7-2022

Water Quality Correlations with Phytoplankton Community Composition in a Polluted Shallow Subtropical Estuary

Connor Joseph Wong

WATER QUALITY CORRELATIONS WITH PHYTOPLANKTON COMMUNITY COMPOSITION IN A POLLUTED SHALLOW SUBTROPICAL ESTUARY

By

CONNOR JOSEPH WONG

B.S., Florida Institute of Technology

A thesis submitted to the College of Engineering and Sciences of Florida Institute of Technology in partial fulfillment of the requirements for the degree of

MASTER OF SCIENCE
in
BIOLOGICAL OCEANOGRAPHY

Melbourne, Florida
July 2022

WATER QUALITY CORRELATIONS WITH PHYTOPLANKTON COMMUNITY COMPOSITION IN A POLLUTED SHALLOW SUBTROPICAL ESTUARY

A THESIS

By

CONNOR JOSPEH WONG

Approved as to style and content by:

_____
Kevin B. Johnson, Ph.D.
Professor
Ocean Engineering and Marine Sciences
Major Advisor

_____
Austin Fox, Ph.D.
Assistant Professor
Ocean Engineering and Marine Sciences

_____
Glenn Miller, Ph.D.
Instructor
Ocean Engineering and Marine Sciences

_____
Richard B. Aronson, Ph.D.
Professor and Department Head
Ocean Engineering and Marine Sciences

July 2022

ABSTRACT

WATER QUALITY CORRELATIONS WITH PHYTOPLANKTON COMMUNITY COMPOSITION IN A POLLUTED SHALLOW SUBTROPICAL ESTUARY

by Connor Joseph Wong, B.S., Florida Institute of Technology

Chairperson of Advisory Committee: Kevin B. Johnson, Ph.D.

The Indian River Lagoon (IRL) estuary has experienced eutrophication and degraded water quality due to high nutrient input, urbanization, and anthropogenic stressors. High nutrient input and restricted estuarine hydrology promotes algal blooms. Algal blooms or harmful algal blooms (HABs) are a global concern as they can cause negative ecological and economic impacts. The frequency and range of HABs is expected to be exacerbated by climate change and altered oceanic and estuarine conditions. Research on the formation and frequency of HABs is an ongoing global effort, but algal blooms are often dynamic and patchy making them difficult to study. This study sought to expand databases of phytoplankton distribution and environmental drivers in the IRL and coastal Atlantic Ocean.

Between the IRL and coastal Atlantic Ocean, salinity was the most influential environmental variable shaping community compositions and biodiversity. However, nutrient data was limited and did not offer compelling evidence of strong influence on phytoplankton distribution, but some associations were determined. Overlap in estuarine and coastal community composition is proposed to be a result of irregular and intermittent coastal and estuarine mixing

associated with the Port Canaveral Locks System, as well as mixing associated with Sebastian Inlet. However, communities within the central BRL were distinct from coastal communities at the same latitude suggesting minimal phytoplankton transport from the coast to the IRL in the central BRL. The taxa driving these similarities in estuarine and coastal communities are likely ubiquitous euryhaline diatoms and some dinoflagellates that dominate in the IRL and coastal ocean. Phytoplankton biodiversity, species richness, and species evenness were also determined to be higher in the coastal ocean and is attributed to osmotic stress along a gradient of decreasing salinities from 10-30 PSU, as found in other estuaries. Diatom abundance in the IRL was significantly higher than the coastal ocean, but dinoflagellates and other plankton were not statistically different between IRL and coastal sites. Cyanobacteria were generally present at low abundances ($<2x10^4$ cells mL^{-1}) except for a unique cyanobacteria bloom referred to as the CyanoHAB of 2020 in the IRL and BRL in 2020. The bloom reached densities of over $5x10^6$ cells mL^{-1} and persisted from July-August to December. Potential bloom drivers were determined to be temperature, nitrate, and phosphate, but limited nutrient data may limit the accuracy of these findings.

TABLE OF CONTENTS

LIST OF FIGURES

LIST OF TABLES

ACKNOWLEDGEMENTS

I would like to express my sincerest gratitude to my major advisor, Dr. Kevin Johnson, for allowing me to conduct research under his guidance and for offering his support and expertise throughout my bachelor and master's degrees. I would also like to express my gratitude for the other members of my thesis committee, Dr. Austin Fox and Dr. Glenn Miller for their help and support in class and during this entire thesis process. My research would not be possible without the help of my peers Sean Crowley, Rachael Stark, Amanda Capuano, Connor Bol, Sophia Byrd, and many others. I am especially appreciative of the Florida Institute of Technology and the Department of Ocean Engineering and Marine Sciences for their constant financial support of my research and education through grants and teaching assistantships.

I would also like to express my gratitude to my parents, siblings, and family for their endless support and constant encouragement through all of my academic endeavors. I hope to make you all proud by being the first in the family to hold a master's and doctorate degree, and I will continue to strive for success. For all those who have helped and encouraged me throughout the years, I cannot express how grateful I am for everything you have done! Lastly, I would like to thank my significant other, Jade Musick, for your love and encouragement throughout our relationship.

CHAPTER 1
INTRODUCTION

The IRL is a shallow, subtropical estuary spanning 250 km along the east coast of Florida and is comprised of three subestuaries: the IRL proper, the Banana River Lagoon (BRL), and the Mosquito Lagoon (Dybas, 2002). The IRL is economically important, contributing $7.6 billion annually to Florida's economy and has been considered by some the most biodiverse estuary in North America (East Central Florida Regional Planning Council, 2016; Dybas, 2002). However, biodiversity and economic value have been impacted through anthropogenic activities in recent years (*e.g.* urbanization, nutrient loading, habitat loss, etc.) (Lapointe *et al*., 2020). Widespread eutrophication in the IRL, facilitated by freshwater nutrient loading and the accumulation of fine-grained, organic-rich sediments, has resulted in seagrass loss and the emergence of persistent and recurring Harmful Algal Blooms (HABs) (*i.e.* shift from benthic to planktonic productivity) (Trefry *et al*, 2007; Lapointe *et al*., 2020). This productivity regime shift began in the northern IRL during the 2011 "superbloom" of a unidentified Pedinophyte (believed to be *Resultor* sp.) and the 2012 *Aureoumbra lagunensis* (brown tide) bloom that increased chlorophyll concentrations, created highly turbid conditions, and smothered 47,000 acres (~60%) of seagrasses from Ponce Inlet to Fort Pierce Inlet (Lapointe *et al*., 2020; Phlips *et al*., 2015). In the following years, Lapointe *et al*. (2020) estimated a 95% reduction in seagrass coverage from 2009 in the same area after another prolonged *A. lagunensis* bloom in 2016 (Lapointe *et al*.,

2020). This regime shift has disrupted ecosystem function, such as high turbidity, hypoxic conditions, and “fish kills” (Phlips *et al.*, 2011) and prompted mitigative efforts to improve water quality and restore seagrass communities in the IRL.

Similar regime shifts in tropical and temperate estuaries are expected to become more ubiquitous in response to climate change and associated weather events (Gobler, 2020; Griffith, 2020). In addition to increased temperatures, climate change may also alter hydrologic patterns, increase storm and drought frequency, and increase freshwater discharge shifting environmental conditions in estuarine and coastal systems (Parkinson *et al*., 2021). Current climate models predict increased intensity, duration, and range expansion of cyanobacteria over eukaryotic phytoplankton in the future (Paerl & Huisman, 2008). This is believed to be a result of many factors including euryhaline and eurythermal tolerances; maximum growth rates at high temperatures; and the efficient use of dissolved phosphorus and atmospheric nitrogen (O’Neil *et al.*, 2012; Quintana, 2011). Frequent and persistent cyanobacteria blooms in estuaries pose many threats including increased cyanotoxins and human-related illnesses; reduced zooplankton grazing and energy transfer; and ecosystem degradation (*e.g.* hypoxia, eutrophication) (Wang & Zhang, 2020; O’Neil *et al.*, 2012).

Phytoplankton blooms are often controlled by nutrient inputs, but nutrient requirements differ between eukaryotic phytoplankton and cyanobacteria. Nutrient stoichiometry in eukaryotic phytoplankton follows the Redfield molar ratio (106C:16N:1P) (Redfield, 1958), but many phytoplankton, including cyanobacteria,

have species-specific nutrient requirements (Paerl & Fulton, 2006). Some eukaryotic phytoplankton thrive in higher N:P ratio environments and cyanobacteria tend to favor lower dissolved inorganic N:P ratios (*i.e.* higher P) (Raateoja *et al*., 2011). Some cyanobacteria require different nutrient species than eukaryotic phytoplankton because many are diazotrophs (N_2-fixers) (Paerl & Fulton, 2006). Consequently, such cyanobacteria can readily acquire and fix abundant atmospheric nitrogen leaving phosphorus as the default limiting nutrient (Kretz *et al*, 2015). Phlips *et al*. (2002) reported higher N:P ratios in the northern IRL suggesting phosphorus is the limiting nutrient controlling phytoplankton growth, with salinity and rainfall as additional factors. Although many cyanobacteria are euryhaline, the distribution of cyanobacteria in marine and estuarine systems is linked to salinity (Rakko & Seppälä, 2014; Buzzani *et al*., 2022). Cyanobacteria strains with the pigment phycocyanin (blue-green algae with phycocyanin or BGAPC) have been found to be more dominant at lower salinities, whereas cyanobacteria strains with phycoerythrin (blue-green algae with phycoerythrin or BGAPE) were more dominant at higher salinities (Ray *et al*., 1989; Wang *et al*., 2011). This natural distinction based on pigments suggests the possibility of quantifying cyanobacteria via pigment fluorescence and flow cytometry. Flow cytometry can also be used to quantify densities of eukaryotic phytoplankton.

The goals of this study are to 1) Find relationships between nutrient concentrations and phytoplankton populations in the IRL and adjacent coastal

Atlantic Ocean and 2) Characterize spatiotemporal trends and environmental relationships in patchy phytoplankton blooms in the IRL. This study also seeks to address these hypotheses:

1. Salinity, temperature, and dissolved phosphate explained the majority of variation in densities of cyanobacteria containing phycocyanin (BGAPC).
2. Densities of BGAPC during the CyanoHAB had a significant inverse linear relationship with salinity and a significant direct linear relationship with temperature in the IRL.
3. Biodiversity of phytoplankton communities was greater in the coastal Atlantic Ocean than in the IRL.

CHAPTER 2
MATERIALS AND METHODS

COMPARING PHYTOPLANKTON DIVERSITY

To assess differences in biodiversity between phytoplankton communities in the IRL and coastal Atlantic Ocean, four standard plankton tows were conducted at three sites in the IRL and three sites in the coastal ocean at the same latitude on a given sampling day from 2019 to 2021 (Figure 1, Table 1 & 2). Each site consisted of 5 sampling stations except for BRNW which consisted of 3 sampling sites (Figure 1 and Table 2). Sample sites were selected because they were logistically feasible options for sampling phytoplankton communities in the IRL and adjacent coastal ocean. Alternative sampling locations were selected for land-based plankton tows and were within 100m of the main sampling stations (Table 2). Plankton tows were conducted within the perimeter of the IRL and coastal stations. Tows were performed using a 25µm plankton net with a mouth diameter of 0.25m and a blind cod end from vessels and from land. Vessels consisted of 5m long skiffs, 7m long pontoons, and an 11m long charter boat. The skiffs and pontoons were powered with outboard motors and the charter boat was powered by an inboard motor.

The plankton net was deployed at the idle speed of the vessel for about two minutes for each replicate with the exact speed (m s^{-1}) and time in seconds being recorded for volume calculations. The sides of the plankton net were rinsed into the cod end using a sprayer and poured into a 20µm PVC filter to reduce sample volume to 500mL for preservation. Each sample was stored in 7% buffered

formalin for later processing. Temperature, salinity, dissolved oxygen (mg L^{-1}), and pH were measured via Yellow Springs Instrument or Aquatroll sondes before each replicate plankton tow.

s: Timetable of phytoplankton tows and associated samples. Four primary categories of samples were collected: cytometer samples (C); plankton tows (T); nutrient samples (N); water quality samples with Secchi Depth (WQ). On each sample date and location, replication was 32 unfiltered water samples for flow cytometry, 4 plankton tows, and 4 replicate water quality profiles.

Date	BRNI	BRNW	BRNO	BRSI	BRSO	VBI	VBO
19-Oct				C|T|WQ			
19-Nov	C|T|WQ	C|T|WQ	C|T|WQ		C|T|WQ		
19-Dec						C|T|WQ	
20-Jan				C|T|WQ	C|T|WQ		C|T|WQ
20-Feb		C|T|WQ	C|T|WQ				
20-Mar	C|T|WQ					C|T|WQ	C|T|WQ
20-May				C|T|WQ			
20-Jun	C|T|WQ					C|T|WQ	
20-Aug				C|T|WQ			
20-Dec	C|T|WQ			C|T|WQ			
21-Feb						C|T|WQ	
21-Mar	C|T|WQ						
21-Apr				C|T|WQ			
21-Jun	C|T|WQ			C|T|WQ			
21-Sep	C|T|WQ|N	C|T|WQ|N	C|T|WQ|N				
21-Oct	C|T|WQ|N	C|T|WQ|N	C|T|WQ|N				

Tow distance was calculated using equation 1,

(1) $D_{Tow} = S * T_{Tow}$

where D_{Tow} = distance of a plankton tow (m), S = the average vessel speed (m s^{-1}) and T_{Tow} = the recorded time of the plankton tow (s).

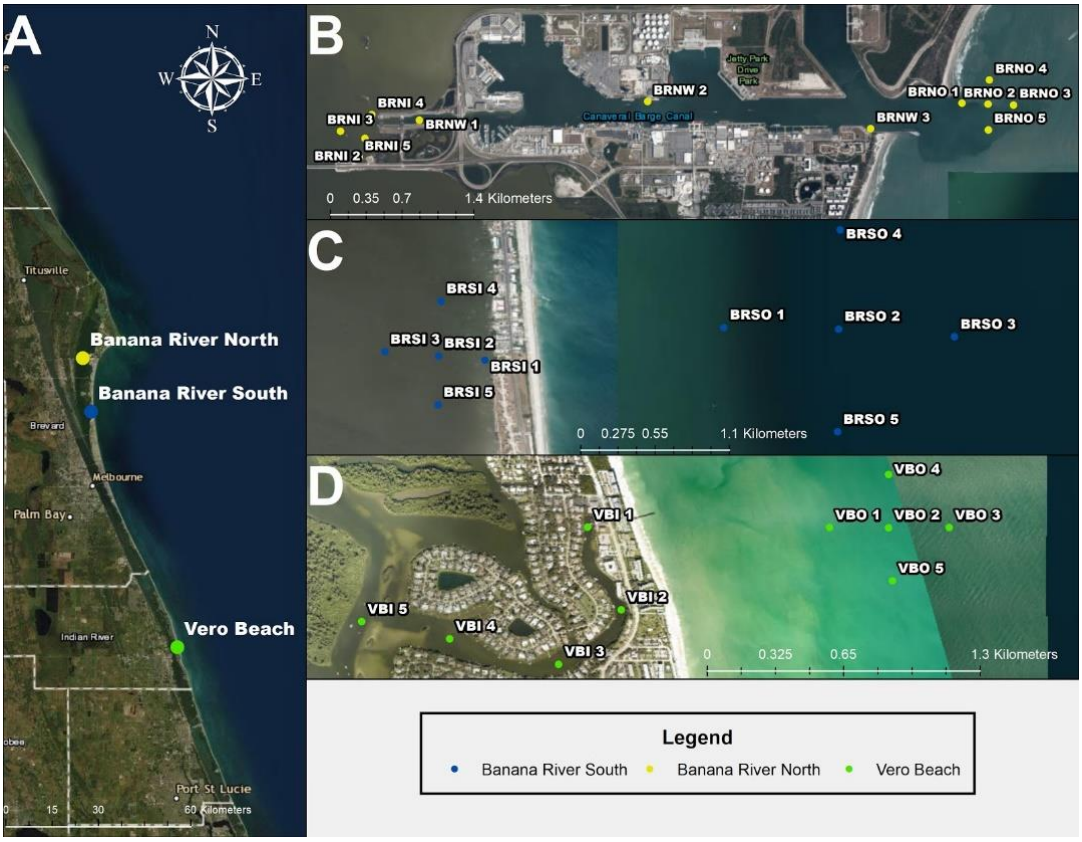

Figure 1: The three latitude locations studied included Banana River North (BRN), Banana River South (BRS), and Vero Beach (VB). A letter after the initial site location name indicates whether the site is in the IRL or ocean (I = IRL, W = within port, and O = outside). A) a map of BRN (yellow), BRS (blue), and VB (green) site locations. B) Expanded map of BRN sites at Port Canaveral. C) Expanded map of BRS sites. D) Expanded map of Vero Beach sites.

Table 2: Geographic coordinates for IRL and ocean sites. Alternative coordinates are other locations close to the proximity of the original coordinates. Location initials include a final initial that indicates inside the estuary (I), within the port (W), and outside in coastal water (O).

Site	Stations	Geographic Coordinates	Alternative Coordinates
Banana River North	BRNI 1	28°24'24.70"N, 80°38'21.39"W	28°24'23.56"N, 80°38'17.93"W
	BRNI 2	28°24'27.43"N, 80°38'30.02"W	28°24'22.66"N, 80°38'23.53"W
	BRNI 3	28°24'29.79"N, 80°38'38.74"W	28°24'21.70"N, 80°38'28.68"W

	BRNI 4	28°24'35.00"N, 80°38'27.51"W	28°24'20.60"N, 80°38'34.51"W
	BRNI 5	28°24'21.54"N, 80°38'32.14"W	28°24'20.28"N, 80°38'38.55"W
	BRNW 1	28°24'33.19"N, 80°38'10.48"W	28°24'32.46"N, 80°37'58.02"W
	BRNW 2	28°24'38.84"N, 80°36'48.75"W	28°24'31.93"N, 80°37'9.22"W
	BRNW 3	28°24'30.04"N, 80°35'28.86"W	28°24'30.29"N, 80°35'41.75"W
	BRNO 1	28°24'37.97"N, 80°34'56.16"W	28°24'31.11"N, 80°35'39.70"W
	BRNO 2	28°24'37.63"N, 80°34'46.87"W	28°24'31.28"N, 80°35'32.16"W
	BRNO 3	28°24'37.33"N, 80°34'37.78"W	28°24'29.26"N, 80°35'26.27"W
	BRNO 4	28°24'45.28"N, 80°34'46.35"W	28°24'29.87"N, 80°35'18.38"W
	BRNO 5	28°24'29.53"N, 80°34'46.80"W	28°24'30.11"N, 80°35'13.28"W
Banana River South	BRSI 1	28°16'17.46"N, 80°36'30.73"W	N/A
	BRSI 2	28°16'18.48"N, 80°36'41.82"W	N/A
	BRSI 3	28°16'19.47"N, 80°36'54.72"W	N/A
	BRSI 4	28°16'31.54"N, 80°36'41.30"W	N/A
	BRSI 5	28°16'6.78"N, 80°36'41.99"W	N/A
	BRSO 1	28°16'25.29"N, 80°35'33.51"W	28°16'18.01"N, 80°36'18.37"W
	BRSO 2	28°16'24.90"N, 80°35'6.03"W	28°16'29.56"N, 80°36'19.36"W
	BRSO 3	28°16'23.07"N, 80°34'38.33"W	28°16'7.79"N, 80°36'17.72"W
	BRSO 4	28°16'48.63"N, 80°35'5.67"W	28°16'35.60"N, 80°36'17.85"W
	BRSO 5	28°16'0.34"N, 80°35'6.33"W	28°16'0.20"N, 80°36'15.75"W
Vero Beach	VBI 1	27°40'11.69"N, 80°21'44.74"W	N/A

	VBI 2	27°39'58.96"N, 80°21'39.54"W	N/A
	VBI 3	27°39'50.54"N, 80°21'49.24"W	N/A
	VBI 4	27°39'54.47"N, 80°22'6.06"W	N/A
	VBI 5	27°39'57.12"N, 80°22'19.66"W	N/A
	VBO 1	27°40'11.64"N, 80°21'7.36"W	N/A
	VBO 2	27°40'11.60"N, 80°20'58.23"W	N/A
	VBO 3	27°40'11.63"N, 80°20'48.85"W	N/A
	VBO 4	27°40'19.83"N, 80°20'58.25"W	N/A
	VBO 5	27°40'3.43"N, 80°20'57.62"W	N/A

Tow volume was calculated using equation 2,

(2) $V_{Tow} = D_{Tow} * r^2 * \pi$

where V_{Tow} = the volume of water filtered through the plankton net (m^3), D_{Tow} = the calculated tow distance (m) and r = the net radius (m)

In the laboratory, preserved tow samples were homogenized and an aliquot (1 - 40µL) was taken and examined via compound light microscopy. Phytoplankton and tintinnids were counted and identified to the lowest taxonomic level. Estimated numbers in the tow sample were then normalized to a field unit of cells L^{-1} using the calculated volume of water collected by the net.

CYANOBACTERIA BLOOM

Samples were collected from four sites in the IRL and two sites in the BRL (Figure 2 and Table 3). Due to the logistics and limitations of sampling, our

sampling period was weekly or biweekly from September to November with one site sampled in July (Table 4). Sampling between July and September and beyond November was not feasible due to various logistical issues. Each sample site

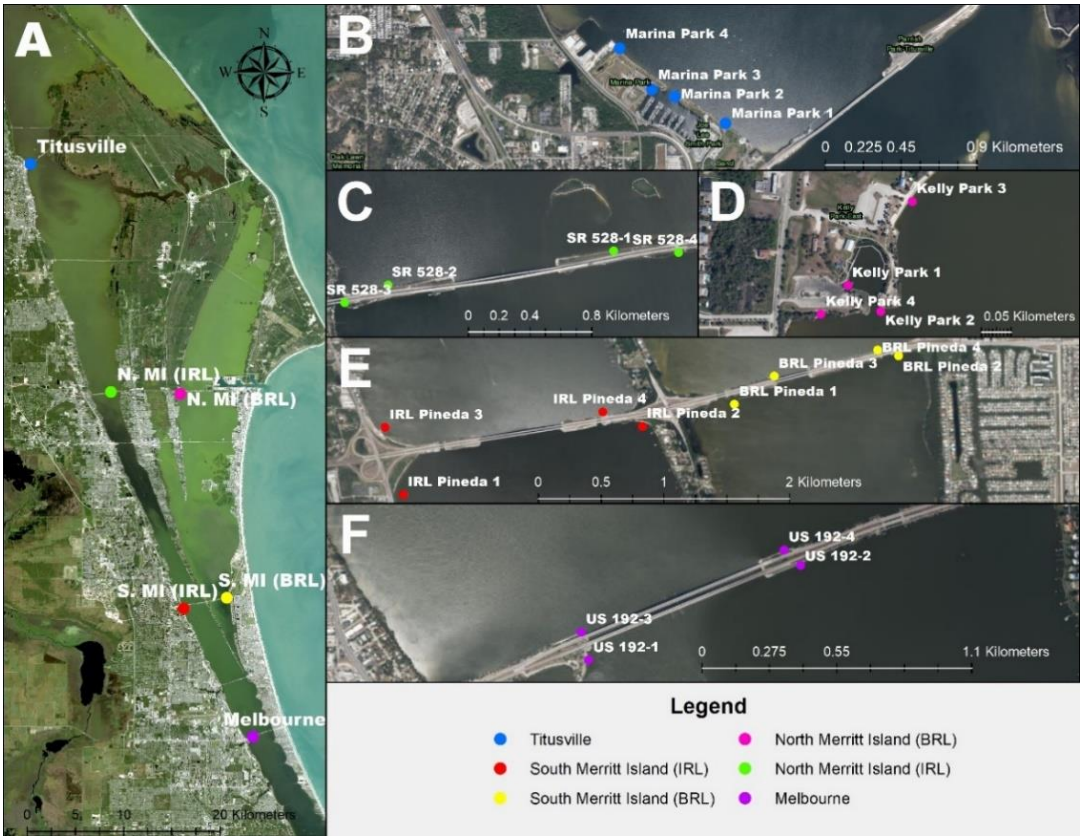

Figure 2: Sampling sites and stations during the "2020 CyanoHAB" in the Northern portion of the IRL. A) The four sites in the IRL and two sites in the BRL. B) Expanded view of the Titusville site in the IRL (blue). C) Expanded view of the north Merritt Island site in the IRL (green). D) Expanded view of the north Merritt Island site in the BRL (pink). E) Expanded view of the south Merritt Island site in the IRL (red) and the BRL (yellow). F) Expanded view of the Melbourne site (purple).

consisted of four onshore subsampling sites where four whole water samples and salinity, temperature, pH, and dissolved oxygen data were collected. Turbidity and chlorophyll data were acquired from the Saint Johns River Water Management

District's (SJRWMD) Continuous Monitoring Program to determine environmental relationships. *In situ* chlorophyll, silica, phosphate, ammonium, and nitrate data were also acquired from SJRWMD. Samples were chilled and processed within hours of collection via BD Accuri C6 Flow Cytometer. The logged number of

Table 3: Geographic coordinates for sampling stations during the bloom.

Site	Stations	Geographic Coordinates
Titusville (IRL)	Marina Park 1	28°37'11.83"N, 80°48'19.57"W
	Marina Park 2	28°37'17.06"N, 80°48'30.60"W
	Marina Park 3	28°37'18.42"N, 80°48'35.60"W
	Marina Park 4	28°37'26.37"N, 80°48'42.71"W
North Merritt Island (IRL)	SR 528-1	28°24'15.12"N, 80°43'39.36"W
	SR 528-2	28°24'8.05"N, 80°44'33.09"W
	SR 528-3	28°24'4.32"N, 80°44'43.44"W
	SR 528-4	28°24'14.76"N, 80°43'23.88"W
South Merritt Island (IRL)	IRL Pineda 1	28°12'7.14"N, 80°39'34.77"W
	IRL Pineda 2	28°12'24.63"N, 80°38'25.04"W
	IRL Pineda 3	28°12'24.52"N, 80°39'40.06"W
	IRL Pineda 4	28°12'28.38"N, 80°38'36.54"W
Melbourne (IRL)	US 192-1	28° 4'55.43"N, 80°35'42.60"W
	US 192-2	28° 5'7.93"N, 80°35'10.71"W
	US 192-3	28° 4'59.13"N, 80°35'43.66"W
	US 192-4	28° 5'10.01"N, 80°35'13.20"W
North Merritt Island (BRL)	Kelly Park 1	28°24'7.70"N, 80°39'45.85"W
	Kelly Park 2	28°24'6.26"N, 80°39'43.83"W
	Kelly Park 3	28°24'12.28"N, 80°39'41.84"W
	Kelly Park 4	28°24'6.12"N, 80°39'47.52"W
South Merritt Island (BRL)	BRL Pineda 1	28°12'30.27"N, 80°37'58.12"W
	BRL Pineda 2	28°12'42.63"N, 80°37'10.21"W
	BRL Pineda 3	28°12'37.47"N, 80°37'46.55"W
	BRL Pineda 4	28°12'44.17"N, 80°37'16.31"W

phycocyanin fluorescent events was plotted against the logged number of chlorophyll fluorescent events to quantify both cyanobacteria strains containing the phycocyanin pigment and "Other" phytoplankton, which includes diatoms, dinoflagellates, and any other non-cyanobacteria cells. The logged number of

phycoerythrin fluorescent events was plotted against the logged number of chlorophyll fluorescent events to quantify cyanobacteria strains containing the phycoerythrin pigment. Cell counts were divided by the volume filtered through the cytometer and normalized to a unit of cells mL^{-1}.

Table 4: Schedule for cyanobacteria bloom sampling.

Site	7/30	9/18	9/25	10/2	10/9	10/21	11/6	11/11
Titusville (IRL)			X	X	X	X	X	X
North Merritt Island (IRL)		X	X	X	X	X	X	X
South Merritt Island (IRL)		X	X	X	X	X	X	X
Melbourne (IRL)			X	X	X	X	X	X
North Merritt Island (BRL)	X	X	X	X	X	X	X	X
South Merritt Island (BRL)		X	X	X	X	X	X	X

NUTRIENT ANALYSES

Water samples were collected at Banana River North sampling stations and filtered through a 0.4μm filter. Concentrations of nitrogen and phosphorus were measured using a SEAL AA3 HR Continuous Segmented Flow Autoanalyzer following the manufacturer's protocol (G-218-98). Dionex (Sunnyvale, CA) 5-Anion Standard was analyzed alongside samples as a reference to verify accuracy.

STATISTICAL ANALYSES

Biodiversity, species richness, and species evenness were calculated using the Shannon-Wiener Diversity Index. Biodiversity and community data were analyzed using ANOVA and Tukey tests, T-tests, n-MDS, PERMANOVA, and ANOSIM. All means are reported as mean ± 1SE. Principal component analysis

(PCA) was used to determine influential environmental parameters and differences between and amongst IRL and coastal sites. Simple linear regressions and a multiple linear regression were performed to determine influential environmental variables with BGAPC during the CyanoHAB of 2020. Two separate PCAs were performed, one using environmental parameters collected at all sites and the other using the limited nutrient data collected in the fall of 2021 at BRN, to be called Environmental Parameters PCA and BRN Nutrient PCA, respectively. The Environmental Parameters PCA used temperature, salinity, dissolved oxygen (DO), and pH for environmental factors. Redundancy Analysis (RDA) was employed on dominant phytoplankton taxa and environmental variables that did not exhibit multicollinearity. Phytoplankton community data from all IRL and coastal sites across all years and seasons and accompanying environmental data (temperature, salinity, DO, and pH) were used to assess the influence of environmental variables on phytoplankton populations via RDA. The influence of nutrients and water quality (temperature, salinity, pH, NO_3, and PO_4) on phytoplankton populations was assessed in a separate RDA due to the limited nutrient samples collected at BRN in the fall of 2021. The influence of environmental parameters on IRL communities and coastal communities were also assessed separately via RDA.

STATISTICAL SOFTWARE AND TRANSFORMATIONS

Microsoft Excel, Google Sheets, and RStudio software were used to transform and run statistical analyses on data. The R packages vegan (Oksanen *et al*., 2020), ggplot2 (Wickham, 2016), ggpubr (Kassambara, 2020), ggfortify

(Horikoshi & Tang, 2016), gridExtra (Auguie, 2017), BiodiversityR (Kindt & Coe, 2005), and faraway (Faraway, 2016) were used for statistical analyses and graphing. Environmental data used in PCA and RDA were log(x+1) transformed before analysis. For RDA, community data were Hellinger transformed and environmental data were log(x+1) transformed. Community data used in n-MDS, ANOSIM, and PERMANOVA were cube root transformed. ANOSIM were performed using Bray-Curtis dissimilarity and 999 permutations. PERMANOVA were also performed using Bray-Curtis dissimilarity.

DOMINANT PHYTOPLANKTON

Dominant phytoplankton species were calculated using equation 3 (Lampitt *et al*., 1993):

$$(1)\ Y = (\frac{n_i}{N})f_i$$

where Y = the species distribution value, n_i = the sum of densities for species i, N = the sum of densities for all species, and f_i = frequency of occurrence of species i. A species distribution value represents the relative abundance (*i.e.* the abundance of a single species divided by the abundance of all species in a sample) multiplied by the frequency of occurrence. That is to say, the species distribution value represents taxa that are abundant and frequent enough in a sample to be considered influential to the community. Taxa were determined to be dominant if their calculated species distribution value (Y) was greater than 0.02.

CHAPTER 3
RESULTS

COMMUNITY COMPOSITION AND ABUNDANCE

Phytoplankton tows across coastal and IRL sites yielded a total of 92 planktonic taxa with the most diverse groups being diatoms (63) and dinoflagellates (16) followed by cyanobacteria (3), a silicoflagellate (1), and 9 miscellaneous or difficult to identify taxa (*i.e.* taxa that have indistinguishable characteristics under light 400x magnification) (Table 5). In this study, 48 taxa were found in both IRL and coastal communities, 33 taxa only belonged to coastal communities, and 11 taxa only belonged to IRL communities (Table 5). Of the 92 taxa identified, ten potentially harmful genera were identified (Table 5). *Pseudo-nitzschia* sp. was the only recognized harmful genus of diatom and *Ceratium* spp., *Dinophysis* spp., *Gonyaulax* sp., *Gymnodinium spp.*, *Peridinium* sp., *Podolampas* sp., *Prorocentrum* spp., *Protoperidinium* spp., and *Pyrodinium bahamense* were the only recognized genera of harmful dinoflagellates. Harmful phytoplankton are defined as taxa notoriously associated with toxin production and/or severe blooms resulting in anoxia, fish kills, ecosystem degradation, and adverse effects on humans (Anderson, 2009). The twenty phytoplankton with the highest mean abundances accounted for 98% of the total phytoplankton cells (Table 6), and the twenty most frequently occurring phytoplankton based upon presence/absence accounted for 66.5% of all phytoplankton occurrences (Table 7).

Table 5: Phytoplankton taxa found in the Indian River Lagoon and corresponding coastal waters. Potentially harmful taxa are bolded. Green indicates taxa present in both the IRL and coastal ocean; blue indicates taxa present only in the coastal ocean; and orange indicates taxa present only in the IRL.

Group	Taxa
Diatom	*Actinoptychus senarius*
	Actinoptychus splendens
	Amphiprora sp.
	Amphitetras sp.
	Amphora proteoides
	Amphora sp.
	Asterionellopsis glacialis
	Bacillaria paxillifera
	Bacteriastrum spp.
	Bellerochea horologicalis
	Bellerochea malleus
	Biddulphia alternans
	Biddulphia rhombus
	Biddulphia sp.
	Chaetoceros spp.
	Climacodium frauenfeldianum
	Corethron spp.
	Coscinodiscus spp.
	Cyclotella meneghiniana
	Cyclotella sp.
	Cylindrotheca closterium
	Cymatosira belgica
	Dactyliosolen fragilissimus
	Delphineis surirella
	Detonula pumila
	Diploneis sp.
	Epithemia sorex
	Eucampia sp.
	Eunotogramma sp.
	Grammatophora marina
	Grammatophora sp.
	Guinardia flaccida

	Guinardia striata
	Gyrosigma fasciola
	Haslea wawrickae
	Hemiaulus hauckii
	Hemiaulus membranaceus
	Hemiaulus sinensis
	Hemiaulus sp.
	Leptocylindrus danicus
	Licmophora sp.
	Lioloma pacificum
	Lithodesmium undulatum
	Melosira moniliformis
	Meuniera membranacea
	Navicula sp.
	Nitzschia longissima
	Nitzschia spp.
	Odontella spp.
	Paralia sulcata
	Pleurosigma sp.
	Pseudofalcula hyalina
	***Pseudo-nitzschia* spp.**
	Rhizosolenia spp.
	Skeletonema costatum
	Stephanopyxis sp.
	Surirella sp.
	Thalassionema frauenfeldii
	Thalassionema nitzschoides
	Thalassiosira sp.
	Triceratium brightwellii
	Triceratium sp.
	Trigonium sp.
Dinoflagellate	*Actiniscus pentasterias*
	***Ceratium* spp.**
	Ceratocorys armata
	***Dinophysis* spp.**
	***Gonyaulax* sp.**

	***Gymnodinium* spp.**
	Oxyphysis sp.
	Oxytoxum sp.
	***Peridinium* sp.**
	Phalacroma argus
	***Podolampas* sp.**
	***Prorocentrum* spp.**
	***Protoperidinium* spp.**
	Pyrocystis fusiformis
	Pyrocystis lanceolata
	Pyrodinium bahamense
Silicoflagellate	***Dictyocha fibula***
Cyanobacteria	*Anabaena* sp.
	Lyngbya sp.
	Oscillatoria sp.
Miscellaneous Plankton	Peridinial Dinoflagellate
	Amphorellopsis sp.
	Cryptophycean
	Eutintinnus sp.
	Helicostomella sp.
	Raphid Bacillariophyceaen Diatom
	Raphidophycean
	Sponge Tylostyle Spicules
	Tintinnopsis sp.

When comparing the three groups of phytoplankton (diatoms, dinoflagellates, and other plankton) in the IRL and coastal ocean, the density of diatoms in the IRL (1,829 cells L^{-1} ± 418) was significantly higher than the density of coastal diatoms (546 cells L^{-1} ± 75) ($t = 3.02$, $df = 79.75$, $p < 0.01$); the density of dinoflagellates in the IRL (420 cells L^{-1} ± 135) was not different than the density of coastal dinoflagellates (541 cells L^{-1} ± 169) ($t = -0.5579$, $df = 100.82$, $p > 0.05$); and the density of other plankton in the IRL (7 cells L^{-1} ± 1) was indistinguishable

from the density of other plankton in coastal waters (6 cells L^{-1} ± 1) (t = 0.39022, df = 100.26, p > 0.05) (Figure 3).

Table 6: Average mean and high densities (cells L^{-1}) of the 20 most abundant phytoplankton taxa from samples collected in the Indian River Lagoon (n=76) and the coastal Atlantic Ocean at corresponding latitude locations (n=48).

Phytoplankton	IRL (n=76)		Coastal (n=48)	
	Average	High	Average	High
Leptocylindrus danicus	1094	11746	18	117
Chaetoceros spp.	425	7497	103	525
Pyrodinium bahamense	333	6897	65	902
Prorocentrum spp.	10	186	362	3406
Rhizosolenia spp.	209	2891	31	318
Ceratium spp.	52	510	86	1241
Skeletonema costatum	66	1873	18	189
Asterionellopsis glacialis	0	1	86	796
Cyclotella meneghiniana	0	0	71	1143
Dactyliosolen fragilissimus	0	13	43	708
Amphora sp.	2	39	32	1449
Coscinodiscus spp.	7	77	21	127
Gymnodinium spp.	1	35	24	318
Gonyaulax sp.	15	350	1	21
Thalassionema nitzschoides	0	3	23	118
Cylindrotheca closterium	7	81	10	80
Pseudo-nitzschia sp.	5	252	13	94
Thalassionema frauenfeldii	0	4	14	101
Odontella spp.	1	32	11	82
Nitzschia spp.	2	32	9	56

Spatial differences in phytoplankton abundances were detected between IRL and coastal sites, but not across seasons. In the fall of 2019, the density of diatoms at BRNI (494 cells L^{-1} ± 80) was significantly higher than the diatom

density at BRNW (170 cells L^{-1} ± 17) ($p<0.02$), but significantly lower than diatom densities at BRNO (1,403 cells L^{-1} ± 66) ($p<0.001$) (Figure 4). Diatoms

Table 7: The percent occurrence of the 20 most frequently occurring phytoplankton taxa. These phytoplankton account for 975 (66.46%) of the 1,467 total occurrences.

Phytoplankton	IRL	Coastal
	% Occurrence (n=76)	% Occurrence (n=48)
Chaetoceros spp.	76%	90%
Rhizosolenia spp.	63%	73%
Coscinodiscus spp.	51%	88%
Ceratium spp.	57%	73%
Nitzschia spp.	33%	79%
Leptocylindrus danicus	46%	56%
Cylindrotheca closterium	36%	67%
Pleurosigma sp.	39%	54%
Prorocentrum spp.	38%	46%
Thalassionema nitzschoides	7%	73%
Paralia sulcata	16%	56%
Navicula sp.	24%	42%
Odontella spp.	14%	54%
Pseudo-nitzschia spp.	9%	52%
Amphora sp.	25%	25%
Skeletonema costatum	13%	38%
Protoperidinium spp.	22%	17%
Gonyaulax sp.	29%	4%
Pyrodinium bahamense	20%	19%
Asterionellopsis glacialis	1%	46%

at BRS in the fall of 2019 showed a reverse trend as BRN during the same year and season. Diatom densities at BRSI (4,449 cells L^{-1} ± 822) during this time were significantly higher than diatom densities at BRSO (645 cells L^{-1} ± 162) ($p<0.02$) (Figure 4). During this same time, densities of diatoms at VBI (142 cells L^{-1} ± 42) were significantly lower than diatom densities at VBO (638 cells L^{-1} ±

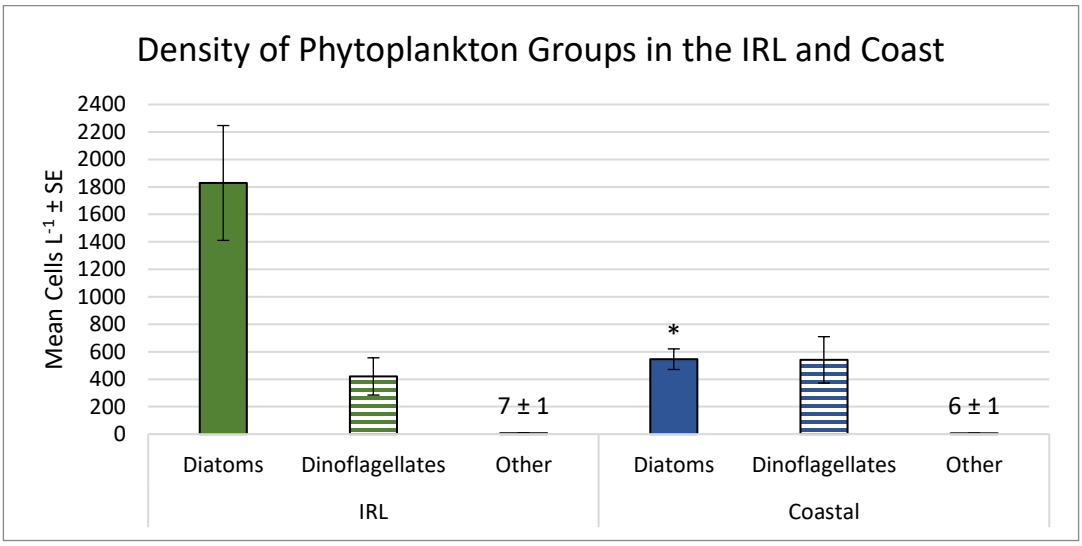

Figure 3: Mean densities of diatoms (solid bars), dinoflagellates (horizontally striped bars), and other plankton (not visible due to relatively low abundance). Green bars represent IRL sites and blue bars represent coastal sites. An asterisk above a coastal group indicates a significant difference between like-groups in the IRL.

18), similar to BRN ($p<0.001$) (Figure 4). In the winter of 2020, diatom densities at BRNI were significantly lower than diatom densities at both BRNW and BRNO ($p<0.01$) (Figure 4). During the same period, the diatom density at BRSI (37 cells $L^{-1} \pm 18$) was not significantly higher than the density of diatoms at BRSO (14 cells $L^{-1} \pm 3$) ($p>0.05$) (Figure 4). Diatom densities at VBI and VBO during the winter of 2020 were relatively low compared to the fall of 2019. Diatom density at VBI (92 cells $L^{-1} \pm 60$) was not significantly lower than diatom density at VBO (101 cells $L^{-1} \pm 24$). In the case of fall of 2021, diatom densities were relatively high at BRNI and significantly lower at BRNW and BRNO for both sampling dates during this period ($p<0.05$) (Figure 4). Dinoflagellate densities were generally lower than that of diatoms.

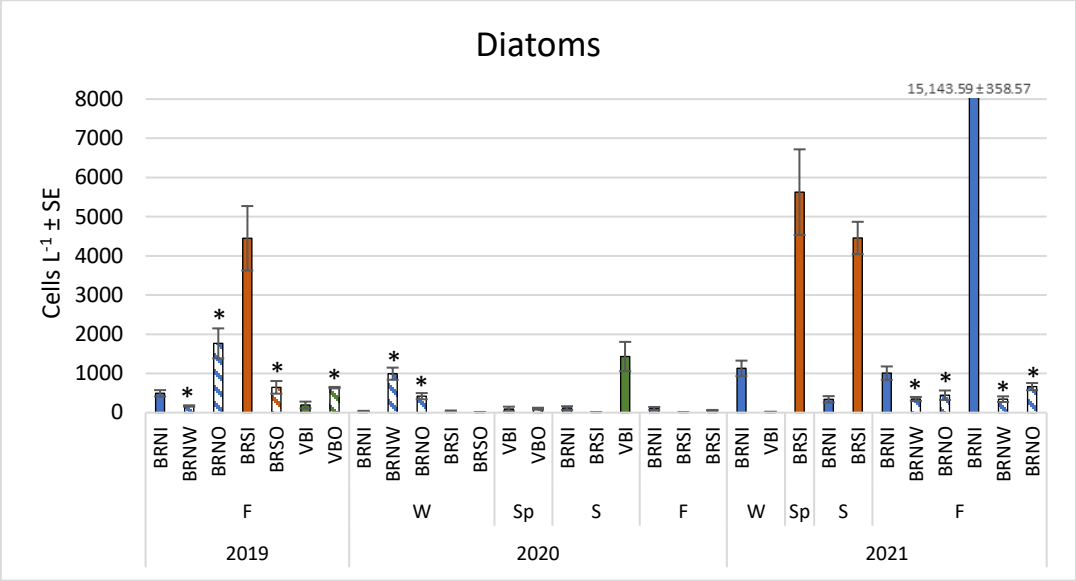

Figure 4: Mean diatom densities (±1SE) by location and season in the IRL (solid bars) and coastal zone (striped bars) from 2019-2021. Locations are Banana River North (BRN, blue bars), Banana River South (BRS, orange bars), and Vero Beach (VB, green bars). The seasons are Fall (F), Winter (W), Spring (Sp), and Summer (S). An asterisk above a coastal site indicates a significant difference between the coastal site and the corresponding IRL site during the same season and year. Some locations are not visible due to low abundance.

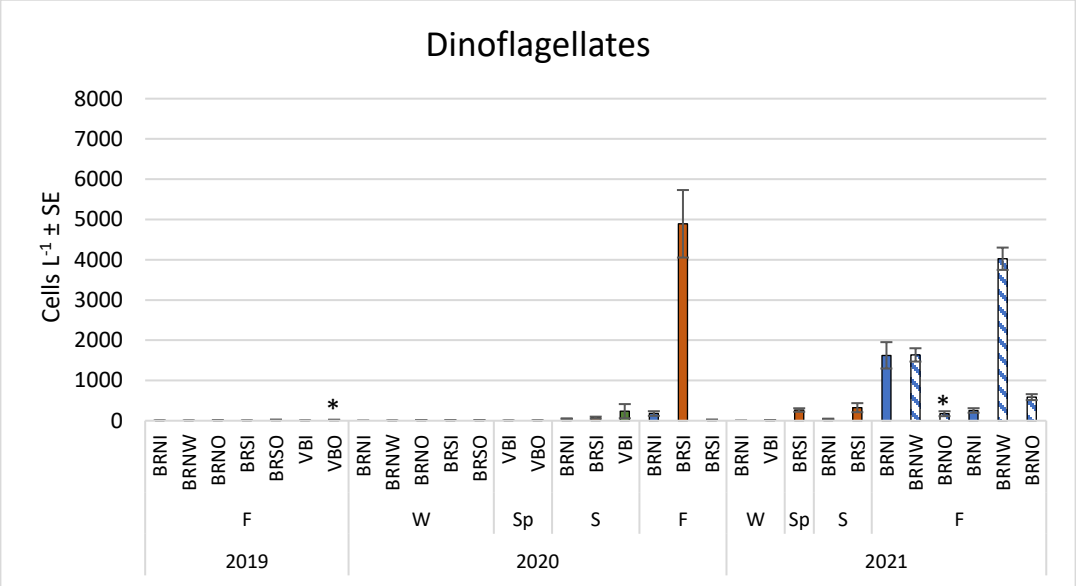

Figure 5: Mean dinoflagellate densities (±1SE) by location and season in the IRL (solid bars) and coastal zone (striped bars) from 2019-2021. Locations are Banana River North (BRN, blue bars), Banana River South (BRS, orange bars), and Vero

Beach (VB, green bars). The seasons are Fall (F), Winter (W), Spring (Sp), and Summer (S). An asterisk above a coastal site indicates a significant difference between the coastal site and the corresponding IRL site during the same season and year. Some locations are not visible due to low abundance.

The dinoflagellate density at BRNI (2 cells L^{-1} ± 1) in the fall of 2019 was not significantly different from BRNW (1 cells L^{-1} ± 0.6) or BRNO (8 cells L^{-1} ± 2) ($p>0.05$). Dinoflagellate densities were relatively low when compared to diatom densities. Dinoflagellate density at BRNI (2 cells L^{-1} ± 1) in the fall of

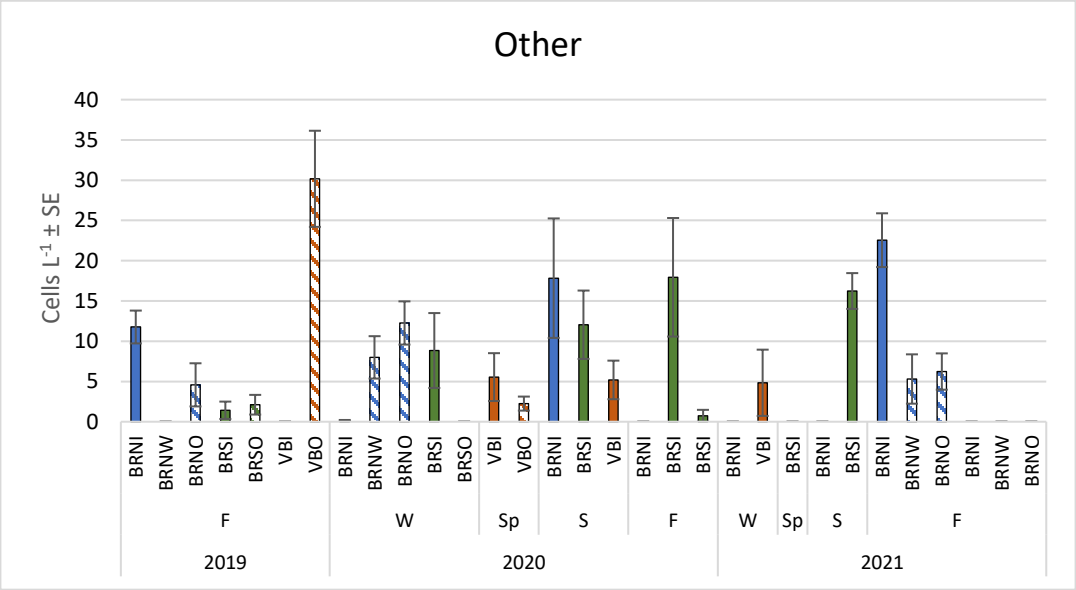

Figure 6: Mean densities of other plankton (±1SE) by location and season in the IRL (solid bars) and coastal zone (striped bars) from 2019-2021. Locations are Banana River North (BRN, blue bars), Banana River South (BRS, orange bars), and Vero Beach (VB, green bars). The seasons are Fall (F), Winter (W), Spring (Sp), and Summer (S). An asterisk above a coastal site indicates a significant difference from the respective IRL site during the same season and year. Some locations are not visible due to low abundance. Please note the y-axis is different from previous graphs due to low abundance of other plankton.

2019 was not significantly different from BRNW (1 cells L^{-1} ± 0.6) or BRNO (8 cells L^{-1} ± 2) ($p>0.05$). In the case of BRS, dinoflagellate densities were not

significantly different between coastal and IRL stations (Figure 5). At VB in the fall of 2019, dinoflagellate densities at coastal stations were significantly higher than dinoflagellate densities at corresponding IRL stations ($p<0.05$). In the winter of 2020, dinoflagellate densities at coastal and IRL stations at BRN, BRS, and VB did not significantly differ ($p>0.05$). During the first sampling in the fall of 2021,

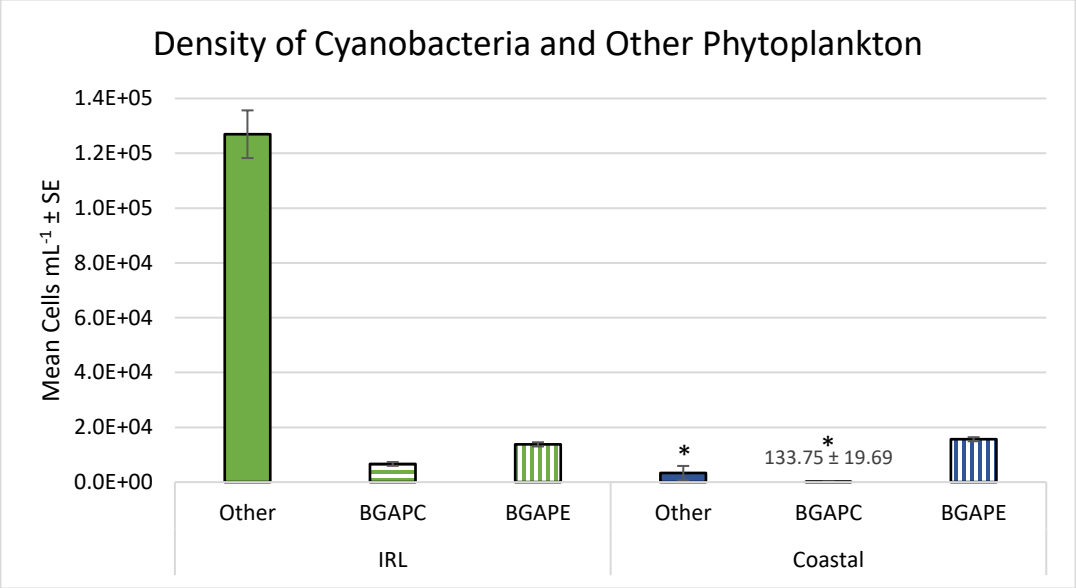

Figure 7: Mean cell densities (±1SE) of cyanobacteria with phycocyanin (BGAPC, horizontal stripes) and phycoerythrin (BGAPE, vertical stripes) pigments and non-cyanobacteria phytoplankton (solid bars) collected via flow cytometry. Green bars symbolize IRL sites and blue bars represent coastal sites. An asterisk above a coastal group indicates a significant difference between like-groups in the IRL.

dinoflagellate densities at BRNI were significantly higher than BRNO ($p<0.01$), but similar to dinoflagellate densities at BRNW ($p=0.99$). During the second sampling period two weeks later, a reverse pattern was observed where dinoflagellate densities at BRNI were similar to BRNO ($p>0.05$), but significantly higher than densities at BRNW ($p<0.001$). Other plankton were present at low

densities and their contribution to the total community abundance was negligible with a collective density of 6.19 cells L^{-1} ± 0.25 (Figure 6).

Abundances of cyanobacteria (BGAPC and BGAPE) and "other phytoplankton" (*e.g.* diatoms, dinoflagellates, and other non-cyanobacteria phytoplankton) were collected via flow cytometry in conjunction with plankton tows. Non-cyanobacteria phytoplankton were the most abundant group of phytoplankton in the IRL with a density of 126,960 cells mL^{-1} ± 8,698, which was significantly higher than the density of non-cyanobacteria in the coastal ocean (6,625 cells mL^{-1} ± 691) ($p<0.001$) (Figure 7). BGAPE were the second most abundant group in the IRL (13,774 cells mL^{-1} ± 761) but their densities were not significantly different from that of coastal waters (15,653 cells mL^{-1} ± 739) ($p>0.05$).

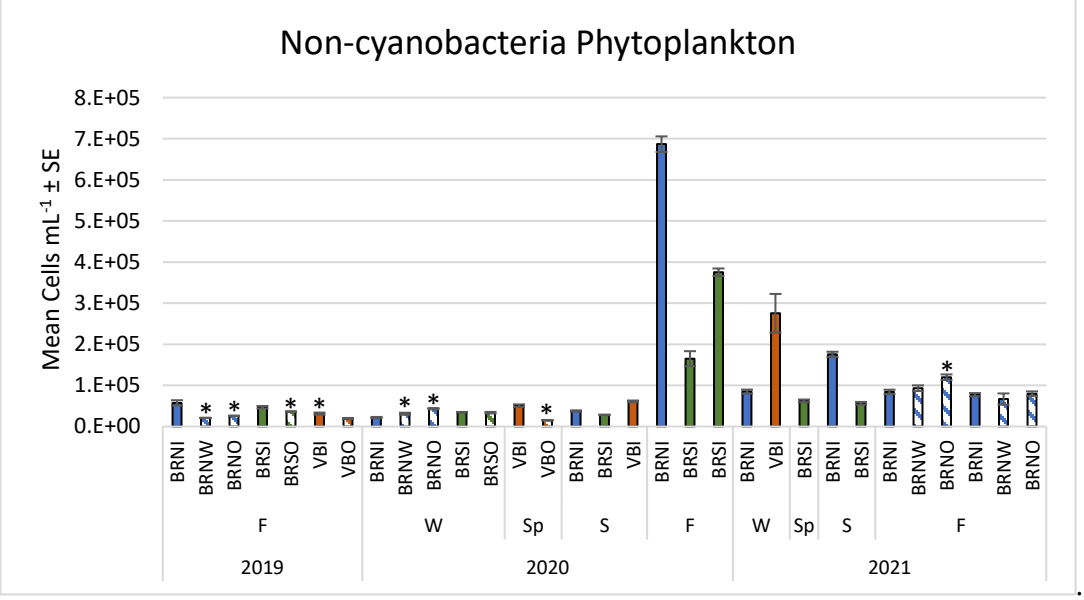

Figure 8: Mean non-cyanobacteria densities (±1SE) by location and season in the IRL (solid bars) and coastal zone (striped bars) from 2019-2021. Locations are Banana River North (BRN, blue bars), Banana River South (BRS, orange bars),

and Vero Beach (VB, green bars). The seasons are Fall (F), Winter (W), Spring (Sp), and Summer (S). An asterisk above a coastal site indicates a significant difference between the coastal site and the corresponding IRL site during the same season and year. Some locations are not visible due to low abundance.

BGAPC were the third most abundant group in the IRL (6,625 cells mL^{-1} ± 691) and densities there were significantly more abundant than BGAPC in coastal waters (134 cells mL^{-1} ± 20) ($p<0.001$). Non-cyanobacteria phytoplankton remained near or below $1x10^5$ cells mL^{-1} in IRL and coastal waters potentially suggesting a background maximum for non-cyanobacteria phytoplankton in both coastal and IRL waters (Figure 8).

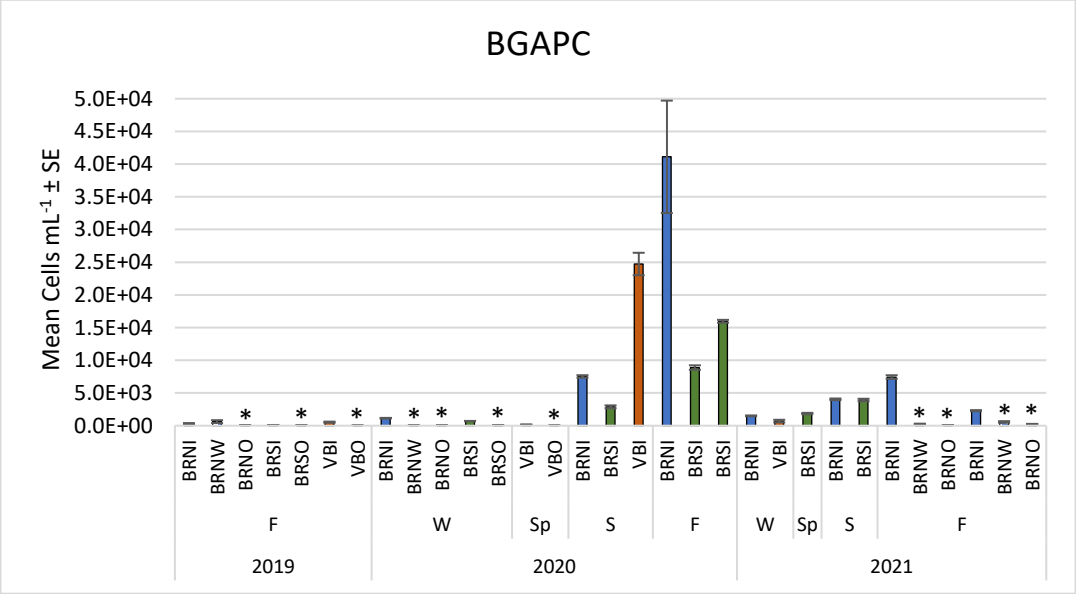

Figure 9: Mean densities of cyanobacteria with phycocyanin (±1SE) by location and season in the IRL (solid bars) and coastal zone (striped bars) from 2019-2021. Locations are Banana River North (BRN, blue bars), Banana River South (BRS, orange bars), and Vero Beach (VB, green bars). The seasons are Fall (F), Winter (W), Spring (Sp), and Summer (S). An asterisk above a coastal site indicates a significant difference between the coastal site and the corresponding IRL site during the same season and year. Some locations are not visible due to low abundance.

IRL sites in the fall of 2020 and winter, spring, and summer of 2021 were the only instances of significant deviation from this background threshold, which may suggest a "bloom period" during this time that was not previously documented in the fall of 2019 or the winter or spring of 2020 (Figure 8). The bloom in the fall of 2020 was due largely to *P. bahamense*. BGAPC densities remained near or below 150 and 1,000 cells mL^{-1} in coastal and IRL waters, respectively. BGAPC significantly deviated from background maximums of the previous year in the summer and fall of 2020, which was slightly earlier than the start of the non-cyanobacteria blooming period (Figure 9). BGAPE remained below a background

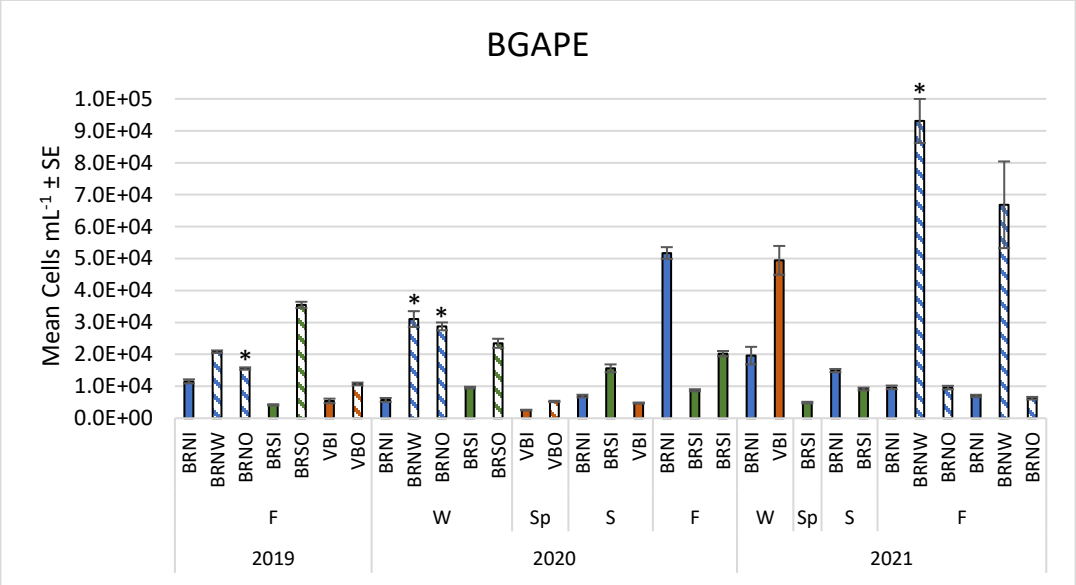

Figure 10: Mean densities of cyanobacteria with phycoerythrin (±1SE) by location and season in the IRL (solid bars) and coastal zone (striped bars) from 2019-2021. Locations are Banana River North (BRN, blue bars), Banana River South (BRS, orange bars), and Vero Beach (VB, green bars). The seasons are Fall (F), Winter (W), Spring (Sp), and Summer (S). An asterisk above a coastal site indicates a significant difference between the coastal site and the corresponding IRL site during the same season and year.

maximum of 20,000 cells mL^{-1} with a few exceptions from coastal sites in the fall of 2019 and the winter of 2020. In the fall of 2020, densities of BGAPE, BGAPC, and non-cyanobacteria exceeded their respective background maxima (Figure 10). At BRNW in the fall of 2021, two deviations from this background maxima can be seen.

Non-metric multidimensional scaling highlights the similarities and differences in phytoplankton communities in the IRL and coastal ocean. Phytoplankton communities at BRN (*e.g.* BRNI vs. BRNW vs. BRNO) were significantly different from each other and showed a strong degree of separation (ANOSIM-R = 0.85, p=0.001). Phytoplankton community distinction between BRN sites for 75% of the variation in BRN communities (p=0.001). Evidence of community structure shifts in the IRL were present, but communities remained relatively distinct from coastal communities (Figure 11). Coastal communities (BRNO) also remained distinct from IRL communities until the fall of 2021, where the coastal community structure shifted to taxa more commonly observed in the IRL (Figure 11). Community structure at BRNW in the fall of 2019 was similar to BRNO, but distinct from BRNI. By the fall of 2021, the community structure of BRNW was relatively similar to communities at BRNO and BRNI, which may suggest the close proximity between sites allows for the occasional development of overlapping community structure. Phytoplankton communities at BRS showed a strong degree of separation and had very little overlap within and amongst IRL and coastal communities (ANOSIM-R = 0.99, p=0.001) (Figure 12). Partitioning

communities by the location within BRS (BRSI or BRSO) during a specific season or year accounted for 71.4% of the variation in phytoplankton communities

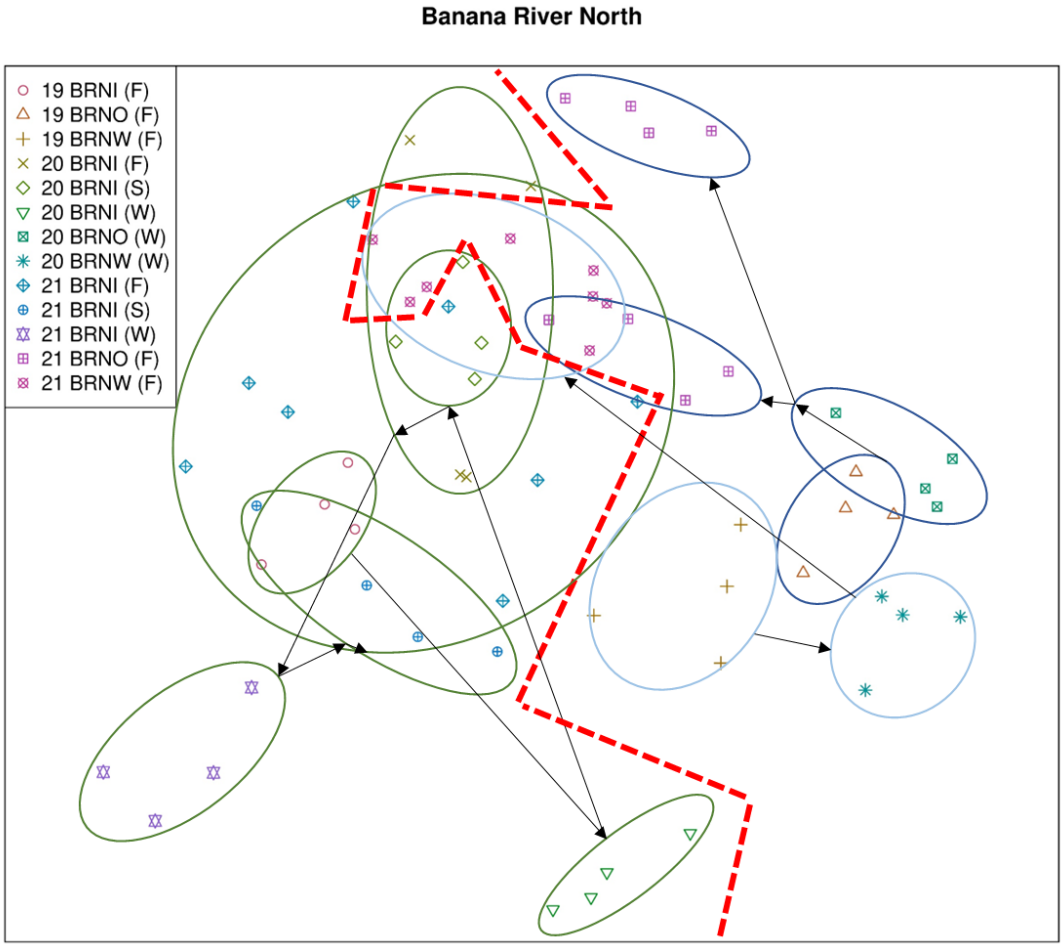

Figure 11: Banana River Lagoon (BRN) phytoplankton community similarities (closely associated plots) and differences (widely separated plots) via non-metric multidimensional scaling (NMDS). BRN sites include estuarine sites (BRNI, grouped by green ellipses), sites within Port Canaveral (BRNW, grouped by light blue ellipses), and coastal sites near the same latitude (BRNO, grouped by dark blue ellipses). Sampling occurred in fall (F), winter (W), spring (Sp), and summer (s) from 2019-2021. Black arrows pointing between clusters follows chronological shifts in phytoplankton communities within the same site. The dashed red line separates IRL and coastal sites, but ellipses may cross this line due to overlapping community structure between coastal sites and IRL sites.

($p<0.01$). Community structure at BRSO was similar between the two seasons sampled, but was distinct from communities at BRSI (*i.e.* few overlapping species). However, the IRL communities were in close proximity to the coastal sites.

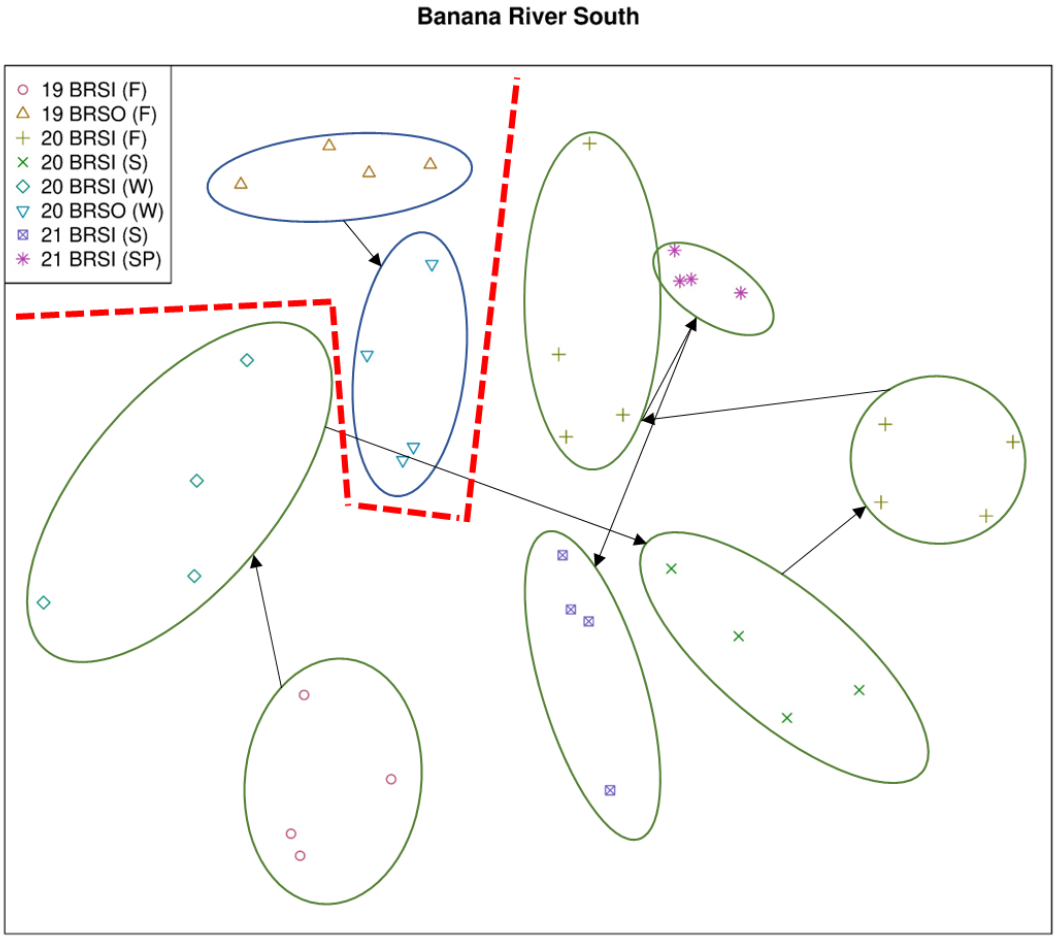

Figure 12: Banana River Lagoon (BRS) phytoplankton community similarities (closely associated plots) and differences (widely separated plots) via non-metric multidimensional scaling (NMDS). BRS sites include estuarine sites (BRSI, grouped by green ellipses) and coastal sites near the same latitude (BRSO, grouped by dark blue ellipses). Sampling occurred in fall (F), winter (W), spring (Sp), and summer (s) from 2019-2021. Black arrows pointing between clusters follows chronological shifts in phytoplankton communities within the same site. The dashed red line separates IRL and coastal sites.

Community structure at VB showed relatively strong separation between coastal and IRL communities, but some overlap in community composition was present between VBI and VBO (ANOSIM-R = 0.79, p=0.001). However, the community structure at VBI in the fall of 2019 was relatively similar to that of VBO in the

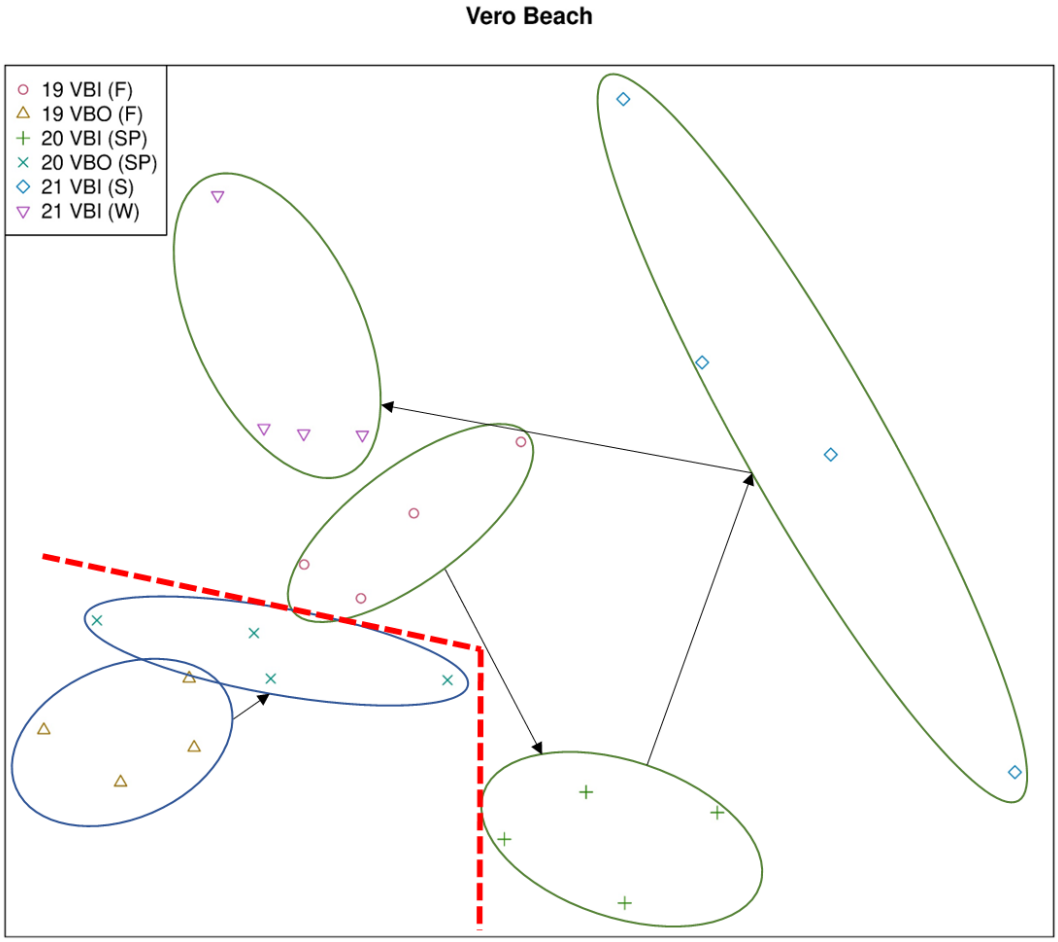

Figure 13: Vero Beach (VB) phytoplankton community similarities (closely associated plots) and differences (widely separated plots) via non-metric multidimensional scaling (NMDS). VB sites include estuarine sites (VBI, grouped by green ellipses) and coastal sites near the same latitude (VBO, grouped by dark blue ellipses). Sampling occurred in fall (F), winter (W), spring (Sp), and summer (s) from 2019-2021. Black arrows pointing between clusters follows chronological shifts in phytoplankton communities within the same site. The dashed red line separates IRL and coastal sites.

spring of 2020 suggesting some degree of similarity in community composition between VBI and VBO. Location within VB for a specific season and year explained 61.9% of the variation in phytoplankton communities ($p<0.01$). VBI communities during the fall of 2019 and winter of 2021 were relatively similar suggesting some degree of overlapping community composition. Winter of 2021 and spring of 2021 communities at VBI were distinct and displayed clear separation from previous seasons (Figure 13). VBI communities in the fall of 2019

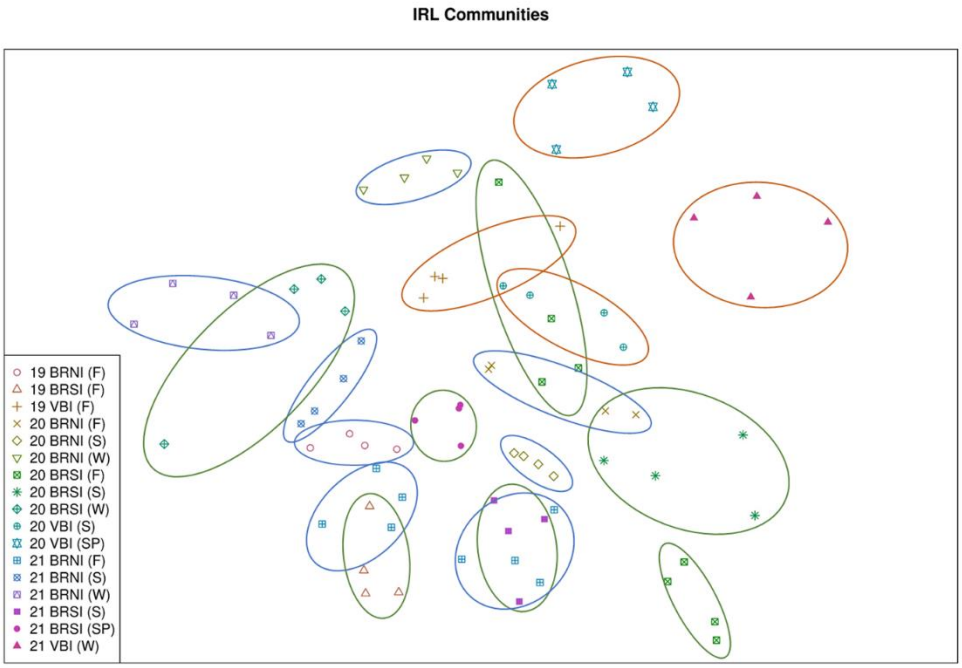

Figure 14: Estuarine phytoplankton community similarities (closely associated plots) and differences (widely separated plots) via non-metric multidimensional scaling (NMDS). Estuarine sites include BRNI (grouped by blue ellipses), BRSI (grouped by green ellipses), and VBI (grouped by orange ellipses). Sampling occurred in fall (F), winter (W), spring (Sp), and summer (S) from 2019-2021.

were relatively similar to VBO communities in the spring of 2020. VBO communities were also similar between both seasons. Separating the communities

by location in the IRL at a particular season and year explained 73.1% of the variation in phytoplankton communities ($p<0.01$). Coastal communities (excluding IRL communities) showed a similar degree of separation as IRL communities (ANOSIM-R = 0.77, $p<0.01$) (Figure 15). However, separating the coastal phytoplankton communities by site during a specific season and year explained 68.4% of the variation in coastal phytoplankton communities ($p<0.01$). BRNO, BRNW, BRSO, and VBI had very similar community compositions in the fall of 2019 (Figure 15). By 2020, community structure at BRNW and BRSO was distinct

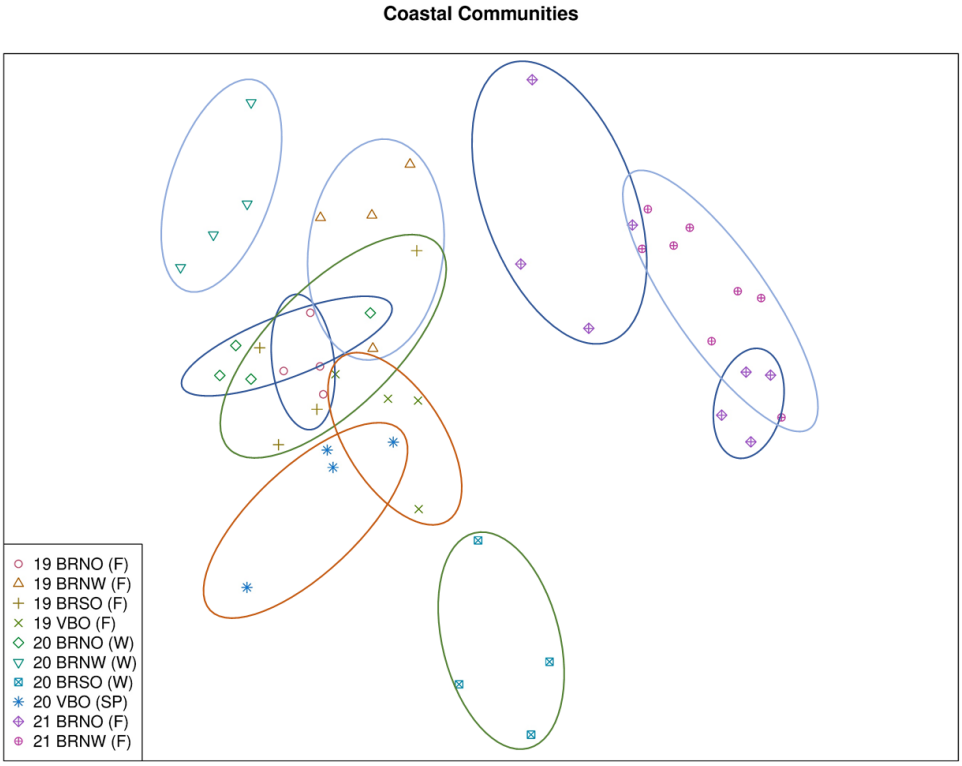

Figure 15: Coastal phytoplankton community similarities (closely associated plots) and differences (widely separated plots) via non-metric multidimensional scaling (NMDS). Coastal sites include BRNO (grouped by dark blue ellipses), BRNW (grouped by light blue ellipses), BRSO (grouped by green ellipses), and VBO (grouped by orange ellipses). Sampling occurred in fall (F), winter (W), spring (Sp), and summer (S) from 2019-2021.

from their respective community structures in 2019. To the contrary, BRNO and VBO did not significantly shift community structure between 2019 and 2020. By the fall of 2021, BRNO and BRNW communities were distinct from their respective communities in 2019 and 2020, but they were relatively similar to each other (Figure 15). Ordinating IRL and coastal sites together showed a fair degree of separation with some overlap between communities (ANOSIM-R = 0.85, $p<0.01$),

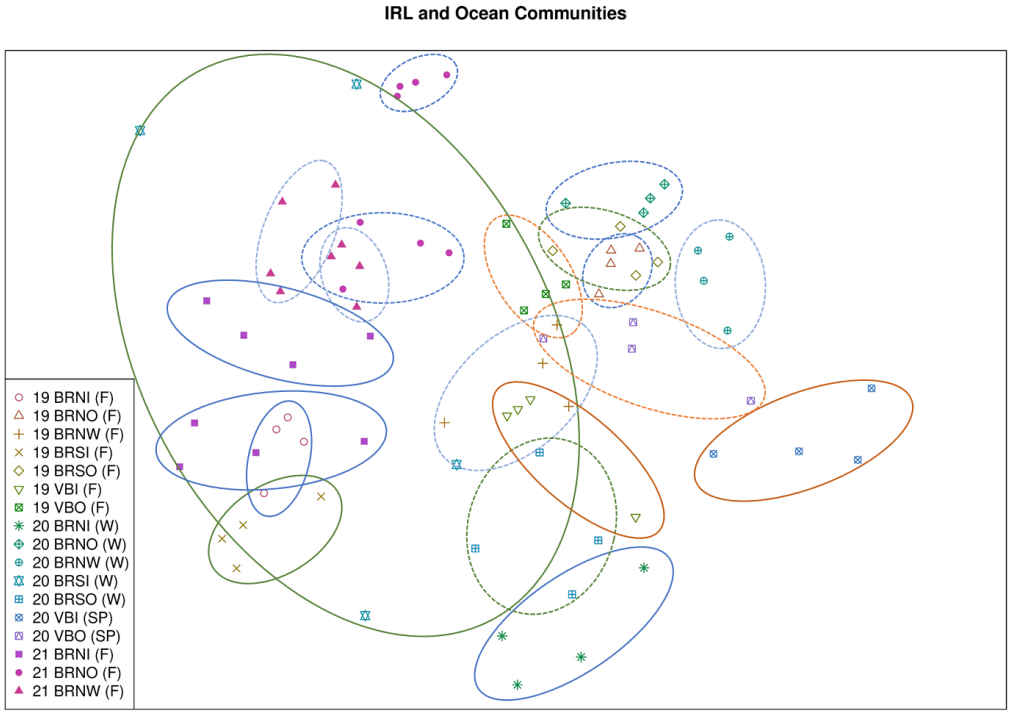

Figure 16: Estuarine and coastal phytoplankton community similarities (closely associated plots) and differences (widely separated plots) via non-metric multidimensional scaling (NMDS). Estuarine sites include BRNI (grouped by blue ellipses), BRSI (grouped by green ellipses), and VBI (grouped by orange ellipses). Coastal sites include BRNO (grouped by dark blue ellipses), BRNW (grouped by light blue ellipses), BRSO (grouped by green ellipses), and VBO (grouped by orange ellipses). Sampling occurred in fall (F), winter (W), spring (Sp), and summer (S) from 2019-2021.

and separating the data by site explained 72.8% of the variation in phytoplankton communities in the IRL and coastal ocean ($p<0.01$) (Figure 16).

BIODIVERSITY, RICHNESS, AND EVENNESS

Shannon-Wiener diversity, species richness, and species evenness were compared between IRL and coastal sampling stations within BRN, BRS, and VB. Diversity across all sites in the IRL was 1.02 ± 0.07, whereas coastal ocean diversity was 1.77 ± 0.08 (Figure 17). Thus, diversity was significantly higher in the coastal ocean ($p<0.001$). Species richness and evenness followed a similar trend with significantly higher richness and evenness in the coastal ocean ($p<0.001$) (Figure 18 & 19). Comparing diversity, species richness, and species evenness

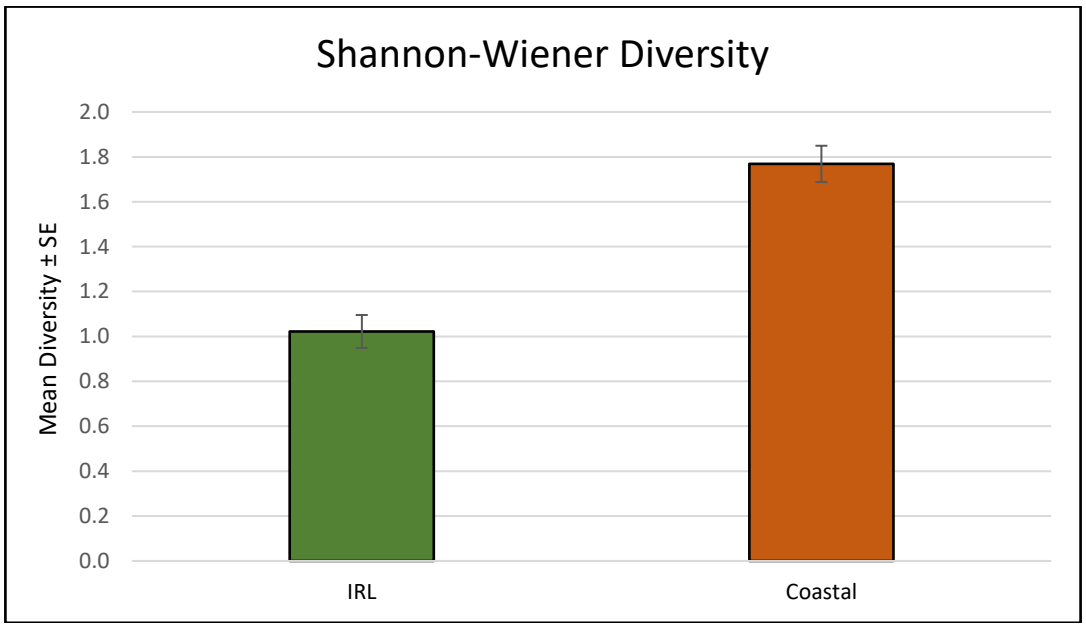

Figure 17 Mean Shannon-Wiener Diversity (±1SE) of the phytoplankton communities in the IRL (green bars) and coastal ocean (orange bars). Shannon-Wiener Diversity was significantly higher in the coastal ocean ($p<0.001$).

between coastal and IRL stations on finer spatial and temporal scales generally yielded similar findings of higher diversity, richness, and evenness in the coastal ocean. However, there are some instances of the opposite being true. In the case of VB during fall of 2019, diversity at IRL stations (1.94 ± 0.06) was statistically indistinguishable from coastal stations (1.71 ± 0.10) ($p>0.05$). However, not all differences in mean diversity were significant (Figure 20). Species richness was higher in all coastal stations across all sites and seasons sampled, but there were four instances of non-significant differences in species richness between IRL and coastal stations (Figure 21).

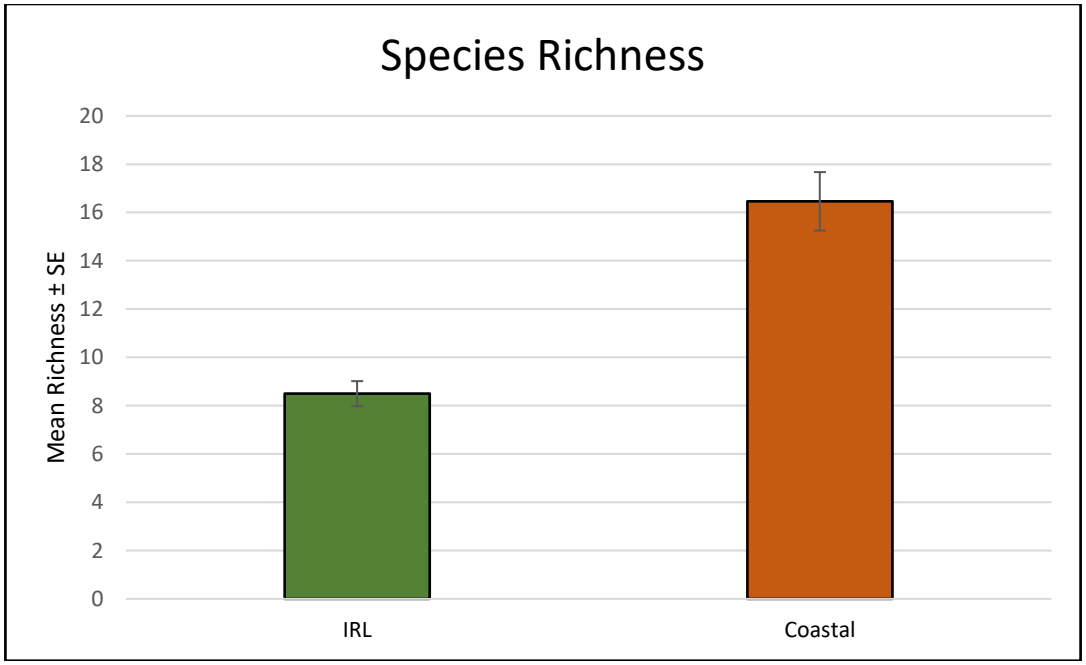

Figure 18: Mean species richness (±1SE) of the phytoplankton communities in the IRL (green bars) and coastal ocean (orange bars). Species richness was significantly higher in the coastal ocean ($p<0.001$).

Species richness was not statistically different between the IRL and coastal stations at BRS in 2020 ($p>0.05$). Similarly, species richness between BRNI and BRNW in the first sampling set of 2021, as well as between both coastal sites and BRNI in the second sampling set of 2021, was not significantly different. However, in the winter of 2020, BNRI was significantly higher than BRNW but significantly lower than BRNO. Species evenness, which is dependent on species richness and the abundance of populations relative to the community, was overall significantly higher in the coastal ocean ($p<0.05$) (Figure 22).

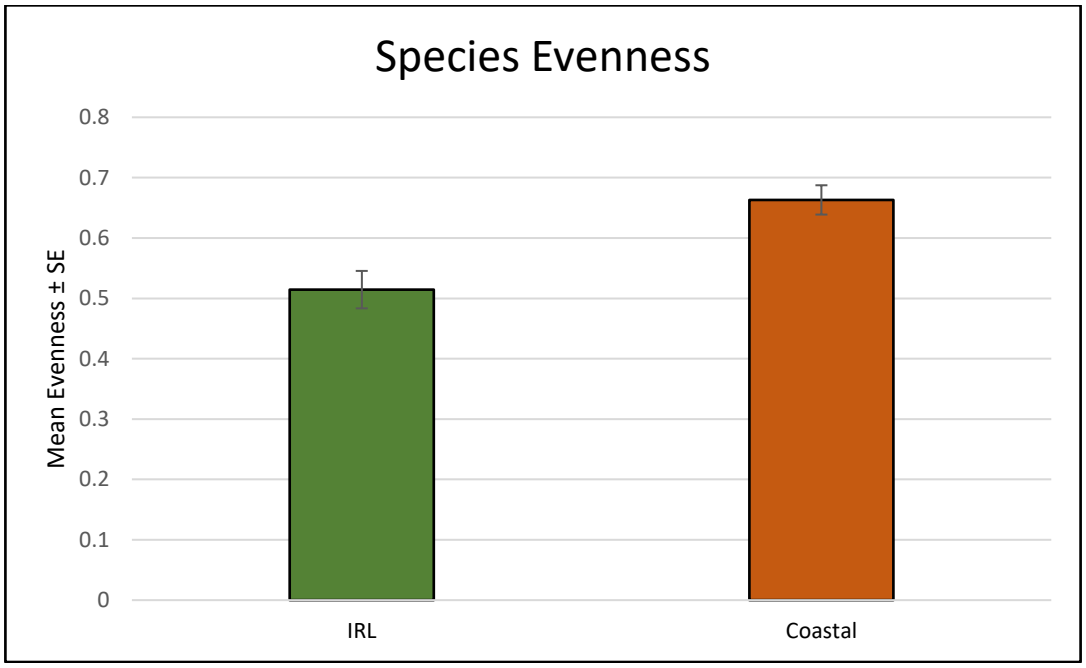

Figure 19: Mean species evenness (±1SE) of the phytoplankton communities in the IRL (green bars) and coastal ocean (orange bars). Species evenness was significantly higher in the coastal ocean ($p<0.001$).

On finer spatial and temporal scales, evenness was generally higher at coastal stations with some exceptions. In the fall of 2019, evenness was statistically

lower at VBO than in VBI ($p<0.05$), which deviated from the trend seen at BRN and BRS during that same period; in the winter of 2020, evenness at BRNW was statistically indistinguishable from BRNI, and evenness BRSO was similar to BRSI ($p>0.05$); in the spring of 2020, evenness at VBO was not different than evenness at VBI ($p>0.05$); and during the second sampling period in the fall of 2021, evenness at BRNW was not different than evenness at BRNI ($p>0.05$) (Figure 22).

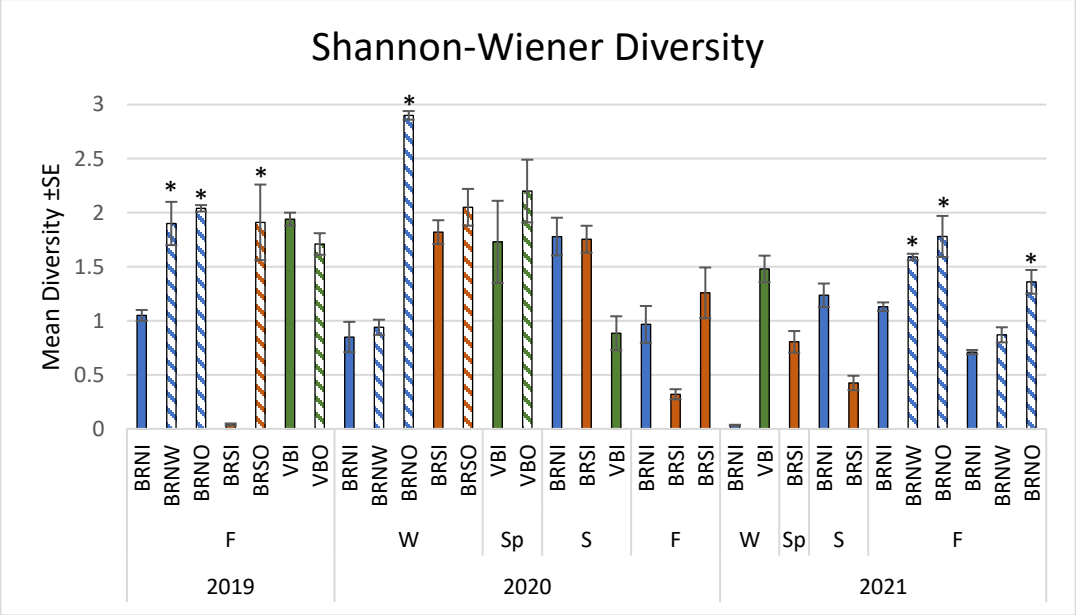

Figure 20: Mean Shannon-Wiener Diversity (±1SE) by location and season in the IRL (solid bars) and coastal zone (striped bars) from 2019-2021. Locations are Banana River North (BRN, blue bars), Banana River South (BRS, orange bars), and Vero Beach (VB, green bars). The seasons are Fall (F), Winter (W), Spring (Sp), and Summer (S). An asterisk above a coastal site indicates a significant difference between the coastal site and the corresponding IRL site during the same season and year.

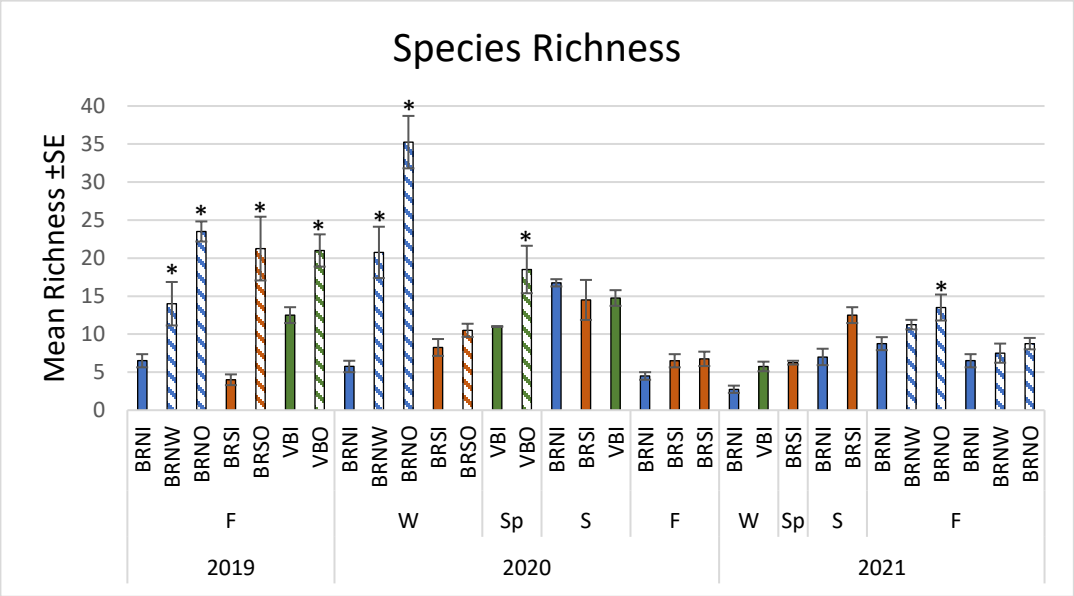

Figure 21: Mean species richness (±1SE) by location and season in the IRL (solid bars) and coastal zone (striped bars) from 2019-2021. Locations are Banana River North (BRN, blue bars), Banana River South (BRS, orange bars), and Vero Beach (VB, green bars). The seasons are Fall (F), Winter (W), Spring (Sp), and Summer (S). An asterisk above a coastal site indicates a significant difference between the coastal site and the corresponding IRL site during the same season and year.

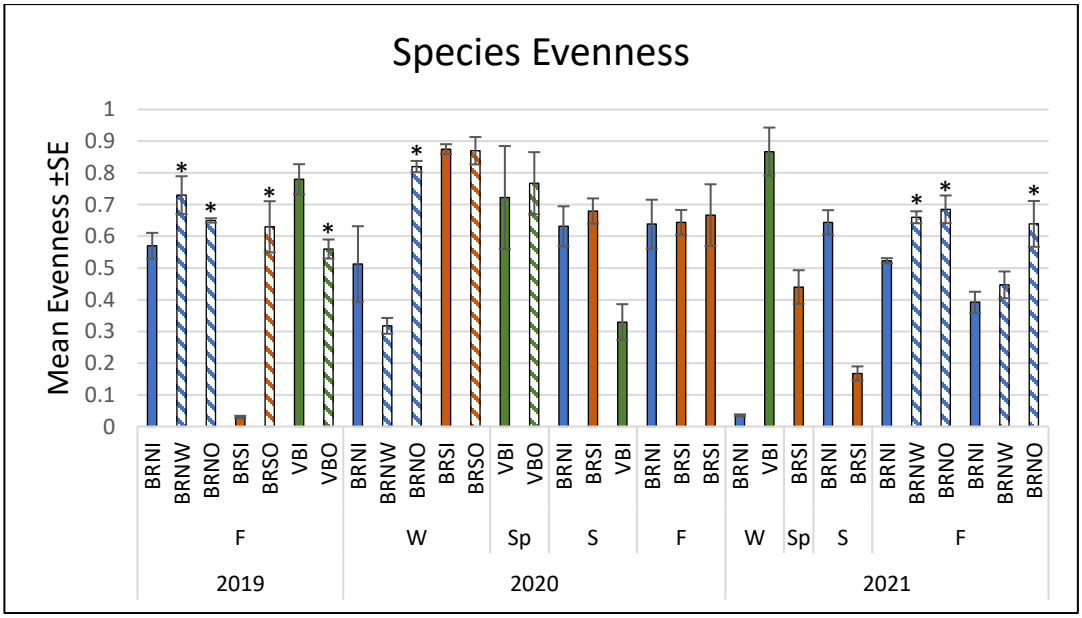

Figure 22: Mean species evenness (±1SE) by location and season in the IRL (solid bars) and coastal zone (striped bars) from 2019-2021. Locations are Banana River North (BRN, blue bars), Banana River South (BRS, orange bars), and Vero Beach

(VB, green bars). The seasons are Fall (F), Winter (W), Spring (Sp), and Summer (S). An asterisk above a coastal site indicates a significant difference between the coastal site and the corresponding IRL site during the same season and year.

ENVIRONMENT AND COMMUNITY

The BRN Nutrient PCA used temperature, salinity, DO, pH, ammonium (NH_4), nitrate (NO_3), Total Dissolved Nitrogen (TDN), Dissolved Inorganic Nitrogen (DIN), Dissolved Organic Nitrogen (DON), phosphate (PO_4), and Silica (Si) as environmental variables. The Environmental Parameters PCA and the BRN Nutrient PCA showed clear separation between IRL and coastal stations especially on the gradient of salinity (Figure 23). Principal components (PC) 1 and 2 of the Environmental Parameters PCA explained 68.5% of the variance in environmental variables. Temperature and pH explained 44% of the variance in PC1 while salinity

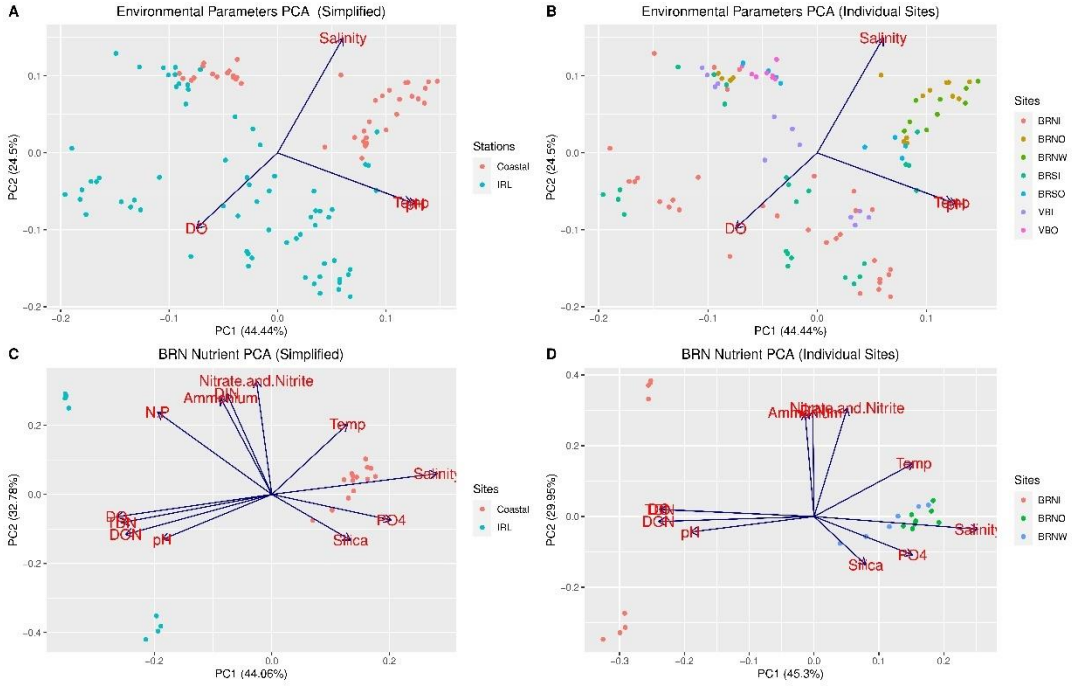

Figure 23: Principal Component Analyses for two sets of environmental data. A) Environmental factors focusing on IRL vs. coastal sites; B) Environmental

variables considering individual sites; C) Environmental variables and nutrients at BRN in the fall of 2021, focusing on IRL vs. coastal sites; D) Environmental variables and nutrients considering individual sites at BRN in the fall of 2021.

and DO explained 24.5% of the variance in PC2. Temperature and pH were directly related, whereas salinity and DO had an inverse relationship. For the BRN Nutrient PCA, PC1 and PC2 explained 75.3% of the variance in environmental factors. PC1 (Salinity, DO, TDN, and DON) accounted for 45.3% of the variation in environmental parameters and PC2 (NH_4, NO_3, and DIN) accounted for 30% of the variance in environmental conditions. Salinity was inversely related to DO, TDN, and DON in PC1, whereas NH_4, NO_3, and DIN all had direct relationships in PC2.

In the Environmental Parameter RDA, temperature, salinity, dissolved oxygen, and pH explained 23% of the variance in dominant phytoplankton populations in RDA1 through RDA4. Salinity accounted for the largest portion of variation in community data in RDA1 (11.6%) followed by dissolved oxygen (4.7%) in RDA2, pH (3.7%) in RDA3, and temperature (3%) in RDA4. Salinity and pH were positively correlated with the abundance of the diatoms *Cyclotella meneghiniana*, *Cylindrotheca closterium*, *Coscinodiscus* spp., *Skeletonema costatum*, and *Asterionellopsis glacialis* (Figure 24). The dinoflagellates *Pyrodinium bahamense*, *Ceratium* spp., *Gonyaulax* spp. *Prorocentrum* spp., and *Peridinium* spp. were positively related to temperature but negatively related to dissolved oxygen. The diatoms *Navicula* spp., *Amphora* spp., *Navicula* spp., *Nitzschia* spp., *Pleurosigma* spp., *Pseudo-nitzschia* sp., *Paralia sulcata*,

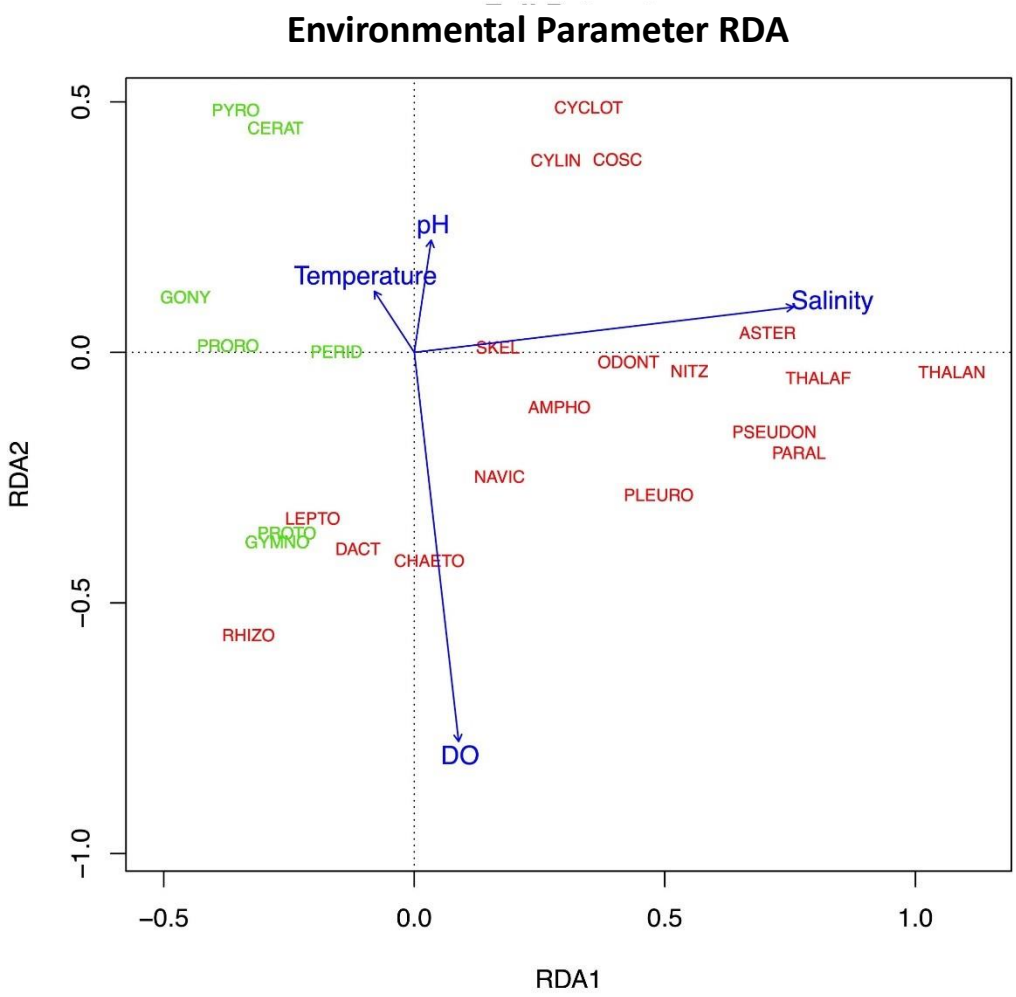

Figure 24: Redundancy analysis for IRL and coastal sites. Dinoflagellate taxa (green) and diatom taxa (red) are abbreviated as follows: NAVIC = *Navicula* spp., THALAF = *Thalassionema frauenfeldii*, THALAN = *Thalassionema nitzschoides* PARAL = *Paralia sulcata*, ODONT = *Odontella* spp., PLEURO = *Pleurosigma* spp., CYCLOT = *Cyclotella meneghiniana*, PSEUDON = *Pseudo-nitzschia* spp., DACT = *Dactyliosolen fragilissimus*, NITZ = *Nitzschia* spp., AMPHO = *Amphora* spp., CYLIN = *Cylindrotheca closterium*, ASTER = *Asterionellopsis glacialis*, COSC = *Coscinodiscus* spp., SKEL = *Skeletonema costatum*, RHIZO = *Rhizosolenia* spp., CHAETO = *Chaetoceros* spp., LEPTO = *Leptocylindrus danicus*, PERID = *Peridinium* sp., PROTO = *Protoperidinium* spp., GYMNO = *Gymnodinium* spp., GONY = *Gonyaulax* sp., CERAT = *Ceratium* spp., PYRO = *Pyrodinium bahamense*, and PRORO = *Prorocentrum* spp. Blue arrows represent environmental parameters. Environmental parameter arrows pointing towards phytoplankton in a quadrant indicate a positive association, whereas environmental parameters pointing away indicate an inverse association.

Thalassionema nitzschoides, and *Thalassionema frauenfeldii* were positively related to dissolved oxygen and negatively related to temperature. *Leptocylindrus danicus*, *Dactyliosolen fragilissimus*, *Rhizosolenia* spp., *Protoperidinium* spp., and *Gymnodinium* spp. were not strongly associated with any of these variables.

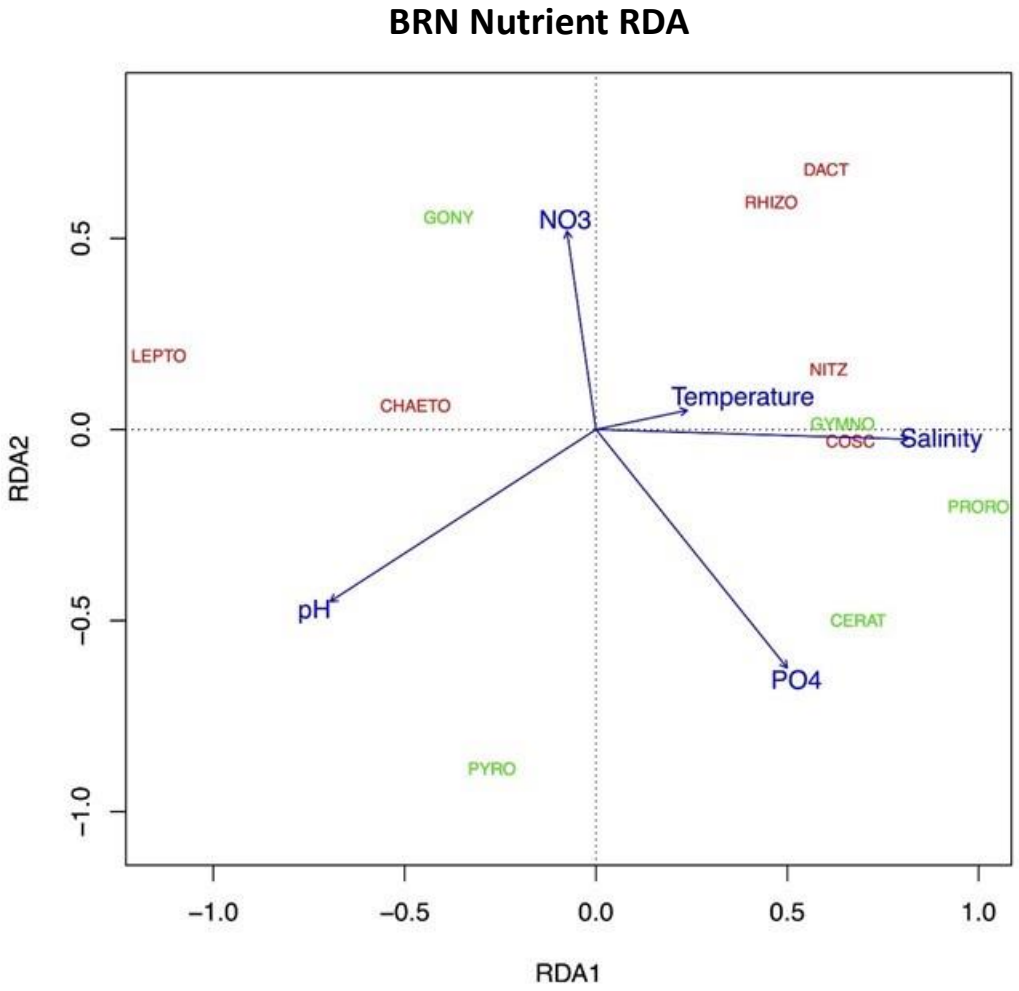

Figure 25: Redundancy analysis using environmental data and dominant phytoplankton collected at BRN. Dinoflagellate taxa (green) and diatom taxa (red) are abbreviated as follows: NITZ = *Nitzschia* spp., DACT = *Dactyliosolen fragilissimus*, COSC = *Coscinodiscus* spp., RHIZO = *Rhizosolenia* spp., CHAETO = *Chaetoceros* spp., LEPTO = *Leptocylindrus danicus*, GYMNO = *Gymnodinium* spp., GONY = *Gonyaulax* sp., CERAT = *Ceratium* spp., PYRO = *Pyrodinium bahamense*, and PRORO = *Prorocentrum* spp.

Temperature, salinity, pH, nitrate, and phosphate accounted for 56.2% of the variation in dominant phytoplankton populations in the BRN Nutrient RDA. Salinity accounted for the majority of variation (31.6%) in RDA1 followed by phosphate (14.3%) in RDA2, temperature (6.4%) in RDA3, and nitrate (3.9%) in RDA4. *Nitzschia* spp., *Rhizosolenia* spp., *Dactyliosolen fragilissimus*, and *Gymnodinium* spp. were positively related to temperature and negatively related to pH (Figure 25). *Pyrodinium bahamense* was positively associated with pH and negatively associated with temperature. *Gonyaulax* spp., *Chaetoceros* spp., and *Leptocylindrus danicus* were positively related to nitrate levels but negatively related to salinity and phosphate, whereas *Ceratium* spp., *Prorocentrum* spp., and *Coscinodiscus* spp. were positively associated with phosphate and salinity and negatively associated with nitrate. These relationships are also evidenced through dominant taxa densities at minima and maxima for environmental parameters (Table 8).

Temperature, salinity, dissolved oxygen, and pH accounted for only 28% of the variation in dominant phytoplankton between IRL sites. Salinity accounted for the majority of variation in dominant IRL phytoplankton (12%) in RDA1 followed by dissolved oxygen (8%) in RDA2, temperature (5%) in RDA3, and pH (3%) in RDA4. *Nitzschia* spp. and *Coscinodiscus* spp. were positively associated with salinity and inversely associated with temperature and pH (Figure 26). Conversely, *Prorocentrum* spp. was positively associated with temperature and pH and inversely associated with salinity. *Protoperidinium* spp., *Rhizosolenia* spp.,

Table 8: Densities of dominant phytoplankton at BRN in the fall of 2021 based on minimum and maximum environmental parameters. The "Min" columns are densities of dominant phytoplankton at the lowest recorded value for an environmental parameter. The "Max" columns are densities of dominant phytoplankton at the highest recorded value for an environmental parameter. Environmental parameters included temperature (range: 26.6-28.5°C), salinity (range: 16.82-36.39 PSU), nitrate (range: 2.7-40.9 μgL^{-1}), phosphate (range: 1.26-14.37 μgL^{-1}), and pH (range: 8.03-9.21).

Phytoplankton	Temperature		Salinity		Nitrate		Phosphate		pH	
	Min	Max	Min	Max	Min	Max	Min	Max	Min	Max
Leptocylindrus danicus	812	16	10568	85	812	11746	10568	85	0	393
Chaetoceros spp.	191	390	4902	149	191	2419	4902	149	0	202
Prorocentrum spp.	16	294	0	891	16	0	0	891	573	21
Pyrodinium bahamense	1592	24	0	764	1592	0	0	764	0	1082
Ceratium spp.	32	24	64	53	32	0	64	53	8	32
Rhizosolenia spp.	0	0	255	0	0	64	255	0	80	0
Gymnodinium spp.	0	0	0	212	0	0	0	212	64	0
Coscinodiscus spp.	16	8	0	42	16	32	0	42	16	0
Dactyliosolen fragilissimus	0	0	0	0	0	0	0	0	708	0
Gonyaulax sp.	0	8	95	0	0	318	95	0	0	0
Nitzschia spp.	0	24	0	11	0	0	0	11	24	11

Chaetoceros spp., and *Pleurosigma* spp. were positively associated with DO. Dissolved oxygen, temperature, pH, and salinity accounted for 33% of the variation in the dominant coastal phytoplankton (Figure 27). Dissolved oxygen accounted for the majority of variation (18%) in RDA1 followed by pH (8%) in RDA2, temperature (6%) in RDA3, and salinity (1%) in RDA4. *Cylindrotheca closterium*, *Guinardia striata*, *Chaetoceros* spp., *Pseudo-nitzschia* spp., *Rhizosolenia* spp., *Thalassionema frauenfeldii*, and *Nitzschia* spp. were positively associated with dissolved oxygen and salinity and inversely associated with pH. *Leptocylindrus danicus*, *Cyclotella meneghiniana*, and *Pyrodinium bahamense* were positively associated with pH and inversely associated with salinity and dissolved oxygen. *Prorocentrum* spp., *Gymnodinium* spp., *Ceratium* spp., and *Dactyliosolen fragilissimus* were positively associated with temperature. Nutrients showed no

associations with dominant phytoplankton in the IRL or coastal ocean due to limited sample size.

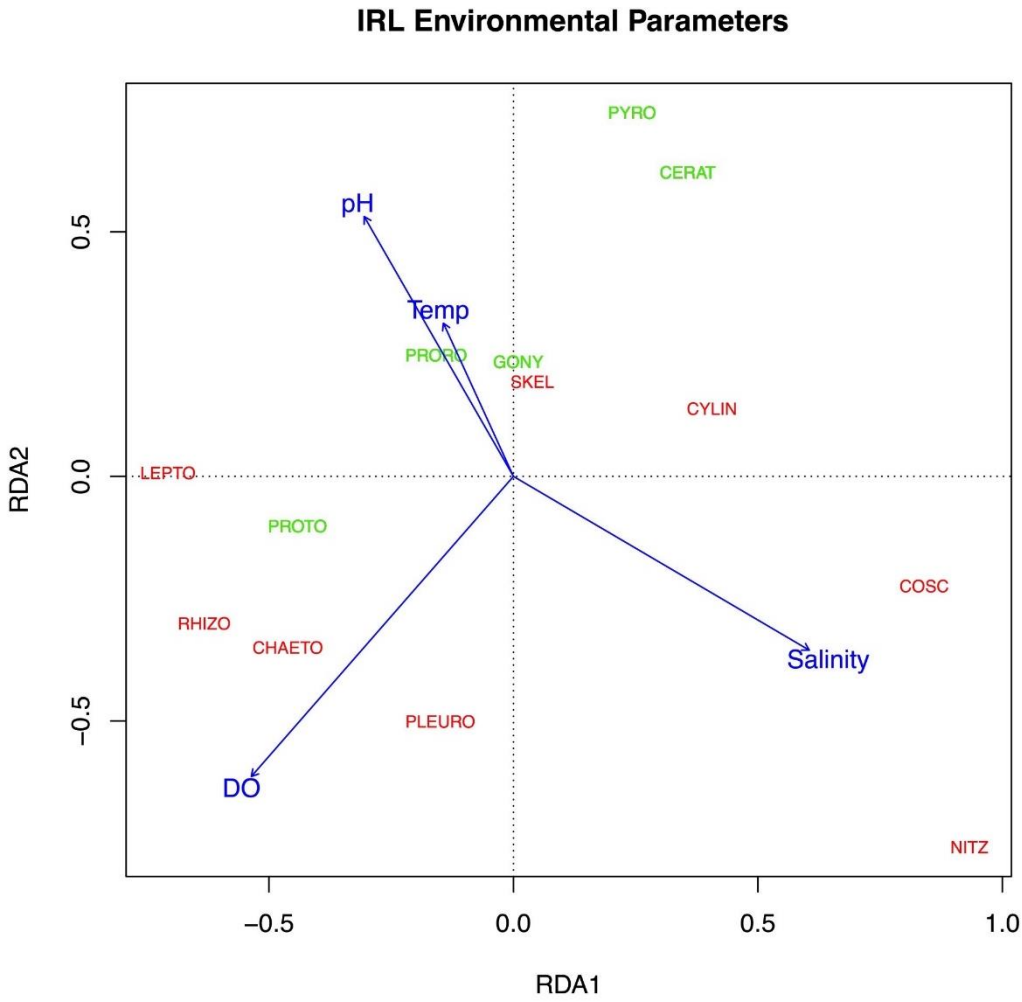

Figure 26: Redundancy analysis using environmental data and dominant phytoplankton collected in the IRL. Dinoflagellate taxa (green) and diatom taxa (red) are abbreviated as follows: LEPTO = *Leptocylindrus danicus*, PRORO = *Prorocentrum* spp., GONY = *Gonyaulax* sp., SKEL = *Skeletonema costatum*, PYRO = *Pyrodinium bahamense*, CERAT = *Ceratium* spp., CYLIN = *Cylindrotheca closterium*, NITZ = *Nitzschia* spp., COSC = *Coscinodiscus* spp., CHAETO = *Chaetoceros* spp., RHIZO = *Rhizosolenia* spp., PROTO = *Protoperidinium* spp., and PLEURO = *Pleurosigma* spp.

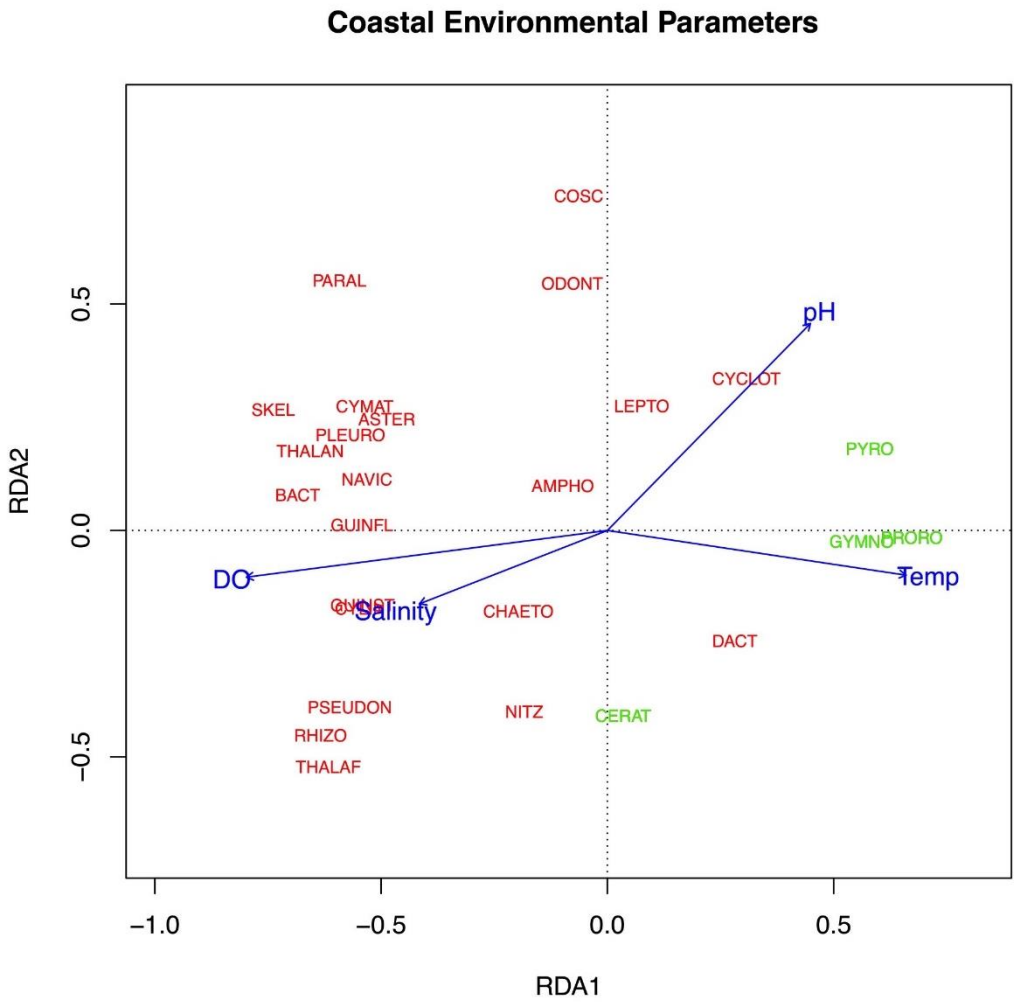

Figure 27: Redundancy analysis using environmental data and dominant phytoplankton collected in the coastal ocean. Dinoflagellate taxa (green) and diatom taxa (red) are abbreviated as follows: NAVIC = *Navicula* spp., COSC = *Coscinodiscus* spp., SKEL = *Skeletonema costatum*, RHIZO = *Rhizosolenia* spp., CHAETO = *Chaetoceros* spp., LEPTO = *Leptocylindrus danicus*, THALAF = *Thalassionema frauenfeldii*, THALAN = *Thalassionema nitzschoides* PARAL = *Paralia sulcata*, ODONT = *Odontella* spp., PLEURO = *Pleurosigma* spp., CYCLOT = *Cyclotella meneghiniana*, PSEUDON = *Pseudo-nitzschia* spp., DACT = *Dactyliosolen fragilissimus*, NITZ = *Nitzschia* spp., AMPHO = *Amphora* spp., CYLIN = *Cylindrotheca closterium*, ASTER = *Asterionellopsis glacialis*, CERAT = *Ceratium* spp., PYRO = *Pyrodinium bahamense*, GYMNO = *Gymnodinium* spp., PRORO = *Prorocentrum* spp., GUINST = *Guinardia striata*, GUINFL = *Guinardia flaccida*, CYMAT = *Cymatosira belgica*, and BACT = *Bacteriastrum* spp.

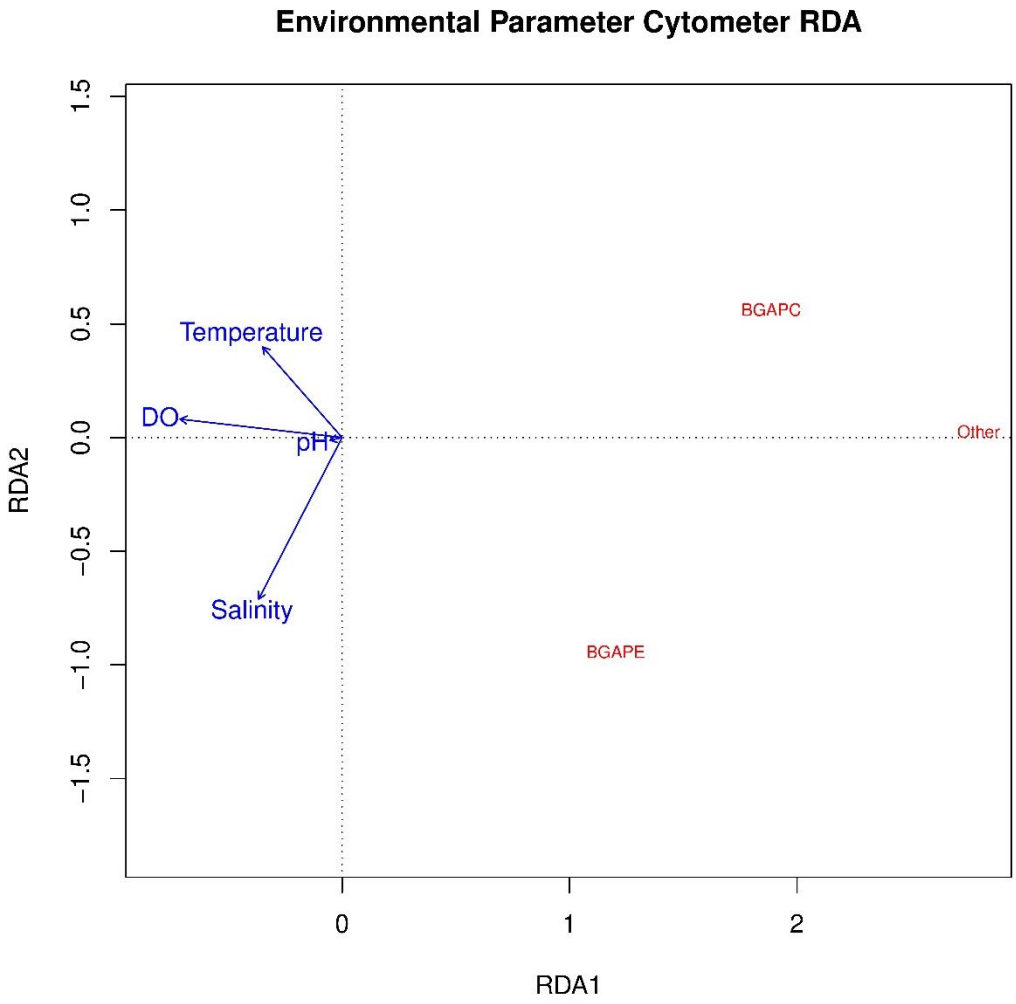

Figure 28: Redundancy analyses using environmental variables across IRL and coastal sites to determine influences on cyanobacteria and non-cyanobacteria phytoplankton.

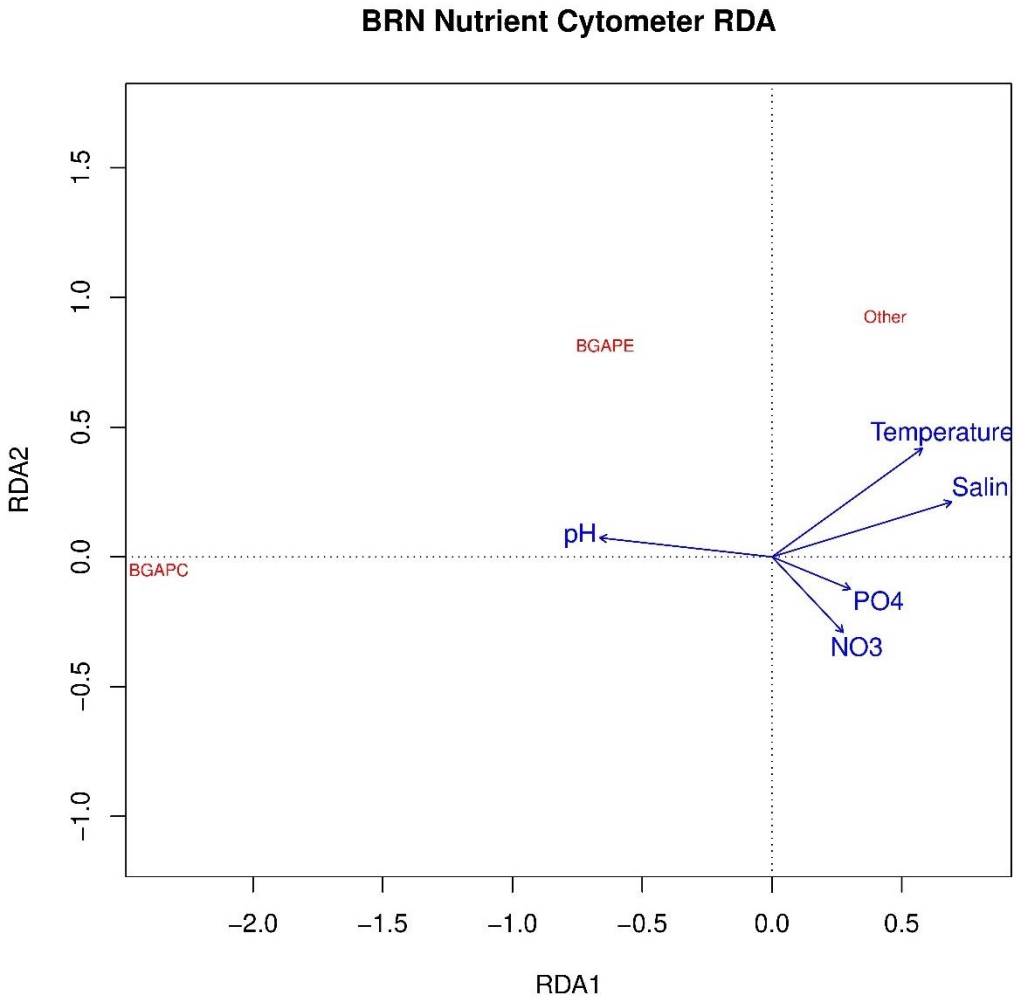

Figure 29: Redundancy analyses using environmental variables and nutrients across IRL and coastal sites at BRN to determine influences on cyanobacteria and non-cyanobacteria phytoplankton.

RDA was also used to determine environmental links between BGAPC, BGAPE, and other (non-cyanobacteria) phytoplankton. The first RDA used temperature, salinity, DO, and pH data from all sites and seasons, yet yielded no relationships with any phytoplankton group sampled (Figure 28). For the RDA that utilized the limited nutrient dataset, salinity and pH (35.2%), temperature (8.7%), and phosphate (<1%) accounted for 43.9% of the variation in cyanobacteria and

other phytoplankton densities (Figure 29). The non-cyanobacteria plankton were positively related to temperature and salinity. BGAPE were positively related to pH, but negatively related to PO_4 and NO_3. BGAPC yielded no relationships with any parameter tested (Figure 29).

CYANOHAB AND ENVIRONMENTAL FACTORS

In mid to late 2020, a cyanobacteria species with strong phycocyanin pigmentation (similar to many species in the Synechococcaceae family of cyanobacteria) dominated the water column (Figure 30). The cyanobacteria rapidly grew in July through September in many parts of the IRL and BRL but reached a plateau in density around 4 to $5.5x10^6$ cells mL^{-1} until subsiding in December.

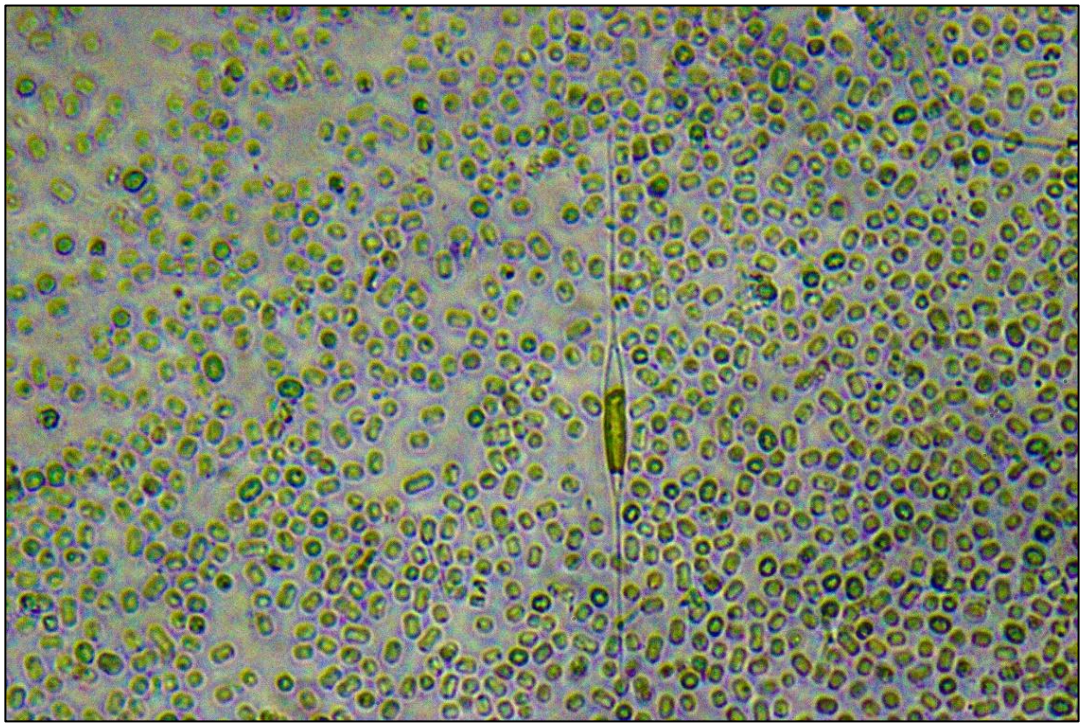

Figure 30: Unidentified cyanobacteria surrounding a single cell of the diatom *Cylindrotheca closterium*. Approximate cell size was 3-5µm.

The bloom likely originated in the Northern portion of the IRL proper (near Merritt Island) and progressed Eastward to the Northern BRL and Southward to the Southern BRL and IRL Proper. However, the progression and spread of the cyanobacteria growth was patchy, inconsistent, and difficult to project beyond a Southward expansion (Figure 31). BGAPC abundances were generally low in the

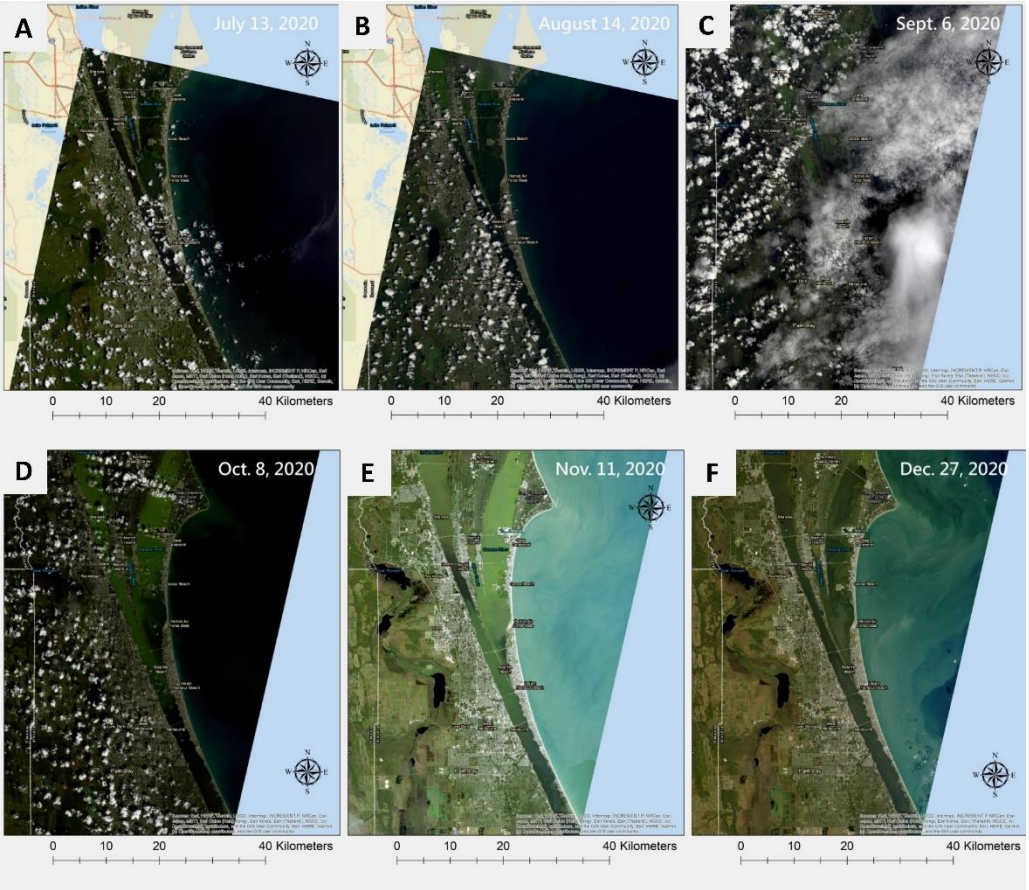

Figure 31: Landsat imagery of the progression of the CyanoHAB in the IRL proper and BRL every month from July to December of 2020. A) No obvious water discoloration in the IRL; B) Green discoloration becoming apparent in the far north IRL and BRL; C) Southward spread of the cyanobacteria to the southern IRL proper; D) A widespread and patchy cyanobacteria bloom that spans most of the Northern IRL proper and BRL; E) The spread and intensification of the cyanobacteria bloom with some patchiness; and F) Minimal water discoloration suggesting the cyanobacteria were no longer blooming.

IRL and coastal ocean. However, the cyanobacteria growth observed in 2020 reached densities as high as $5.87x10^6$ cells mL^{-1} and persisted for several months.

BGAPC densities in the northern BRL in July of 2020 were higher than earlier densities by two orders of magnitude, and the bloom continued to grow between July and November 2020. Therefore, it is inferred that the proliferation of cyanobacteria containing phycocyanin in the Northern BRL began blooming at the end of July or during August and continued exponential growth. Observed densities started at $4.58x10^5$ ± 52,987 cells mL^{-1} on July 30th and increased to $2.08x10^6$ ± 27,195 cells mL^{-1} by September 18th (an observed 353% increase in BGAPC density over a 50 day period) (Figure 32). One week later on September 25th, BGAPC densities increased by 87% to $3.9x10^6$ ± 25,458 cells mL^{-1} and plateaued near that density for at least 75 days until November 11th. No additional data were collected beyond November 11th and the subsidence of the bloom, presumed to have been in December, was not captured via flow cytometry. In the southern portion of the BRL, BGAPC density remained an order of magnitude lower than in the Northern BRL. On September 18th, BGAPC densities were $3.11x10^5$ ± 10,479 cells mL^{-1} and increased to $4.71x10^5$ ± 24,404 cells mL^{-1} one week later. By October 2nd, the BGAPC densities had dropped back to $2.05x10^5$ ± 75,590 cells mL^{-1}, but then rallied through October 21st to $4.62x10^5$ ± 54,194 cells mL^{-1}. Densities then crashed to $1.42x10^4$ ± 2,621 cells mL^{-1} by November 6th, but then surged to $6.23x10^5$ ± 31,703 cells mL^{-1} on November 11th. This sudden decrease and increase in BGAPC density may be a result of patchy bloom transport around

the lagoon, with the high density water mass moving away from, and then back to, the sampling site.

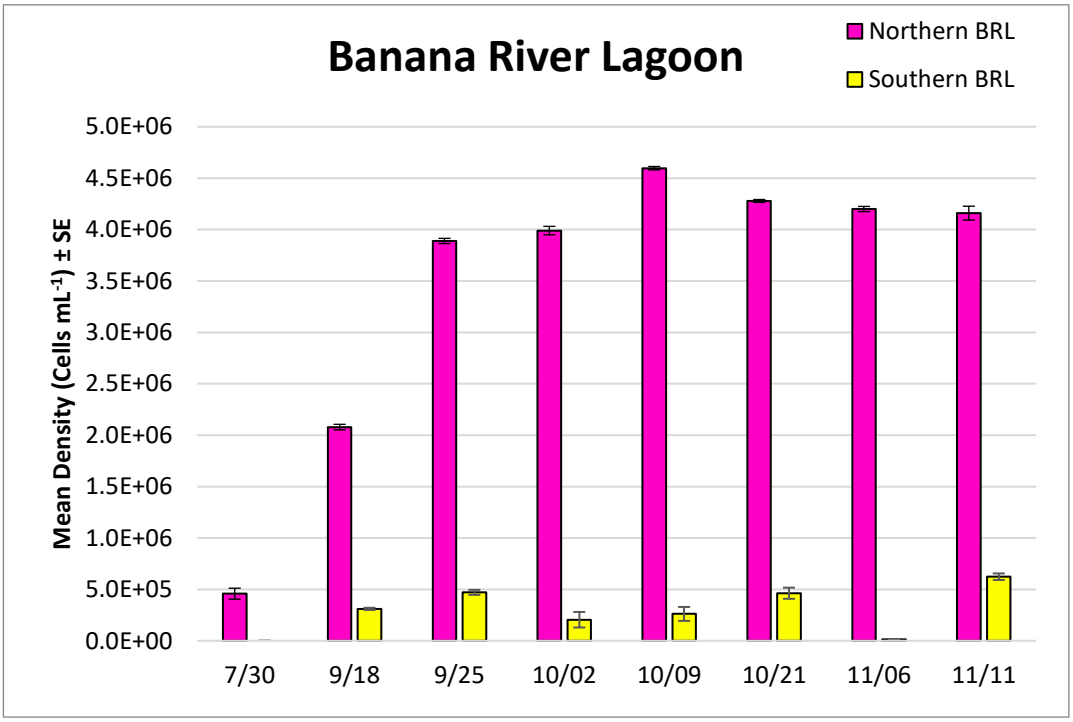

Figure 32: Mean BGAPC densities (±1SE) in the northern BRL (pink) and southern BRL (yellow). No data was collected in the southern BRL on July 30th, 2020.

BGAPC densities in the IRL proper varied spatially (Figure 33). Densities in the IRL proper near Titusville remained under 1.5 and $2.7x10^6$ cells mL^{-1} from September to November with no apparent exponential growth period (Figure 32). In the IRL Proper near North Merritt Island, BGAPC densities remaining around $4.5x10^6$ cells mL^{-1} until November where they exhibited a slight decline to $3.46x10^6 \pm 16{,}547$ cells mL^{-1}.

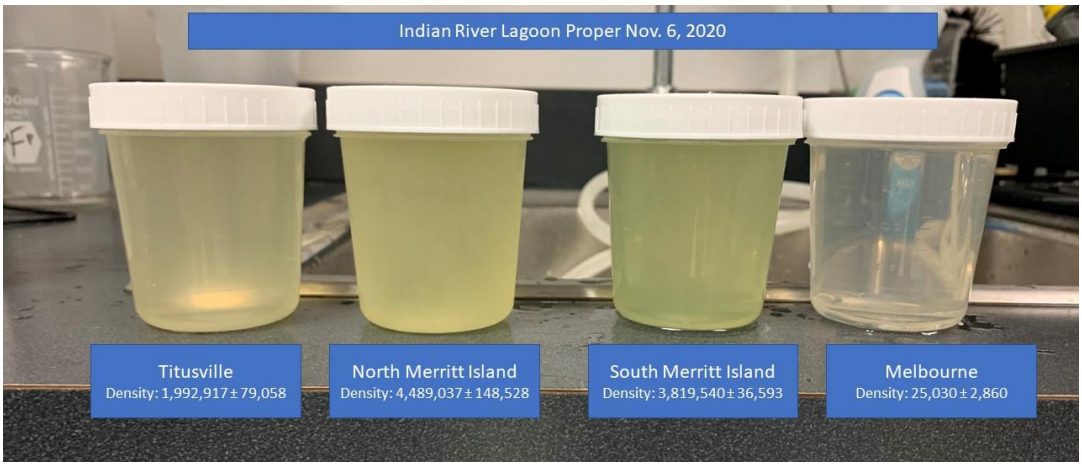

Figure 33: Whole water samples with coloration and opacity representing BGAPC densities (cells mL^{-1}) on November 6th, 2020 from the north to south (from left to right: northern IRL to the southern IRL). Water discoloration is apparent from Titusville to South Merritt Island, but not in Melbourne.

This slight decrease in density may have been the beginning of the bloom's decline. BGAPC densities in the IRL Proper near south Merritt Island appears to have exhibited all three stages of a bloom, with background-level densities in September, a sharp growth period from late September to October reaching a peak abundance of $4.59x10^6 \pm 49{,}202$ cells mL^{-1}, and then a hint of decline at the last sampling in mid-November. The BGAPC densities at the southernmost site in the IRL Proper (Melbourne) usually remained at or below $2x10^5$ cells mL^{-1}, but a sharp rise and decline in density ($8.99x10^5 \pm 136{,}954$ cells mL^{-1}) was observed from September to October (Figure 34).

The northern BRL bloom began subsiding in late November to early December, dissipating almost entirely by late December.

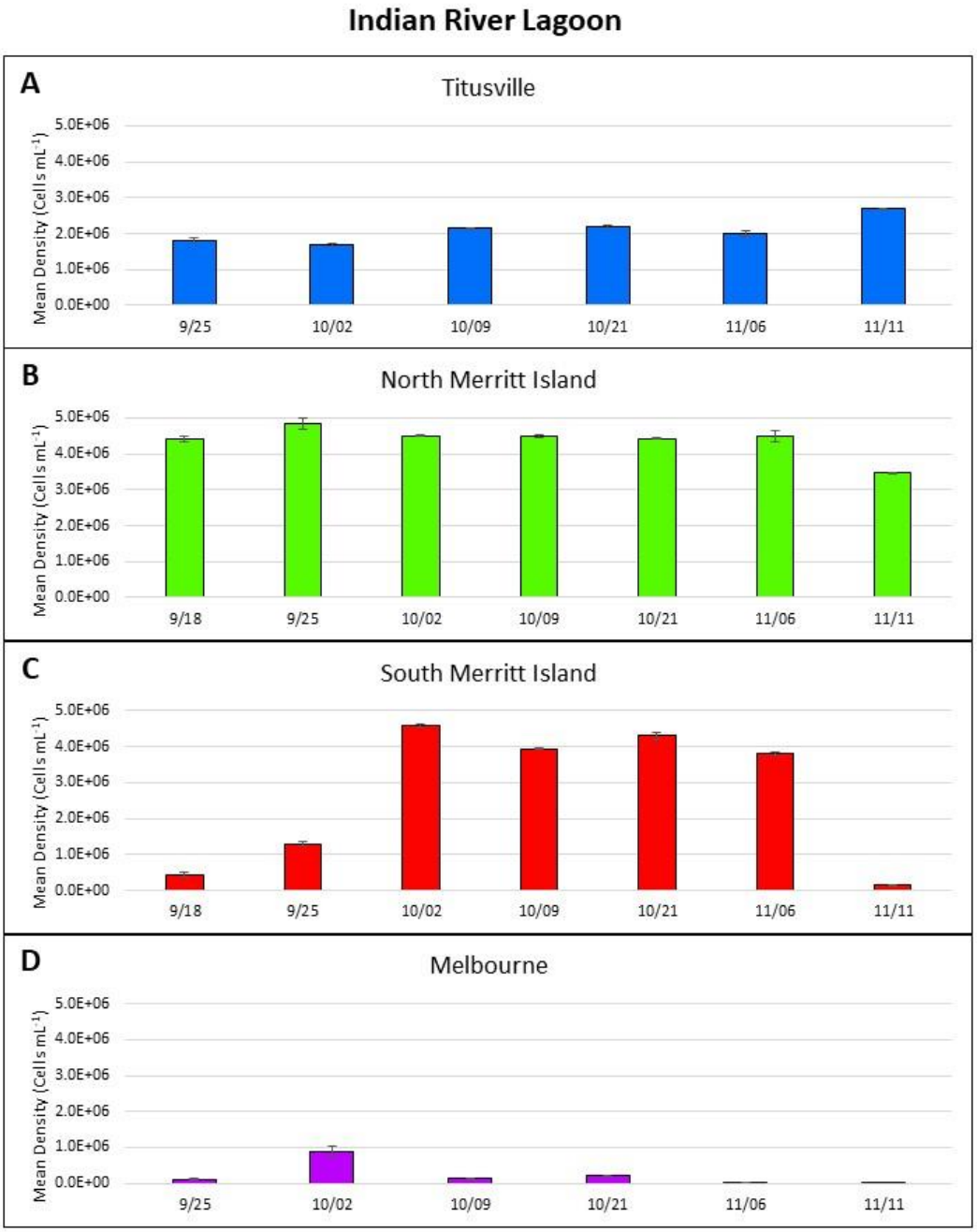

Figure 34: Mean cyanobacteria densities (±1SE) in four regions of the IRL proper, sampled biweekly from September 25th – November 11th, 2020. IRL regions were, from north to south, A) Titusville, B) north Merritt Island, C) south Merritt Island, and D) Melbourne.

To test this, turbidity and chlorophyll data from the Saint John's River Water Management District's Continuous Water Quality Monitoring Portal (SJRWMD) were tested for viability as a proxy for BGAPC density via simple linear regression. The turbidity and BGAPC density yielded a strong, significant relationship (R^2 = 0.71, p<0.001) and chlorophyll yielded no association with BGAPC (R^2 = 0.062, p<0.001) (Figure 35). Based on the stronger relationship between turbidity and BGAPC density, turbidity was used as a proxy for BGAPC densities.

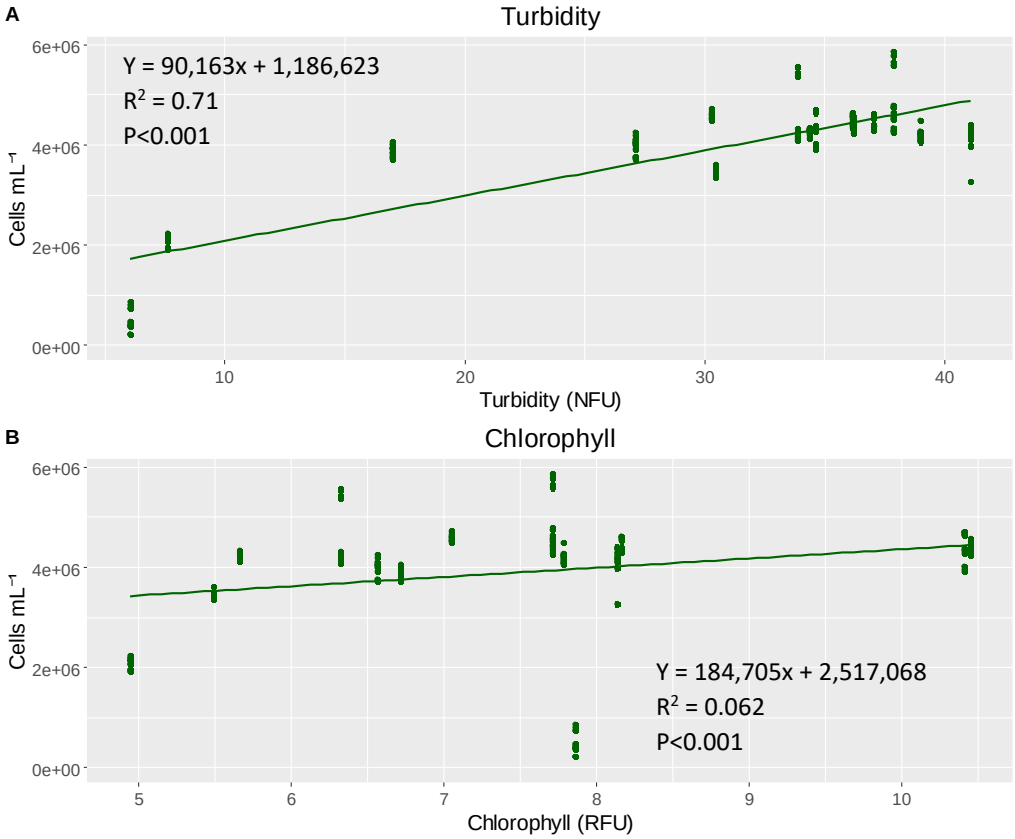

Figure 35: Linear regressions of BGAPC densities (cells mL^{-1}) against A) turbidity and B) chlorophyll during the CyanoHAB. The linear models, r^2 values, and significances are reported in the graph's fields, respectively.

To demonstrate the growth, climax, and decline of the CyanoHAB beyond November 11th, regional turbidity was plotted over time (Figure 36). In the northern IRL, turbidity began rapidly increasing in July, climaxing in early October, and then declining from October to December. We therefore infer that, in the northern BRL, after BGAPC bloomed and plateaued, it declined from October to December. The progression of the CyanoHAB in the Northern IRL was fairly symmetrical, meaning the rate of decline mirrored the rate of the bloom's increase, whereas the CyanoHAB in the BRL took longer to start increasing, leading to staggered population growth curves for the two groups (Figure 36). The delay of bloom increase in the BRL suggests the CyanoHAB began in the Northern IRL, and then spread to the Northern BRL.

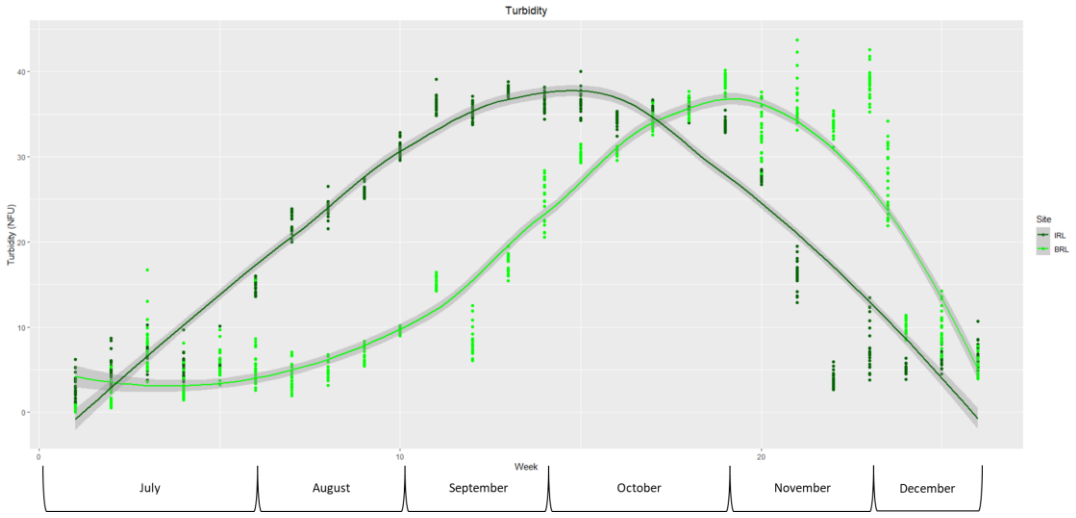

Figure 36: Turbidity (Nephelometric Formazin Units or NFU) measurements over time in the Northern IRL (dark green) and BRL (light green) near Northern Merritt Island during the development and decline of the CyanoHAB bloom (July-December, 2020).

Temperature, salinity, dissolved oxygen, and pH were collected alongside BGAPC samples to examine potential environmental links between these parameters and algal densities. BGAPC during the CyanoHAB did not have significant correlations with temperature, salinity, or ammonium ($p>0.05$) (Figure 37). However, BGAPC did have significant relationships with dissolved oxygen, pH, chlorophyll, silica, phosphate, and nitrate ($p<0.05$). BGAPC had the strongest relationship with chlorophyll ($R^2=0.91$), silica ($R^2=0.87$), phosphate ($R^2=0.22$), pH ($R^2=0.22$), and nitrate ($R^2=0.11$). Multiple linear regression indicated temperature, nitrate, and phosphate were the most influential variables during the CyanoHAB and yielded the fitted regression model: BGAPC = 253,833.5*(Temperature) + 254,459,145.6*(Nitrate) + 101,637,009.5*(Phosphate) + 8,726,565.2 ($R^2_{adj}=0.9$, $p < 2.2x10^{-16}$).

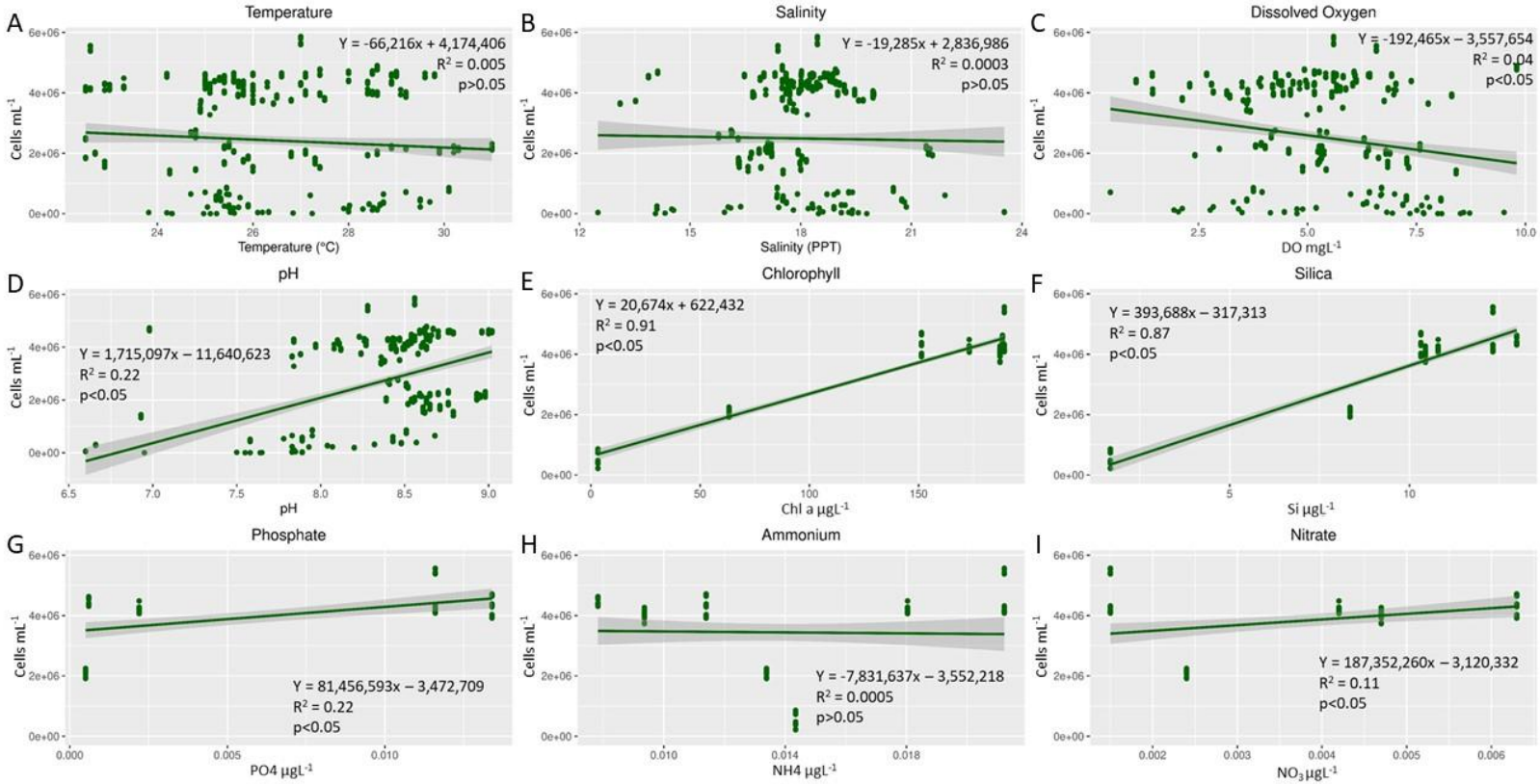

Figure 37: Linear regressions of BGAPC densities (cells ml^{-1}) from all sites in the IRL against various environmental and nutrient parameters, including A) temperature, B) salinity, C) dissolved oxygen, D) pH, E) chlorophyll, F) silica, G) phosphate, H) Ammonium, and I) Nitrate. Displayed on each plot is the linear model, regression coefficient, and significance value.

CHAPTER 4
DISCUSSION

DIATOMS AND DINOFLAGELLATES

This study represents a baseline comparison of phytoplankton community structure and diversity, environmental drivers, and community shifts between and within the Indian River Lagoon (IRL) estuary and the coastal Atlantic Ocean. There are, however, few other studies that compare phytoplankton communities and environmental drivers between estuaries and coastal waters in tandem, but they tend to focus on other factors that contribute to differences in estuarine and coastal phytoplankton communities. For example, O'Boyle and Silke (2010) reviewed the physical processes that influenced coastal and estuarine phytoplankton communities in Ireland. They determined that coastal phytoplankton assemblages and biomass were primarily influenced by seasonal stabilization and destabilization of the water column, tidal/thermohaline fronts, wind and coastal upwelling, advection of oceanic water masses landward, and currents while estuarine phytoplankton communities were influenced by the periodic ebb and flood of the tides and episodic shifts in riverine discharge. The review emphasized that physical processes play a crucial role in shaping phytoplankton assemblages, but the major shortcomings of this research, highlighted by the authors, were the lack of data regarding competition between phytoplankton for resources (*e.g.* nutrients) and the influence of other bloom controllers (*e.g.* zooplankton grazing). There is also limited spatial/temporal comparisons between estuarine and coastal phytoplankton

communities and environmental regimes (*i.e.* bloom controllers) for the IRL. This study documents the phytoplankton species and abundances in the IRL estuary and corresponding coastal waters and expands the databases of environmental drivers and community shifts.

Phytoplankton dominance in the IRL and coastal Atlantic Ocean is known to alternate primarily between diatoms, dinoflagellates, cyanobacteria, cryptophytes, and chlorophytes (Badylak & Phlips, 2004; Wachnicka *et al*., 2020). The results of our study indicate that diatoms dominated the IRL and coastal ocean followed by dinoflagellates, while other groups of plankton were present in low densities. Elevated diatom densities generally corresponded with genuinely or relatively low dinoflagellate densities (*e.g.* VBI in the summer of 2020, BRSI in the spring of 2021, the second sampling of BRNI fall of 2021). The reverse trend was observed at BRSI in the fall of 2020, BRNI/BRNW in the first sampling at BRN in the fall of 2021, and at BRNW in the second sampling at BRN in the fall of 2021. *Pyrodinium bahamense,* a potentially toxin-producing dinoflagellate, bloomed at BRSI in the fall of 2020 showed an instance of dominance with densities exceeding those of diatoms by three orders of magnitude (Dinoflagellates: 4,892 cells L^{-1} ± 838 vs. Diatoms: 1 cell L^{-1} ± 0.8). Phlips *et* al. (2021), reported a similar peak in *P. bahamense* biomass in the summer of 2020 in the central BRL attributing the bloom to warmer water temperatures (above 30°C) and higher rainfall associated with El Niño periods. Between 20 sampling dates from 1997 to 1999, Badylak and Phlips (2004) found that the dominant bloom-forming diatoms in the IRL were

Skeletonema costatum, Dactyliosolen fragilissimus, Skeletonema menzelii, Cerataulina pelagica, Odontella regia, Chaetoceros lorenzianus, Rhizosolenia setigera and Thalassionema nitzschioides, whereas our study determined that, in addition to *S. costatum*, *D. fragilissimus*, *Odontella* spp., *Chaetoceros* spp., *Rhizosolenia* spp., and *T. nitzschioides*, *Leptocylindrus danicus*, *Coscinodiscus* spp., *Asterionellopsis glacialis*, *Cylindrotheca closterium*, *Amphora* sp., *Nitzschia* spp., *Pseudo-nitzschia* spp., *Cyclotella meneghiniana*, *Pleurosigma* spp., *Paralia sulcata*, *Thalassionema frauenfeldii*, and *Navicula* spp. were also dominant bloom-forming diatoms. These diatom genera were present in both the IRL and coastal ocean except for *Cyclotella meneghiniana*, which was only present in the coastal ocean. Badylak and Phlips (2004) also determined that the common bloom-forming dinoflagellates in the IRL were *Pheopolykrikos hartmannii*, *Akashiwo sanguinea*, *Prorocentrum micans*, *Pyrodinium bahamense* and *Prorocentrum minimum*. In our study, *Prorocentrum* sp., *Pyrodinium bahamense*, *Peridinium* sp., *Protoperidinium* spp., *Gymnodinium* spp., *Gonyaulax* sp., and *Ceratium* spp. were the dominant dinoflagellates. A greater number of dominant diatoms (18 genera) in contrast to dinoflagellates (7 genera) may be a result of different bloom strategies between the two groups. For instance, Smayda and Reynolds (2003) described diatom blooms as a predictable and diverse guild of multiple, complimentary species, whereas dinoflagellate blooms were described as unpredictable and often monospecific. They characterized diatom and dinoflagellate blooms in this manner because dinoflagellates are generally habitat specialists, blooming alone under very specific

conditions, while diatoms tend to bloom alongside other species under a broad range of conditions. These different bloom patterns observed in coastal phytoplankton may explain why diatoms bloomed more frequently and why there were few competing phytoplankton when *Pyrodinium bahamense* was blooming at BRSI in the fall of 2020. In the Baltic Sea, Spilling *et al*. (2018) attributed higher growth rates in diatoms as the main driver in diatom dominance over dinoflagellates, and linked dinoflagellate blooms to water column stratification. Similarly, in the Caloosahatchee River Estuary, Florida, Fugate and Andresen (2020) associated chlorophyll maxima with areas of maximum stratification within the estuary. Further associations between dinoflagellates and water column stratification were found by Yñiguez *et al*. (2018) who determined that declines in *Pyrodinium bahamense* blooms in the Sorsogon Bay Estuary (Philippines) was associated with diminished water column stratification due to higher salinities and relatively low temperatures. In instances of higher diatom abundance and slightly elevated dinoflagellate abundance (*e.g.* VBI in the summer of 2020), higher growth rates in diatoms may explain why diatoms generally outcompeted dinoflagellates. In cases of dinoflagellate blooms (*e.g. Pyrodinium bahamense* bloom at BRSI in the fall of 2020), water stratification may be an underlying factor, as Phlips *et al*. (2021) reported peak *Pyrodinium bahamense* biovolumes in 2020 during warmer temperatures (*i.e.* development of a thermocline) and increased rainfall (*i.e.* development of a halocline and increase in nutrients). Diatom or dinoflagellate success in the IRL and adjacent coastal Atlantic Ocean is dependent on taxon-

specific bloom strategies, physiological adaptations to the environment, and competition for resources.

The diversity and richness of phytoplankton communities along environmental gradients may be shaped by taxon-specific physiological tolerances. In this study, collective diversity, species richness, and species evenness were all significantly higher in the coastal ocean. When assessed on seasonal scales, diversity and species richness were significantly higher in the coastal ocean during eight of the 12 sampling dates, of which the remaining four sampling dates were not statistically different between coastal and IRL sites. Similarly on seasonal scales, species evenness was significantly higher in the coastal ocean during seven of the 12 sampling dates, while one sampling date showed significantly higher evenness in the IRL and the remaining three sampling dates showed no statistical difference between IRL and coastal sites. Olli *et al*. (2019) established that phytoplankton diversity in the Baltic Sea and Chesapeake Bay was intermediate at lower salinities (0-5 PSU), decreased to a diversity minimum at mesohaline salinities (7-9 PSU), and increased along the salinity gradient from brackish to marine salinities (10-30 PSU), which is known as the Remane concept/curve (Remane, 1934). Virta *et al.* (2020) found similar results with diatom richness being highest at lower (0-5 PSU) and higher salinities (10-30 PSU), and a diversity minimum at salinities around 6-9 PSU. This phenomenon of minimal diversity at intermediate salinities is attributed to the inability of strictly fresh and marine phytoplankton to tolerate these salinities (Virta *et al.*, 2020). Estuarine

phytoplankton commonly exhibit high tolerance to salinity fluctuations, whereas coastal phytoplankton only show an intermediate tolerance (Brand, 2005). Phytoplankton communities in the IRL and coastal ocean appear to follow this trend of low diversity at intermediate salinities, which may be due to the compartmentalized hydrologic structure of the IRL limiting blooms of exclusively estuarine species. Lower diversity and evenness in the IRL may also be a result of high phytoplankton productivity (*i.e.* blooms) by one or multiple species while a few other species are present at lower densities (Zhong *et al*., 2021). Chalar (2009) determined that phytoplankton diversity was intermediate at lower phytoplankton abundances, optimal at intermediate abundances, and minimal at higher abundances in the Salto Grande reservoir. Higher phytoplankton abundance can limit resource availability (*e.g.* light, nutrients) subsequently increasing competition resulting in lower species richness (Hutchinson, 1961). Higher abundances of phytoplankton in the IRL may cause a similar phenomenon of lower diversity by increasing competition for resources and favoring selected phytoplankton (*e.g.* faster growth rates, more efficient nutrient uptake, etc.).

Changes in phytoplankton community composition along salinity gradients may be shaped by taxon-specific responses to changes in environmental conditions. Generally in our study, phytoplankton community compositions were unique between IRL and coastal sites, but some overlap in community structure was observed. The majority of overlap between coastal and IRL communities was at BRN and VB. For instance, at BRN during the fall of 2021, *Leptocylindrus danicus*,

Chaetoceros spp., and *Pyrodinium bahamense* were the most prolific phytoplankton, but *Prorocentrum* spp. and *Ceratium* spp. were present at lower densities; BRNW was dominated by *Coscinodiscus* spp., *Chaetoceros* spp., *Prorocentrum* spp., and *Pyrodinium bahamense*, with lower densities of *Leptocylindrus danicus* and *Ceratium* spp. present; and communities at BRNO were dominated by *Chaetoceros* spp. and *Prorocentrum* spp., with lower abundances of *Pyrodinium bahamense* and *Leptocylindrus danicus*. Each site had its own number of unique species, but the main overlap is between the species mentioned due to their relatively high abundance and ubiquity between BRN sites. BRN was unique in regard to its proximity to the Port Canaveral Lock System (PCL), which is opened on demand to allow vessels to travel between the IRL and ocean. Tidal forcing at the PCL has not been documented (Weaver *et al*., 2016), but it is assumed that there is some mixing when the PCL is intermittently opened. The relatively greater overlap in IRL and coastal community composition at BRN (ANOSIM-R=0.85) compared to BRS (ANOSIM-R=0.99) may suggest the PCL is a potential vector for euryhaline phytoplankton to travel between on a small scale. The most overlap in IRL and coastal communities was observed at VB, which was approximately 24km from Sebastian Inlet. Sebastian Inlet accounts for an estimated 15% of the exchange between the IRL and coastal ocean (Smith, 2016), which would likely explain the greater degree of overlap at VB.

The relatively higher diversity in coastal sites and inherent overlap in potentially euryhaline species may also account for overlap in community structure.

As mentioned before, seventeen of the eighteen dominant diatoms and dinoflagellates in this study were present in both the IRL and coastal ocean (except for *Cyclotella meneghiniana*), which may be indicative of euryhaline tolerances in some species. Estuarine phytoplankton are highly tolerant to salinity fluctuations while coastal phytoplankton are moderately tolerant (Brand, 2005). However, there are few exclusively estuarine phytoplankton species (*i.e.* species that exclusively live in estuaries) due to this requirement to tolerate salinity fluctuations (Virta *et al*., 2020). Therefore, marine phytoplankton with this ability to acclimate to osmotic stress through various species-specific mechanisms dominate in estuaries and other regions of highly variable salinity, such as the IRL and coastal Atlantic Ocean.

BGAPC, BGAPE, AND NON-CYANOBACTERIA PHYTOPLANKTON

Collectively, non-cyanobacteria phytoplankton (diatoms, dinoflagellates, etc.) densities (determined via flow cytometry) from 2019 to 2021 were significantly higher in the IRL, which is consistent with plankton tow data. Higher abundances of non-cyanobacteria phytoplankton in the IRL may be a result of broad estuarine and intermediate coastal salinity tolerances in phytoplankton described by Brand (2005) or differences in nutrient regimes between the IRL and coastal ocean. BGAPC were also significantly higher in the IRL, but BGAPE were not statistically different between the IRL and coast. This may suggest BGAPC in the IRL have an affinity for lower salinities, while BGAPE were not influenced by salinity gradients. Generally, the distribution of BGAPC and BGAPE in estuaries is defined by salinity gradients. For instance, in the Pearl River Estuary located in

China, Jiang *et al*., 2016 found that the abundance of *Synechococcus* sp. containing phycoerythrin was directly correlated with salinity (maximum at 11 PSU; range: 0 to 35 PSU) while the abundances of *Synechococcus* sp. containing phycocyanin were inversely correlated with salinity (maximum at 15 PSU; range: 0 to 32 PSU). The authors also determined that maximum abundances of *Synechococcus* sp. containing phycoerythrin were roughly half the maximum abundances of *Synechococcus* sp. containing phycocyanin. BGAPC in the IRL followed this inverse relationship to salinity, but BGAPE deviated from the direct correlation with salinity. Waterbury *et al*. (1986) determined that some cyanobacteria with phycoerythrin pigments had physiological requirements for elevated concentrations of dissolved ions, whereas some cyanobacteria that lacked phycoerythrin did not have these requirements and could survive in freshwater. Additionally, Rajaneesh and Mitbavkar (2013) determined that three *Synechococcus* spp. strains that contained phycoerythrin each had different salinity tolerances ranging from freshwater to marine in the Zuari Estuary (India). This may suggest that analyses of BGAPE on broad scales (*i.e.* as a single group), such as in our study, are not precise enough to explain distributions based on salinity gradients. In an analysis on the community structure of cyanobacteria in the Baltic Sea, Haverkamp *et al*. (2009), found that areas of intermediate turbidity (*e.g.* coastal areas and lakes) offer sufficient niches for the coexistence and diversification of cyanobacteria with phycoerythrin as a result of physiological adaptations to light. Thus, BGAPE in the

IRL may need to be analyzed on strain or species-specific scales to accurately depict salinity tolerances.

Non-cyanobacteria phytoplankton and BGAPC remained consistently below $1x10^5$ cells mL^{-1} and $5x10^3$ cells mL^{-1}, respectively, from the fall of 2019 to the summer/fall of 2020. By the fall of 2020, a phytoplankton bloom ensued at BRNI consisting of elevated densities of BGAPC, BGAPE, and non-cyanobacteria phytoplankton. However, diatoms and dinoflagellate densities were not elevated during this period in phytoplankton tow data. This may suggest, the elevated non-cyanobacteria densities detected via flow cytometry were smaller pico- or nano-phytoplankton that were too small to be captured with a 25µm plankton net. The spike in BGAPC, BGAPE, and non-cyanobacteria productivity immediately proceeded the regression of a high biomass picocyanobacteria bloom of a *Synechococcus* sp.-like species with phycocyanin fluorescence in the IRL proper and BRL (referred to as the CyanoHAB of 2020). The CyanoHAB of 2020 progressed from July/August to November/December of 2020 and dominated the phytoplankton community reaching densities as high as $5x10^6$ cells mL^{-1}. The high degree of turbidity generated by this cyanobacterial bloom may have limited the growth of other BGAPC, as well as BGAPE and non-cyanobacteria phytoplankton until the subsidence of the bloom in November/December where BGAPC, BGAPE, and non-cyanobacteria phytoplankton densities were elevated following the bloom. In eutrophic freshwater lakes, cyanobacteria can lyse rapidly and release nutrients directly into surface waters where other cyanobacteria and phytoplankton (*e.g.*

diatoms, dinoflagellates) can use these nutrients (Keating, 1978). Similarly, in the Baltic Sea, diazotrophic cyanobacteria blooms have the potential to increase nitrogen flux into coastal waters and estuaries comparable to anthropogenic nitrogen loading (Spilling *et al*., 2018). Adam *et al*. (2016), found that dissolved nitrogen (ammonium) produced by diazotrophic cyanobacterial blooms did not accumulate, but rather transferred to diatoms (*Chaetoceros* spp.) and other phytoplankton, as well as copepods. Additionally, Tamminen and Anderson (2007) found that increased nitrogen input from cyanobacteria blooms could increase biomass transport to sediments upon lysing causing a subsequent increase in sediment-oxygen demand and stimulating a flux of phosphorus to the water column. A similar scenario may be possible in the IRL due to rapid decline of a high biomass CyanoHAB and potential fluxes of nutrients into the water column. This may also suggest that cyanobacteria blooms in the IRL have the potential to stimulate secondary blooms in the wake of a major bloom event as seen immediately following the CyanoHAB of 2020.

SALINITY INFLUENCES ON DOMINANT PHYTOPLANKTON

Resource availability (*e.g.* nutrients, light) and environmental conditions play an important role in the inhibition and promotion of phytoplankton blooms. The relative influence of nutrients and other environmental parameters were assessed on dominant phytoplankton taxa between the IRL and coastal ocean to explain differences and overlap in community structure. Collectively across IRL and coastal sites for all seasons, temperature, salinity, DO, and pH accounted for

just 23% of the variation in dominant phytoplankton abundance and the majority of variation remains unexplained. Salinity was the most influential variable influencing dominant IRL and coastal phytoplankton attributing to 11.6% of the variation in phytoplankton abundance while pH, dissolved oxygen, and temperature accounted for a collective total of 11.4% of the variation. Across all IRL and coastal sites and seasons, the diatoms *Cylindrotheca closterium, Coscinodiscus* spp., *Cyclotella meneghiniana*, *Skeletonema costatum*, and *Asterionellopsis glacialis* were positively associated with salinity. The highest growth rates of *Cylindrotheca closterium* (at optimal temperatures) tend to occur at higher salinities (15-33 PSU) (Glaser & Karsten, 2020) and *Asterionellopsis glacialis* is well-adapted to coastal surf zones and experiences optimal growth between 20 and 30 PSU and can tolerate a wide range of brackish to full marine salinities (15-40 PSU) (Rörig *et al*., 2017). *Skeletonema costatum* is documented as a euryhaline species that can grow at salinities ranging from 1 to 35 PSU (Balzano *et al*., 2011). *Cyclotella meneghiniana* is sometimes referred to as a euryhaline freshwater diatom that is capable of surviving in salinities from 0 to 33 PSU with a growth optimum at 18 PSU (Roubeix & Lancelot, 2008). Mukherjee *et al*. (2013) determined that *Coscinodiscus centralis* and *C. radiatus*, common species present in the IRL and coastal waters around Florida, decreased linearly in size along increasing salinity gradients from 5 to 25 PSU, but were able to survive in a wide range of salinities. *Cylindrotheca closterium, Coscinodiscus* spp., *Cyclotella meneghiniana*, *Skeletonema costatum*, and *Asterionellopsis glacialis* in the IRL showed preference

to higher salinities, and salinity appeared to be a significant factor driving differences in IRL and coastal phytoplankton.

Salinity (31.6%), phosphate (14.3%), temperature (6.4%), and nitrate (3.9%) accounted for 56.2% of variation in phytoplankton abundance at BN in the fall of 2021. *Prorocentrum* spp., *Ceratium* spp., and *Coscinodiscus* spp. displayed correlations with higher salinities. *Prorocentrum minimum,* a species present in the IRL, is preferential to lower salinities and can survive in estuarine and marine environments, but they experience high mortality at around 8 PSU due to osmotic stress (Skarlato *et al*., 2018). In an analysis of *Ceratium* salinity and temperature tolerances in the coastal waters of Virginia, Mulford (1963) determined that *Ceratium candelabrum* (32.52-32.95 PSU), *Ceratium extensum* (31.49-32.95 PSU), and *Ceratium contortum* (31.02-32.95) (species also present in and around the IRL) preferred higher salinity, which is also evidenced in our RDA findings. *Gonyaulax* sp., *Chaetoceros* spp., and *Leptocylindrus danicus* showed negative correlations with salinity, likely due to salinity stress at higher salinities. For instance, *Leptocylindrus danicus* is sometimes referred to as a brackish species and thrives in salinities below 31 PSU (Yoon *et al*., 2022). Similarly, *Gonyaulax spinifera*, a species sometimes found in the IRL, is proposed to have a euryhaline tolerance (17.5-39.1 PSU) (Rodrigues *et al*., 2019). Thus, in the case of salinity correlations across all sites and seasons and at BRN in the fall of 2021, salinity was the most significant environmental variable influencing phytoplankton abundance between the IRL and coastal ocean and taxa-specific salinity tolerances likely explain some

of the phytoplankton distributions between the IRL and coastal ocean. Temperature, pH, dissolved oxygen, nitrogen, and phosphorous account for additional variation.

In the IRL, salinity was the most influential environmental variable accounting for 12% of the variation in dominant phytoplankton. *Coscinodiscus* spp. and *Nitzschia* spp., dominant phytoplankton in IRL and coastal communities, showed a strong association with higher salinities within the IRL. Saifullah *et al*. (2019) found similar distributions of *Coscinodiscus* spp. and *Nitzschia* spp. at higher salinities in the Sibuti Mangrove Estuary attributing their success in the estuarine environment to euryhaline tolerances. A similar scenario is likely in the IRL, which may explain some overlap in community composition within the IRL and between the IRL and coastal ocean. *Prorocentrum* spp. was found to be inversely associated with salinity in the IRL, as reported in other estuaries with broad salinity tolerances attributing to its success in marine and estuarine environments (Skarlato *et al*., 2018). The relatively strong influence of salinity on dominant phytoplankton in this study reinforces the significance of salinity gradients on species distributions along an estuary-coastal continuum and highlights the relative success of euryhaline diatoms and dinoflagellates.

TEMPERATURE INFLUENCES ON DOMINANT PHYTOPLANKTON

Temperature increases can raise photosynthetic and metabolic rates in phytoplankton (Regaudie & Duarte, 2012). However, at the species level, temperature dependence is often unimodal and skews negatively (Barton & Yvon-Durocher, 2019). Across all sites and seasons, temperature ranged between 14.7

and 31.9°C and only accounted for 3% of the variation in phytoplankton abundance. The dominant dinoflagellates (*Pyrodinium bahamense*, *Ceratium* spp., *Gonyaulax* sp., *Prorocentrum* spp., and *Peridinium* spp.) were correlated with higher temperatures. Conversely, the dominant diatoms (*Navicula* spp., *Amphora* spp., *Nitzschia* spp., *Pleurosigma* spp., *Pseudo-nitzschia* sp., *Paralia sulcata*, *Thalassionema nitzschoides*, and *Thalassionema frauenfeldii*) were negatively associated with temperature. In the literature, there are other cases of dinoflagellate densities increasing with higher temperatures, and this inverse correlation between diatoms and temperature has been documented in other estuaries (Rong *et* al., 2021; Morse *et al.*, 2013; Jiang *et al.*, 2015). The RDA results confirm these temperature relationships between and within IRL and coastal communities. Diatom growth during cooler periods giving way to dinoflagellate growth during warmer periods may be a result of competition or thermal niche partitioning between diatoms and dinoflagellates. Thermal niche partitioning is known to occur amongst some strains (Pittera *et al*., 2014) and ecotypes of algae (Johnson et al., 2006). Evidence of diatom-dinoflagellate competition and alternating succession of "blooming" diatom and dinoflagellate taxa have been documented in other systems, with controlling variables including nutrient concentrations and temperature (Rong *et al.*, 2021; Zhou *et al*., 2017). Temperature is a significant controller of phytoplankton bloom activity and intensity, and temperature has the potential to double phytoplankton growth rates with every 10°C increase in temperature (Rose & Caron, 2007). In this study, temperatures were between 19 and 31.9°C during 24 of the 29 sampling days.

This range encompasses temperature thresholds for optimal growth for some dinoflagellates, such as *Pyrodinium bahamense* (27-32°C) (Phlips *et al*., 2021) and *Ceratium* spp. (16-27°C) (Mulford, 1663), and some diatoms, such as *Pseudo-nitzschia pungens* (15.1-32.9°C) (Kim *et* al., 2014). Overlapping thermal optima amongst dominant diatoms and dinoflagellates would serve to reduce the overall influence of temperature as a factor driving species. Simulated scenarios of large phytoplankton communities (>60 species) with overlapping thermal optima suggests the potential for phytoplankton species to coexist (and compete) with relatively similar thermal niches and similar environmental requirements (Scranton & Vasseur, 2016). Temperature likely plays a small role in overall differences between IRL and coastal sites due to overlapping thermal niches amongst phytoplankton, but is not expected to be the primary driving force.

At BRN in the fall of 2021, temperature ranged from 26.6-28.5°C and accounted for 6.4% of the variation in phytoplankton abundance. The diatoms *Dactyliosolen fragilissimus, Rhizosolenia* spp., and *Nitzschia* spp., and the dinoflagellate *Gymnodinium* spp. were positively correlated with temperature, whereas *Pyrodinium bahamense* was inversely correlated with temperature. *Rhizosolenia* spp. is proposed to be a eurythermal species (Ye *et al*., 2018), but other studies found correlations between *Rhizosolenia* spp. and temperature (Mohd-Din *et al.*, 2022). Mohd-Din *et al.* (2022) found that both *Rhizosolenia* spp. and *Dactyliosolen fragilissimus* were positively correlated with temperature, which are consistent with findings in this study. The positive correlation between *Nitzschia* sp.

and temperature at BRN in the fall of 2021 appears contradictory to RDA findings across all sites and seasons (*i.e.* negative correlation with temperature); however, the observed thermal range of *Nitzschia longissima*, a common species in and around the IRL, ranges between 10 and 30°C and is optimal at 20°C (Papry *et al*., 2019), which is within the range of temperatures observed during this period in the IRL. Similarly, the inverse correlation between *Pyrodinium bahamense* and temperature appears contradictory to the RDA findings across all sites and seasons; however, IRL strains of *Pyrodinium bahamense* range from 18 and 34°C and reach maximum biovolumes between 27 and 32°C (Phlips *et al*., 2011).The narrow range of observed temperatures during this period may not have stressed phytoplankton such as *Nitzschia* spp. and *Pyrodinium bahamense*, and would not be expected to drive phytoplankton community responses.

PH INFLUENCES ON DOMINANT PHYTOPLANKTON

Phytoplankton can both influence, and be influenced by, pH. Across all sites and seasons, pH ranged from 7.16 to 8.97 and accounted for only 3.7% of the variance in phytoplankton abundance. The diatoms *Cylindrotheca closterium*, *Coscinodiscus* spp., *Cyclotella meneghiniana*, *Skeletonema costatum*, and *Asterionellopsis glacialis* were, however, determined to be correlated with higher pH. Shifts in pH can be a result of high productivity (pH increases) and bloom decomposition/respiration (pH decreases) (López-Archilla *et al*., 2004), but also has the potential to influence metabolic processes and growth rates in phytoplankton (Hinga, 2002). Some diatoms have been found to prefer higher pH,

and they are sometimes considered pH biosensors due to this sensitivity (Carpenter and Waite, 2000), which may offer insight as to why diatoms between the IRL and coastal were observed at higher pH. For instance, decreasing pH in *Nitzschia closterium* and *Skeletonema costatum* cultures resulted in corresponding decreases to growth rates, biomass, and nitrogen uptake (Gu *et al*., 2017).

At BRN in the fall of 2021, pH ranged from 8.03 to 9.21. The diatoms *Dactyliosolen fragilissimus*, *Rhizosolenia* spp., and *Nitzschia* spp., and the dinoflagellate *Gymnodinium* spp. were negatively correlated with pH, while the dinoflagellate *Pyrodinium bahamense* had positive correlations with pH. Huang *et al*. (2021), found evidence that increases in dissolved CO_2 (*i.e.* a decrease in pH) and increase in temperature worked synergistically to inhibit diatom to dinoflagellate succession in mesocosm experiments. In their study, dinoflagellate blooms only began to form after the regression of existing diatom blooms. In our study, a similar inverse response to pH and positive response to temperature was observed in diatoms (*Dactyliosolen fragilissimus*, *Rhizosolenia* spp., and *Nitzschia* spp., and the dinoflagellate *Gymnodinium* spp.). Mohd-Din *et al.* (2022) found that both *Rhizosolenia* spp. and *Dactyliosolen fragilissimus* were negatively correlated with pH, consistent with the findings of this study. The growth rate of *Nitzschia* spp. is optimal around a pH of 8.5-10 (Zhang *et al*., 2018). Similarly, some species of *Gymnodinium* spp. can tolerate a wide range of pH (Adam *et al*., 2011).

NUTRIENT INFLUENCES ON DOMINANT PHYTOPLANKTON

Nutrients, such as nitrogen, phosphate, and silica, are strongly influential environmental variables for estuarine phytoplankton (Phlips *et al*., 2002). *Gonyaulax* sp., *Leptocylindrus danicus*, and *Chaetoceros* spp. were positively associated with nitrate and negatively associated with salinity and phosphate. *L. danicus* has been labeled an "oligotrophic" diatom and experiences optimal growth in nitrogen-depleted environments due to its ability to adapt to low nitrogen conditions (Watanabe *et al*., 2017; Gao *et al*., 2020). This is in contrast to the positive association between nitrate and *L. danicus* in this study and at least one other (Baek *et al.*, 2019). Baek et al. (2019) did not offer a compelling explanation for this seeming contradiction. We propose that *L. danicus* either has a more robust capability to take advantage of different nitrate concentrations than its presumption as oligotrophic suggest or competition to *L. danicus* lacked mechanisms to adapt to lower concentrations of nitrate allowing *L. danicus* to be successful relative to other species in the community. This study's negative phosphate correlations with *Chaetoceros* spp. and *Gonyaulax* spp. are also at variance with some published findings. Kesaulya *et al*. (2022) found positive correlations between nutrients (nitrogen, phosphorous, and silica) and these taxa. One explanation may be that we were only able to identify these cells to genus, and congeners can have very different physiologies (*e.g.* Trowbridge, 1995). Phosphate is potentially a limiting nutrient for the strains of *L. danicus*, *Chaetoceros* spp., and *Gonyaulax* spp. in this

study. However, these nutrient associations are complex and require further investigation.

In contrast to the species above, *Prorocentrum* spp., *Ceratium* spp., and *Coscinodiscus* spp. displayed correlations with higher phosphates and lower nitrates. *Ceratium furca* and *Ceratium fusus* have the potential to physiologically adjust to low nutrient concentrations (Baek *et al*., 2008). This may suggest that nitrogen and phosphorous alone are poor predictors of *Ceratium* spp. population dynamics due to their plasticity in nutrient requirements. *Prorocentrum minimum* was observed to have inhibited growth at high nitrate levels (Abassi & Ki, 2022), and this is consistent with findings in this study. Phosphate limitation and N:P stoichiometry influenced competition between *Prorocentrum donghaiense* and *Skeletonema costatum* (Cao & Wang, 2012); and bioavailable nickel may promote their growth (Huang *et* al., 2016). This suggests that unexamined variables (e.g., interspecific competition, dissolved nickel, and other nutrients) may also be important in driving or inhibiting phytoplankton populations

CYANOBACTERIA ENVIRONMENTAL ASSOCIATIONS

Collectively, BGAPC, BGAPE, and other non-cyanobacteria phytoplankton had no apparent correlations with temperature, salinity, pH, or dissolved oxygen over the course of 2019 to 2021. This is likely a result of the representation of many species within these groups, each with their own unique combination of environmental requirements and drivers (as was the case of dominant diatoms and dinoflagellates). For instance, diatoms and dinoflagellates in the IRL have

demonstrated species level tolerances and environmental preferences in this study but are grouped together due to the presence of chlorophyll a. At BRN in the fall of 2021, our results determined that salinity and pH (35.2%), temperature (8.7%) and phosphate (<1%) accounted for only 43.9% of the variation in BGAPE and non-cyanobacteria, but no apparent relationships were observed between BGAPC and any of these variables. BGAPE at BRN during the fall of 2021 were correlated with pH and inversely correlated with phosphate and nitrate. Cyanobacteria are often diazotrophs, can use atmospheric nitrogen, and may sometimes be limited by phosphorous (Paerl & Fulton, 2006). In marine environments, high productivity can influence pH. In turn, higher pH may affect the bioavailability of trace elements necessary for photosynthesis or inhibit phosphate uptake by cyanobacteria (Nguyen *et al*., 2022). Rather than driving BGAPE presence, the high productivity may have instead created higher pH and lower nutrient conditions. The other non-cyanobacteria phytoplankton were positively associated with temperature and salinity and appeared to thrive with the higher temperature and salinity conditions of the sampling period.

CYANOHAB ENVIRONMENTAL REGRESSIONS

Densities of the dominant cyanobacterium during the CyanoHAB of 2020 showed significant linear relationships between dissolved oxygen (R^2 = 0.04), pH (R^2 = 0.22), chlorophyll a (R^2 = 0.91), silica (R^2 = 0.87), phosphate (R^2 = 0.22), and nitrate (R^2=0.11). The cyanobacterium exhibited an affinity for higher temperatures persisting at densities higher than $4x10^6$ cells mL^{-1} at temperatures of 22.5-31°C.

The cyanobacterium may also be stenohaline, but with a preference of lower salinity (~18 PSU). Dissolved oxygen was a poor predictor of cyanobacteria density. The cyanobacterium had a positive relationship with pH, which may have been due to high primary productivity driving up the pH (Zepernick *et al*., 2021). Cyanobacteria have been documented to use the subsequent increase in alkalinity to outcompete diatoms and other silicious phytoplankton because the biosilicification process that allows silica deposition is pH dependent (Zepernick *et al*., 2021). A strong positive relationship between silica and the cyanobacteria supports these findings and suggests inhibited diatom (and other silicious phytoplankton) growth during this period. In the Xinkai Lake (Russia), Sun *et al*. (2007) determined that an increase in dissolved silicate stimulated the growth and number of diatoms present and suppressed the biomass of chlorophytes and cyanobacteria. This could explain a scenario in which high BGAPC production during the CyanoHAB increased alkalinity causing a subsequent decrease in biosilicification, which led to the accumulation of dissolved silica that ultimately inhibited the growth of the BGAPC. This may also explain the increase in non-cyanobacteria phytoplankton (possibly diatoms) immediately following the subsidence of bloom. The strong relationship between chlorophyll and the cyanobacteria densities is a clear result of increased cyanobacteria productivity and further suggests inhibition of non-cyanobacteria growth. That is to say, the cyanobacterium dominated the water column during the CyanoHAB. Phosphate and nitrate had fair, positive relationships with the cyanobacterium. For instance, Hughes and Marion (2021),

determined that growth rates of cyanobacteria containing phycocyanin in hypereutrophic lakes did not increase with the addition of either nitrate of phosphate, but rather only increased when nitrate and phosphate were added together, which align with the results of our multiple regression. Simple linear regression did not prove useful in explaining the effects of temperature on the cyanobacterium, but multiple regression indicated temperature partially explained the distribution of BGAPC in the IRL during the CyanoHAB. Therefore, the it appears the interactions of this bloom with environmental parameters was relatively complex. Nitrate, phosphate, and temperature may have had some effects on the distribution of this bloom and the subsequent rise in pH and silica as a result of the bloom may have helped to suppress non-cyanobacteria phytoplankton until after the bloom had subsided, but much remains unexplained as to why or how this bloom emerged.

CHAPTER 5
CONCLUSION

This study determined that temperature, salinity, dissolved phosphate, and other environmental variables poorly explained the distribution of BGAPC in the IRL and coastal ocean, which is likely a result of categorizing multiple species into a single category (Hypothesis I). Densities of BGAPC during the "CyanoHAB" cyanobacteria bloom of 2020 did not have linear relationships with most environmental parameters and is proposed to have a more complex relationship with environmental parameters than the multiple regression suggests (Hypothesis II). Biodiversity of phytoplankton communities was greater in the coastal Atlantic Ocean than in the IRL due to osmotic stress at lower salinities leading to a biodiversity decrease along a coast to estuary gradient, often referred to as the Remane Curve (Hypothesis III). Salinity gradients between the IRL and coastal ocean, as well as within the IRL, explained the majority of variation in dominant phytoplankton communities, which further emphasizes the significance of salinity on phytoplankton distribution in the IRL and differences in community structure between the coastal ocean and IRL. Phytoplankton communities in the IRL and coastal ocean were relatively distinct with some exceptions. Communities in the IRL and coastal ocean at BRS were revealed to be highly distinct from each other, which was likely a result of limited hydrologic connectivity between central BRL and costal Atlantic Ocean. IRL communities at BRN showed more overlap with its respective coastal communities than BRS, which may be due to the close proximity

of BRN to the intermittently open Port Canaveral Locks allowing some mixing between estuarine and coastal communities. IRL and coastal communities at VB showed the most overlap in community structure, which is likely a result of its close proximity to Sebastian Inlet allowing free exchange between coastal and estuarine water.

LITERATURE CITED

Abassi, S., & Ki, J.-S. (2022). Increased nitrate concentration differentially affects cell growth and expression of nitrate transporter and other nitrogen-related genes in the harmful dinoflagellate Prorocentrum minimum. *Chemosphere*, 288(Part 2).

Adam, B., Klawonn, I., Sveden, J. B., Bergkvist, J., Nahar, N., Walve, J., Littmann, S., Whitehouse, M. J., Lavik, G., & Kuypers, M. M. (2016, January 1). N2-fixation, ammonium release and N-transfer to the microbial and classical food web within a plankton community. *ISME JOURNAL*, 10(2), 450–459.

Adam, A., Mohammad-Noor, N., Anton, A., Saleh, E., Saad, S., & Shaleh, S. R. M. (2011). Temporal and spatial distribution of harmful algal bloom (HAB) species in coastal waters of Kota Kinabalu, Sabah, Malaysia. *Harmful Algae*, 10(5), 495-502.

Anderson, D. M. (2009). Approaches to monitoring, control and management of harmful algal blooms (HABs). *Ocean & coastal management*, 52(7), 342-347.

Auguie, B. (2017). gridExtra: Miscellaneous Functions for "Grid" Graphics. R package version 2.3. https://CRAN.R-project.org/package=gridExtra

Badylak, S., & Phlips, E. J. (2004). Spatial and temporal patterns of phytoplankton composition in subtropical coastal lagoon, the Indian River Lagoon, Florida, USA. *Journal of Plankton Research*, 26(10), 1229–1247.

Baek, S. H., Kim, D., Kim, Y. O., Son, M., Kim, Y.-J., Lee, M., & Park, B. S. (2019). Seasonal changes in abiotic environmental conditions in the Busan coastal region (South Korea) due to the Nakdong River in 2013 and effect of these changes on phytoplankton communities. *Continental Shelf Research*, 175, 116–126.

Baek, S. H., Shimode, S., Han, M.-S., & Kikuchi, T. (2008). Growth of dinoflagellates, Ceratium furca and Ceratium fusus in Sagami Bay, Japan: The role of nutrients. *Harmful Algae*, 7(6), 729–739.

Balzano, S., Sarno, D., & Kooistra, W. H. C. F. (2011). Effects of salinity on the

growth rate and morphology of ten Skeletonema strains. *Journal of Plankton Research*, 33(6), 937–945.

Barton, S. & Yvon-Durocher, G. (2019). Quantifying the temperature dependence of growth rate in marine phytoplankton within and across species. *Limnology and Oceanography*, 64(5), 2081-2091.

Brand. L. E. (2005). The salinity tolerance of forty-six marine phytoplankton isolates. Estuarine, Coastal and Shelf Science, 18, 543–556.

Buzzani, A., Paranhos, R., Mello, M. P., Abreu, F., dos Santos, A. A., Martins, R., & Bianco, K. (2022). Rainfall governs picocyanobacterial ecology in a tropical estuary (Guanabara Bay, Brazil). *Hydrobiologia*, 849(1), 175.

Cao Jing, Wang, Jiangtao. (2012). The Inhibitory Degree Between Skeletonema costatum and Dinoflagellate Prorocentrum donghaiense at Different Concentrations of Phosphate and Nitrate/Phosphate Ratios. *Journal of Ocean University of China*, 2, 153.

Carpenter, K. D., & Waite, I. R. (2000). Relations of Habitat-Specific Algal Assemblages to Land Use and Water Chemistry in the Willamette Basin, Oregon. *Environmental Monitoring and Assessment*, 64(NO 1), 247–257.

Chalar, G. (2009). The use of phytoplankton patterns of diversity for algal bloom management. *Limnologica*, 39(3), 200–208.

Dybas, C. L. (2002). Florida's Indian River Lagoon: An Estuary in Transition. *BioScience*, 52(7), 554.

East Central Florida Regional Planning Council, 2016. Indian River Lagoon Economic Valuation Update, p. 69.

Julian Faraway (2016). faraway: Functions and Datasets for Books by Julian Faraway. R package version 1.0.7. https://CRAN.R-project.org/package=faraway

Gao, P., Wang, P., Chen, S., Bi, W., Lu, S., He, J., Wang, X., & Li, K. (2020). Effect of Ambient Nitrogen on the Growth of Phytoplankton in the Bohai Sea: Kinetics and Parameters. *Journal of Geophysical Research*. Biogeosciences, 125(12), 1–15.

Glaser, K., & Karsten, U. (2020). Salinity tolerance in biogeographically different

strains of the marine benthic diatom Cylindrotheca closterium (Bacillariophyceae). *Journal of Applied Phycology*, 32(6), 3809–3816.

Gobler, C. J. (2020). Climate Change and Harmful Algal Blooms: Insights and perspective. *Harmful Algae*, 91.

Griffith, A. W., & Gobler, C. J. (2020). Harmful algal blooms: A climate change co-stressor in marine and freshwater ecosystems. *Harmful Algae*, 91.

Gu, X., Li, K., Pang, K., Ma, Y., & Wang, X. (2017). Effects of pH on the growth and NH4-N uptake of Skeletonema costatum and Nitzschia closterium. *Marine Pollution Bulletin*, 124(2), 946–952.

Haverkamp, T. H., Schouten, D., Doeleman, M., Wollenzien, U., Huisman, J., & Stal, L. J. (2009). Colorful microdiversity of Synechococcus strains (picocyanobacteria) isolated from the Baltic Sea. The ISME journal, 3(4), 397-408.

Hinga, K. R. (2002). Effects of pH on coastal marine phytoplankton. Marine Ecology Progress Series, 238, 281–300.

Horikoshi, M. and Tang, Y. (2016). ggfortify: Data Visualization Tools for Statistical Analysis Results. https://CRAN.R-project.org/package=ggfortify

Huang, X.-G., Lin, X.-C., Li, S., Xu, S.-L., & Liu, F.-J. (2016). The influence of urea and nitrate nutrients on the bioavailability and toxicity of nickel to Prorocentrum donghaiense (Dinophyta) and Skeletonema costatum (Bacillariophyta). *Aquatic Toxicology*, 181, 22–28.

Huang, R., Sun, J., Yang, Y., Jiang, X., Wang, Z., Song, X., and Gao, K. (2021). Elevated pCO2 Impedes Succession of Phytoplankton Community From Diatoms to Dinoflagellates Along With Increased Abundance of Viruses and Bacteria. *Frontiers in Marine Science*, 1212.

Hughes, S. E., & Marion, J. W. (2021). Cyanobacteria growth in nitrogen-& phosphorus-spiked water from a hypereutrophic reservoir in Kentucky, USA. *Journal of Environmental Protection*, 12(2), 75-89.

Hutchinson, G. E. (1961). The paradox of the plankton. *The American Naturalist*, 95(882), 137-145.

Jiang, Z., Chen, J., Shou, L., Chen, Q., Wang, K., Zhou, F., Tao, B., & Yan, X.. (2015). Controlling factors of summer phytoplankton community in the Changjiang (Yangtze River) Estuary and adjacent East China Sea shelf. *Continental Shelf Research*, 101, 71–84.

Johnson, Z. I., Zinser, E. R., Coe, A., McNulty, N. P., Woodward, E. M. S., & Chisholm, S. W. (2006). Niche partitioning among Prochlorococcus ecotypes along ocean-scale environmental gradients. *Science*, 311(5768), 1737.

Kahru, M., Elmgren, R., Kaiser, J., Wasmund, N., & Savchuk, O. (2020). Cyanobacterial blooms in the Baltic Sea: Correlations with environmental factors. *Harmful Algae*, 92.

Kassambara, A. (2020). ggpubr: 'ggplot2' Based Publication Ready Plots. R package version 0.4.0. https://CRAN.R-project.org/package=ggpubr

Keating, K. I. (1978). Blue-Green Algal Inhibition of Diatom Growth: Transition from Mesotrophic to Eutrophic Community Structure. *Science*, 199(4332), 971–973.

Kesaulya, I., Rumohoira, D. R., & Saravanakumar, A. (2022). The Abundance of Gonyaulax polygramma and Chaetoceros sp. Causing Blooming in Ambon Bay, Maluku. *Indonesian Journal of Marine Sciences*, 27(1), 13–19.

Kim, J. H., Park, B. S., Kim, J., Wang, P., Han, M., & Cock, M. (2015). Intraspecific diversity and distribution of the cosmopolitan species Pseudo-nitzschia pungens (Bacillariophyceae): morphology, genetics, and ecophysiology of the three clades. *Journal of Phycology*, 51(1), 159–172.

Kindt, R. & Coe, R. (2005) Tree diversity analysis. A manual and software for common statistical methods for ecological and biodiversity studies. World Agroforestry Centre (ICRAF), Nairobi. ISBN 92-9059-179-X.

Kretz C. B., Bell D. W., Lomas, D. A., Lomas M. W., & Martiny A. C. (2015). Influence of growth rate on the physiological response of marine Synechococcus to phosphate limitation. *Frontiers in Microbiology*, 6.

Lampitt, R. S., Wishner, K. F., Turley, C. M., & Angel, M. V. (1993). Marine snow studies in the Northeast Atlantic Ocean: distribution, composition and role as a food source for migrating plankton. *Marine Biology*, 116(4), 689.

Lapointe, B. E., Herren, L. W., Brewton, R. A., & Alderman, P. K. (2020). Nutrient

over-enrichment and light limitation of seagrass communities in the Indian River Lagoon, an urbanized subtropical estuary. *Science of the Total Environment*, 699.

López-Archilla AI, Moreira D, López-García P, Guerrero C. (2004). Phytoplankton diversity and cyanobacterial dominance in a hypereutrophic shallow lake with biologically produced alkaline pH. *Extremophiles: Life Under Extreme Conditions*. 8(2):109-115.

Mohd-Din, M., Hii, K. S., Abdul-Wahab, M. F., Mohamad, S. E., Gu, H., Leaw, C. P., & Lim, P. T. (2022). Spatial-temporal variability of microphytoplankton assemblages including harmful microalgae in a tropical semi-enclosed strait (Johor Strait, Malaysia). *Marine Environmental Research*, 175.

Morse, R. E., Mulholland, M. R., Hunley, W. S., Fentress, S., Wiggins, M., & Blanco-Garcia, J. L. (2013). Controls on the initiation and development of blooms of the dinoflagellate Cochlodinium polykrikoides Margalef in lower Chesapeake Bay and its tributaries. *Harmful Algae*, 28, 71–82.

Mukherjee, A., Basu, A., Chakraborty, S., Das, S., & De, T. K. (2013). Salinity might be the most influential governing factor of cell surface size of Coscinodiscus in well mixed tropical estuarine waters. *International Journal for Life Sciences and Education Research*, 1, 81-90.

Mulford, R. A. (1963). Distribution of the Dinoflagellate Genus Ceratium in the Tidal and Offshore Waters of Virginia. *Chesapeake Science*, 4(2), 84–89.

Nguyen, A. T., Dao, T.-S., Strady, E., Nguyen, T. T. N., Aimé, J., Gratiot, N., & Némery, J. (2022). Phytoplankton characterization in a tropical tidal river impacted by a megacity: the case of the Saigon River (Southern Vietnam). *Environmental Science and Pollution Research*, 29(3), 4076–4092.

O'Boyle, S., & Silke, J. (2010). A review of phytoplankton ecology in estuarine and coastal waters around Ireland. *Journal of Plankton Research*, 32(1), 99–118.

Oksanen, J., Blanchet, F . G., Friendly, M., Kindt, R., Legendre, P., McGlinn, D., Minchin, P. R., O'Hara, R.B., Simpson, G. L., Solymos, P., Henry, M., Stevens, H., Szoecs, E., and Wagner, H. (2020). vegan: Community Ecology Package. R package version 2.5-7. https://CRAN.R-project.org/package=vegan

Olli, K., Ptacnik, R., Klais, R., & Tamminen, T. (2019). Phytoplankton species richness along coastal and estuarine salinity continua. *American Naturalist*, 194(2), E41–E51.

O'Neil. J. M., Davis, T. W., Burford, M. A., & Gobler, C. J. (2012). The rise of harmful cyanobacteria blooms: The potential roles of eutrophication and climate change. *Harmful Algae*, 14, 313–334.

Paerl, H. W., & Fulton, R. S. (2006). Ecology of harmful cyanobacteria. In *Ecology of harmful algae* (pp. 95-109). Springer, Berlin, Heidelberg.

Paerl H. W., & Huisman, J. (2008). Blooms like It Hot. *Science*, 320(5872), 57–58.

Papry, R. I., Ishii, K., Mamun, M. A. A., Miah, S., Naito, K., Mashio, A. S., Maki, T., & Hasegawa, H. (2019). Arsenic biotransformation potential of six marine diatom species: effect of temperature and salinity. *Scientific Reports*, 9(1).

Parkinson, R. W., Seidel, V., Henderson, C., & De Freese, D. (2021). Adaptation Actions to Reduce Impairment of Indian River Lagoon Water Quality Caused by Climate Change, Florida, USA. *Coastal Management*, 49(2), 215–232.

Phlips, E. J., Badylak, S., & Grosskopf, T. (2002). Factors Affecting the Abundance of Phytoplankton in a Restricted Subtropical Lagoon, the Indian River Lagoon, Florida, USA. Estuarine, *Coastal and Shelf Science*, 55(3), 385–402.

Phlips, E. J., Badylak, S., Christman, M., Wolny, J., Brame, J., Garland, J., Hall, L., Hart, J., Landsberg, J., Lasi, M., Lockwood, J., Paperno, R., Scheidt, D., Staples, A., & Steidinger, K. (2011). Scales of temporal and spatial variability in the distribution of harmful algae species in the Indian River Lagoon, Florida, USA. *Harmful Algae*, 10(3), 277–290.

Phlips E. J., Badylak S., Lasi M. A., Chamberlain R., Green W. C., Hall L. M., Hart J. A., Lockwood J. C., Miller J. D., Morris L. J., & Steward J. S. (2015). From Red Tides to Green and Brown Tides: Bloom Dynamics in a Restricted Subtropical Lagoon Under Shifting Climatic Conditions. *Estuaries and Coasts*, 38(3), 886–904.

Phlips E. J., Badylak S., Nelson, N. G., Hall L. M., Jacoby C. A., Lasi M. A., Lockwood J. C., & Miller, J. D. (2021). Cyclical Patterns and a Regime Shift in the Character of Phytoplankton Blooms in a Restricted Sub-

Tropical Lagoon, Indian River Lagoon, Florida, United States. *Frontiers in Marine Science*, 8.

Pittera, J., Humily, F., Thorel, M., Grulois, D., Garczarek, L., & Six, C. (2014). Connecting thermal physiology and latitudinal niche partitioning in marine Synechococcus. ISME Journal: *Multidisciplinary Journal of Microbial Ecology*, 8(6), 1221–1236.

Quintana, N., Van der Kooy, F., Van de Rhee, M. D., Voshol, G. P., & Verpoorte, R. (2011). Renewable energy from Cyanobacteria: energy production optimization by metabolic pathway engineering. *Applied Microbiology & Biotechnology*, 91(3), 471–490.

Raateoja, M., Kuosa, H., & Hällfors, S. (2011). Fate of excess phosphorus in the Baltic Sea: A real driving force for cyanobacterial blooms? *Journal of Sea Research*, 65(2), 315–321.

Rajaneesh, K. M., & Mitbavkar, S. (2013). Factors controlling the temporal and spatial variations in Synechococcus abundance in a monsoonal estuary. *Marine environmental research*, 92, 133-143.

Rakko A., & Seppälä, J. (2014). Effect of salinity on the growth rate and nutrient stoichiometry of two Baltic Sea filamentous cyanobacterial species. *Estonian Journal of Ecology*, 55.

Ray, R. T., Haas, L . W., & Sieracki. M. E. (1989). Autotrophic picoplankton dynamics in a Chesapeake Bay sub-estuary. *Marine Ecology Progress Series*, 52(3), 273–285.

Redfield, A. (1958). The biological control of chemical factors in the environment. *American Scientist*, 46(3), 205-221.

Regaudie-de-Gioux, A., & Duarte, C. M. (2012). Temperature dependence of planktonic metabolism in the ocean. *Global Biogeochemical Cycles*, 26(1).

Remane, A. (1934). Die Brackwasserfauna. Verhandlunge Der Deutschen Zoologischen Gesellschaft, 36, 34–74.

Rodrigues, R. V., Patil, J. S., K, S., & Anil, A. C. (2019). Dinoflagellate

planktonic-motile-stage and benthic-cyst assemblages from a monsoon-influenced tropical harbour: Elucidating the role of environmental conditions. Estuarine, *Coastal and Shelf Science*, 226.

Roubeix, V., & Lancelot, C. (2008). Effect of salinity on growth, cell size and silicification of an euryhaline freshwater diatom: Cyclotella meneghiniana Kütz. *Transitional waters bulletin*, 2(1), 31-38.

Rong Bi, Zhong Cao, Stefanie M. H. Ismar-Rebitz, Ulrich Sommer, Hailong Zhang, Yang Ding, & Meixun Zhao. (2021). Responses of Marine Diatom-Dinoflagellate Competition to Multiple Environmental Drivers: Abundance, Elemental, and Biochemical Aspects. *Frontiers in Microbiology*, 12.

Rörig, L. R., Honorato, M. C., Itokazu, A. G., de Macedo, C. X., Deschamps, F., Lins, J. V. H., Maraschin, M., Ramlov, F., Gressler, P. D., & Filho, J. P. (2017). Ecophysiological and biochemical variation of the surf zone diatom asterionellopsis glacialis sensu lato from Santa Catarina, Southern Brazil. *Brazilian Journal of Oceanography*, 65(4), 695–708.

Rose, J. M., & Caron, D. A. (2007). Does Low Temperature Constrain the Growth Rates of Heterotrophic Protists? Evidence and Implications for Algal Blooms in Cold Waters. *Limnology and Oceanography*, 52(2), 886–895.

Saifullah, A. S. M., Kamal, A. H. M., Idris, M. H., & Rajaee, A. H. (2019). Community composition and diversity of phytoplankton in relation to environmental variables and seasonality in a tropical mangrove estuary. *Regional Studies in Marine Science*, 32.

Scranton, K., & Vasseur, D. A. (2016). Coexistence and emergent neutrality generate synchrony among competitors in fluctuating environments. *Theoretical Ecology*, 9(3), 353-363.

Skarlato, S., Filatova, N., Knyazev, N., Berdieva, M., & Telesh, I. (2018). Salinity stress response of the invasive dinoflagellate Prorocentrum minimum. *Estuarine, Coastal and Shelf Science*, 211, 199–207.

Smayda, T. J., & Reynolds, C. S. (2003). Strategies of marine dinoflagellate survival and some rules of assembly. *Journal of Sea Research*, 49(2), 95–106.

Smith, N. P. (2016). Transport pathways through southern Indian River Lagoon. *Florida Scientist*, 79(1), 39–50

Spilling, K., Olli, K., Lehtoranta, J., Kremp, A., Tedesco, L., Tamelander, T. and Tamminen, T. (2018). Shifting diatom—dinoflagellate dominance during spring bloom in the Baltic Sea and its potential effects on biogeochemical cycling. *Frontiers in Marine Science*, 5, 327.

Sun, L., Jin, X. C., Yang, W., Xu, M., Zhong, Y., Zhu, L., & Zhuang, Y. Y. (2007). Effects of silicate on the community structure of phytoplankton in enclosures. *Huan Jing ke Xue Huanjing Kexue*, *28*(10), 2174-2179.

Tamminen, T., & Andersen, T. (2007). Seasonal phytoplankton nutrient limitation patterns as revealed by bioassays over Baltic Sea gradients of salinity and eutrophication. *Marine Ecology Progress Series*, 340, 121-138.

Trefry, J. H., Trocine, R. P., & Woodall, D. W. (2007). Composition and Sources of Suspended Matter in the Indian River Lagoon, Florida. *FLORIDA SCIENTIST*, 4, 363.

Trowbridge, CD. 1995. Establishment of the green algae Codium fragile ssp. tomentosoides on New Zealand rocky shores: current distribution and invertebrate grazers. *Journal of Ecology* 83:949-965.

Virta, L., Soininen, J., & Norkko, A. (2020). Diversity and distribution across a large environmental and spatial gradient: Evaluating the taxonomic and functional turnover, transitions and environmental drivers of benthic diatom communities. *Global Ecology and Biogeography*, 29(12), 2214–2228.

Wachnicka, A., Browder, J., Jackson, T., Louda, W., Kelble, C., Abdelrahman, O., Stabenau, E., & Avila, C. (2020). Hurricane Irma's Impact on Water Quality and Phytoplankton Communities in Biscayne Bay (Florida, USA). *Estuaries and Coasts: Journal of the Coastal and Estuarine Research Federation*, 43(5), 1217–1234.

Wang, K., Wommack, K. E., & Chen, F. (2011). Abundance and Distribution of Synechococcus spp. and Cyanophages in the Chesapeake Bay. *Applied and Environmental Microbiology*, 21, 7459.

Wang, J., & Zhang, Z. (2020). Phytoplankton, dissolved oxygen and nutrient patterns along a eutrophic river-estuary continuum: Observation and modeling. *Journal of Environmental Management*, 261.

Watanabe, T., Taniuchi, Y., Kakehi, S., Sakami, T., & Kuwata, A. (2017). Seasonal succession in the diatom community of Sendai Bay, northern Japan, following the 2011 off the Pacific coast of Tohoku earthquake. *Journal of Oceanography*, 73(1), 133–144.

Waterbury, J. B. (1986). Biological and ecological characterization of the marine unicellular cyanobacterium Synechococcus. *Photosynthetic picoplankton*, 71-120.

Weaver, R. J., Johnson, J. E., & Ridler, M. (2016). Wind-Driven Circulation in a Shallow Microtidal Estuary: The Indian River Lagoon. *Journal of Coastal Research*, 32(6), 1333–1343.

Wickham, H. ggplot2: Elegant Graphics for Data Analysis. Springer-Verlag New York, 2016.

Ye, Y., Chen, K., Zhou, Q., Xiang, P., Huo, Y., & Lin, M. (2018). Impacts of Thermal Discharge on Phytoplankton in Daya Bay. *Journal of Coastal Research*, 83, 135–147.

Yñiguez, A. T., Maister, J., Villanoy, C. L., Deauna, J. D., Peñaflor, E., Almo, A., & Azanza, R. V. (2018). Insights into the dynamics of harmful algal blooms in a tropical estuary through an integrated hydrodynamic-Pyrodinium-shellfish model. *Harmful Algae*, 80, 1-14.

Yoon, J. N., Lee, M., Jin, H., Lim, Y. K., Ro, H., Park, Y. G., & Baek, S. H. (2022). Summer Distributional Characteristics of Surface Phytoplankton Related with Multiple Environmental Variables in the Korean Coastal Waters. *Journal of Marine Science and Engineering*, 10(7), 850.

Zepernick, B. N., Gann, E. R., Martin, R. M., Pound, H. L., Krausfeldt, L. E., Chaffin, J. D., & Wilhelm, S. W. (2021). Elevated pH Conditions Associated With Microcystis spp. Blooms Decrease Viability of the Cultured Diatom Fragilaria crotonensis and Natural Diatoms in Lake Erie. *Frontiers in Microbiology*, 11.

Zhang, D., Wen, S., Wu, X., & Cong, W. (2018). Effect of culture condition on the

growth, biochemical composition and EPA production of alkaliphilic Nitzschia plea isolated in the Southeast of China. *Bioprocess & Biosystems Engineering*, 41(6), 831–839.

Zhong, Q., Xue, B., Noman, M. A., Wei, Y., Liu, H., Liu, H., Zheng, L., Jing, H., & Sun, J. (2021). Effect of river plume on phytoplankton community structure in Zhujiang River estuary. *Journal of Oceanology and Limnology*, 39(2), 550–565.

Zhou, Y., Zhang, Y., Li, F., Tan, L., & Wang, J. (2017). Nutrients structure changes impact the competition and succession between diatom and dinoflagellate in the East China Sea. *Science of the Total Environment*, 574, 499–508.